

2484- 2580

g 557

TECHNICAL REPORT

69-25-CE

AD 714224

PASSIVE THERMAL CONTROL SYSTEMS FOR ADVANCED SPACE SUIT CONCEPTS

by

Louise V. Dusablon, Ferdinand Votta, Jr.,
Nathaniel S. Schneider and Leo A. Spano

November 1968

UNITED STATES ARMY
NATICK LABORATORIES
Natick, Massachusetts 01760



Clothing & Personal Life
Support Equipment Laboratory
C&OM-54

This document has been authorized for public release and sale; its distribution is unlimited.

The findings in this report are not to be construed as an official Department of the Army position unless so designated by other authorized documents.

Citation of trade names in this report does not constitute an official indorsement or approval of the use of such items.

Destroy this report when no longer needed. Do not return it to the originator.

This document has been approved
for public release and sale;
its distribution is unlimited.

AD _____

TECHNICAL REPORT

69-25-CE

PASSIVE THERMAL CONTROL SYSTEMS FOR ADVANCED SPACE SUIT CONCEPTS

by

Louise V. Dusablon
Ferdinand Votta, Jr.
Nathaniel S. Schneider
Leo A. Spano

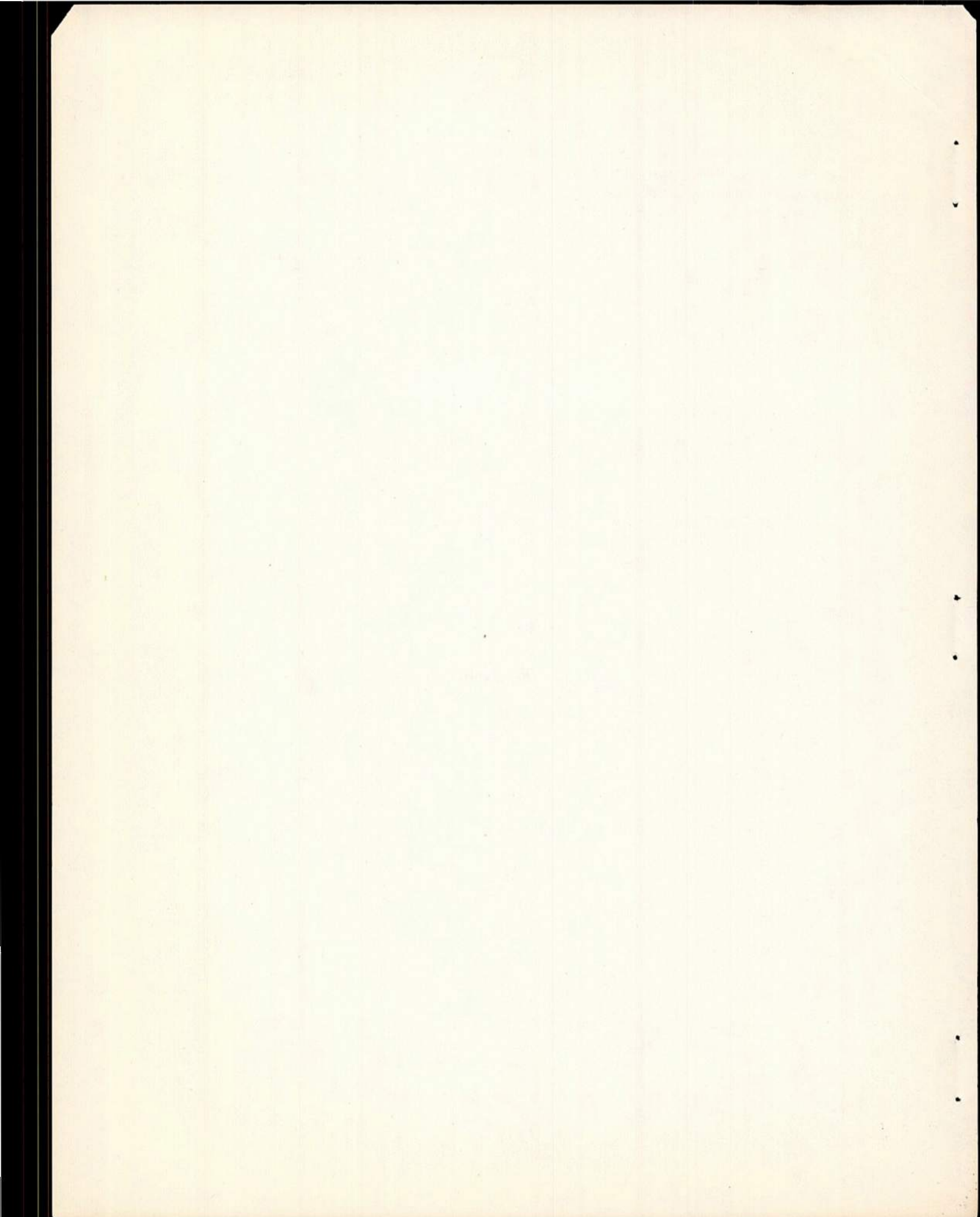
November 1968

Project Reference:

Series: C&OM-54

NASA R-135

CLOTHING & PERSONAL LIFE SUPPORT EQUIPMENT LABORATORY
U. S. ARMY NATICK LABORATORIES
Natick, Massachusetts 01760



FOREWORD

This final report represents the work done by the Advance Projects Branch, Clothing & Personal Life Support Equipment Laboratory, U. S. Army Natick Laboratories, under NASA Project Number R-135. The object of this program was to investigate and develop novel passive thermal control systems for use in space suit designs.

The report summarizes the performance during the contract period January 1964 to January 1968.

CONTENTS

	<u>Page</u>
ABSTRACT	vi
I INTRODUCTION	1
II DISCUSSION	1
A. Semipassive Pervaporative Thermal Control System	2
B. Passive Thermal Control Systems	5
1. Electroendosmosis	5
2. Ionically Modulated Diffusion	8
3. Studies in the Design of a High MVP Polyurethane	10
III CONCLUSIONS AND RECOMMENDATIONS	14
APPENDIXES	
A. Experimental Study of a Passive Thermal Control System	16
B. Electroendosmosis and Water Transport	32
C. Evaluation of "IOPLEX" for Ionically Modulated Diffusion	47
D. Experimental Study of Polyurethanes	76

LIST OF FIGURES

<u>Figure</u>		<u>Page</u>
1	Heat Regulation by Evaporative Cooling	3
2	Electroendosmosis in a Cylindrical Tube	7

LIST OF TABLES

<u>Table</u>		
1	Steady-State Flux	11

ABSTRACT

Pervaporation of water from a space suit has been proposed as a method of cooling an astronaut. The purpose of this program was to investigate the various principles, techniques and material designs applicable to the engineering of a system capable of transferring up to 3000 Btu/hr. Four different approaches were investigated with an eventual prototype kept in view.

Simple diffusion of water through a membrane requires the development of a polymer with strong physical properties and chemical characteristics necessary for its application to a space suit. Presently no polymer has both required properties. Research was begun to design an appropriate polymer.

A composite membrane was tested where the matrix had the required physical characteristics and a "filler" polymer enhanced the existing permeation qualities of the matrix. This system came within a factor of two of the required permeation rate of 1100 gms/24 hrs/100 in². A matrix with higher permeation rates and a more uniform method of mixing is needed before this method can be incorporated in a prototype design.

The principle of electroendosmosis was examined as a means of electrically controlling water transport through a membrane. It was shown to be theoretically capable of removing a sufficient quantity of moisture at no great cost of power. However, much developmental research is needed to bring the system to the prototype stage.

A semipassive system ready for prototype development was also tested. With this method, the temperature of the man would be controlled by a valve which allows regulated amounts of water to evaporate and thus remove heat.

I INTRODUCTION

Investigations were initiated to design passive-type thermal controls for space suit systems for extra-vehicular and lunar surface operations. Several investigators have explored the use of passive heat regulation devices to control the heat absorption and emission of orbiting satellites and space vehicles. However, no passive thermoregulatory system to protect man in space has been achieved, although on a theoretical basis such a system appears quite promising. The purpose of this program was to investigate various principles, techniques, material designs and physiological and psychological parameters applicable to the engineering of such passive protective systems.

In order to define the parameters against which the space suit or protective system must be functional, the environment to which the astronaut could be exposed must be defined for orbital and surface operations away from earth. As man proceeds away from the surface of the earth, a number of environmental factors are altered. Of these factors, pressure, temperature, radiation, and reduced gravity must be considered.

In space, there is negligible heat added or removed from the suited man by the rarefied gas molecules. The temperature of the extra-vehicular man is controlled by metabolic heat + solar energy. Atmospheric pressures are essentially zero. The effect of weightlessness on the ability to function, and the protection from ultraviolet and infrared effects must also be considered in the development of a personal protective system. Radiation effects, i.e., the penetration of materials by high energy particles, and the ranges and energy losses in many elements for a wide range of particle energies, must also be taken into account.

Several methods have been proposed for the passive thermal regulation of man in space of which pervaporative cooling (vaporization across a diffusive barrier) is the one whose state-of-the-art permits design work to start. The heat of evaporation liberated by the water or perspiration diffusing across a membrane into outer space would be used to keep an astronaut comfortable. Several pervaporative systems have been proposed and explored. Other cooling schemes would be conductive cooling by use of a water-conditioned suit and the reduction of the thermal gradient from front to back of the suited astronaut by the use of heat of fusion techniques.

II DISCUSSION

Pervaporation of moisture from a space suit has been proposed as a method of cooling an astronaut in free space. In this process, liquid water from inside the suit is transported through a permselective barrier in the suit wall and is discharged as a vapor to the

vacuum of space. About 1000 BTU can be removed from the suit for each pound of water transported through the suit wall via this barrier-moderated evaporation process. The success of this cooling scheme relies on the development of a suitable barrier material with high moisture permeability and lower air permeability. This perm-selective character of the barrier is essential in order to prevent excessive loss of life-supporting air gases from the pressurized suit while pervaporation of large amounts of moisture is taking place. The barrier material must also be reasonably tough and flexible, although properties such as tear resistance and dimensional stability can presumably be provided by laminating the barrier material to reinforcing structures such as fabrics and foams.

The cooling load for an average-size man has been estimated to be 3000 Btu/hr including both the metabolic energy being generated by the astronaut and the net solar energy being absorbed by the suit. With about 20 ft² of suit area available for pervaporation, the barrier would have to be capable of transporting water at the rate of about 1100 gms/(100 in² X 24 hrs). For maximum comfort it is also desirable for the major portion of the cooling load to be handled by mechanisms other than by sweating, i.e., have another source of moisture available. For long missions the man should be in a dry environment and subjected to only insensible perspiration most of the time.

Two pervaporative, thermal control systems have been proposed and explored. The first is a completely passive system making use of a selective moisture permeable membrane to provide the necessary cooling effect. The second or alternate system is passive except for a small amount of gas flow necessary to remove insensible perspiration next to the skin and a temperature sensitive pressure control valve.

A. SEMIPASSIVE PERVAPORATIVE THERMAL CONTROL SYSTEM

The semipassive pervaporative thermal control system discussed below is presently the only technically feasible passive method available. The essential components of this system are shown in Figure 1. The skin would be separated from an impermeable membrane by a narrow air gap controlled by a spacer material. The air gap would allow for some circulation of the gas next to the skin and would contain the life support gas at the required pressure. The impermeable membrane which would keep the life support gas from escaping, would be in contact with a wet wick which would itself be covered by a permeable membrane. The permeable membrane would be separated from an outer impermeable membrane by a porous vapor space. For operation in a vacuum environment such as in space, the vapor space would vent to the surroundings through a pressure control valve.

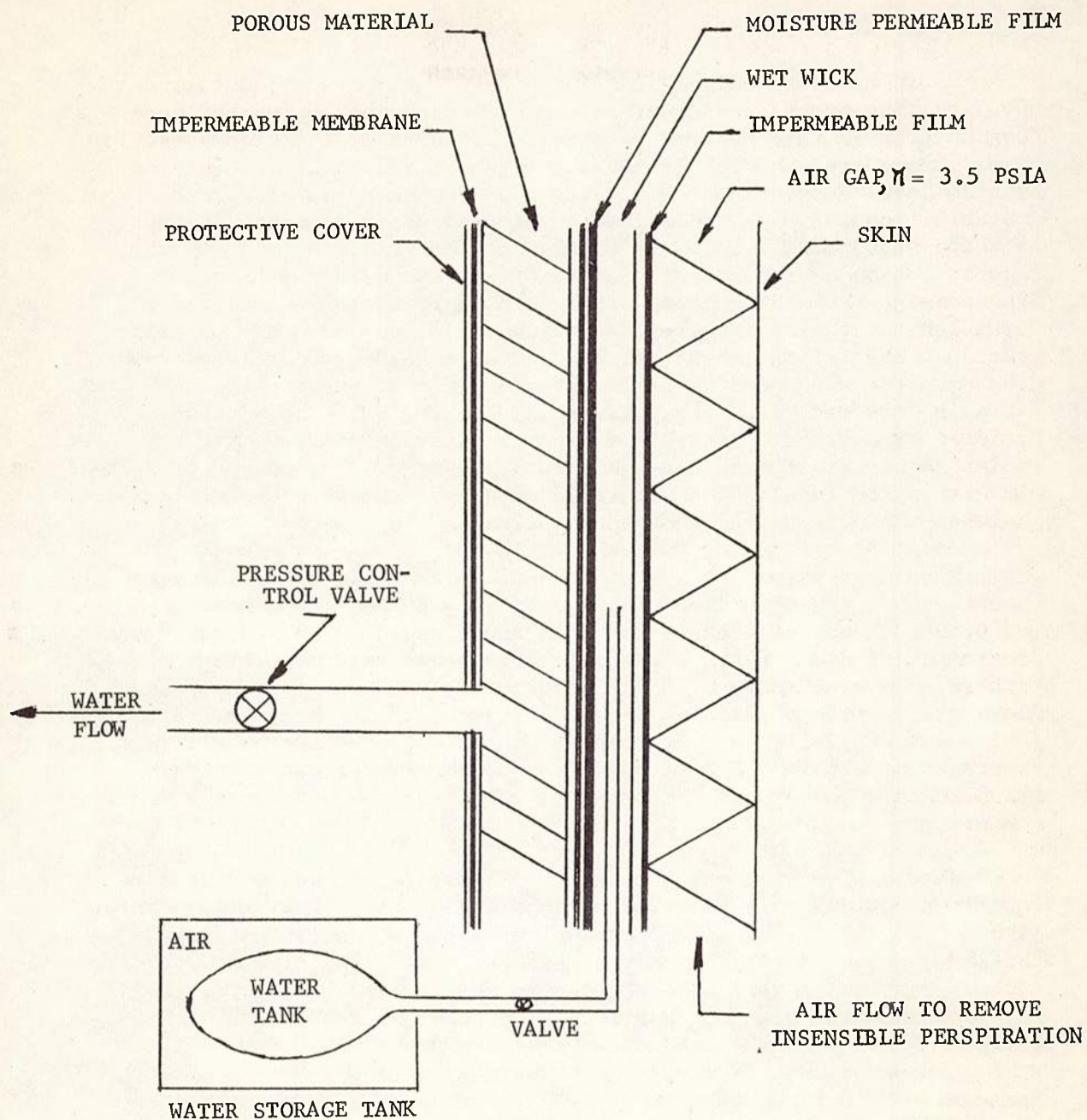


FIGURE 1. HEAT REGULATION BY EVAPORATION COOLING

Equipment was designed and tests were run to experimentally evaluate the proposed concept and several clothing composites were evaluated with this system. A detailed account of the theory, equipment, procedure, and results is contained in Appendix A. Clothing system No. 1 consisted of a .285-inch polyurethane-saran spacer material mounted over the skin simulator so as to form an air gap. A white rubberized fabric was mounted on the outside of the spacer and it became an impermeable membrane separating the air gap from the remainder of the system. The water distribution was obtained by a length of 1/16-inch Teflon tubing coiled outside the rubberized fabric. The Teflon tubing was punched by a needle about every two inches. The wick consisted of a single layer of absorbent paper toweling covered by a single layer of woven nylon. The wick was covered by a tightly fitting layer of leather which served as the moisture permeable membrane. The entire system was then wound tightly with nylon tape so that it would withstand the pressure differential between the air gap and the vapor space.

Clothing system No. 2 consisted of a layer of cotton shirting mounted over the skin simulator. The air gap was formed by a layer of 0.10 inch-polyethylene-saran spacer which was in contact with the cotton shirting. The impermeable membrane and water distribution system used were the same as in No. 1. The wick was formed by six layers of cotton shirting covered by a layer of woven nylon. Suit No. 3 was similar to No. 2 except that the cotton shirting wick was replaced by a nylon felt wick and the leather layer was eliminated. Thus suits No. 2 and No. 3 contained the identical air gap spacer material.

With a simulated skin temperature of 91°F., it was possible to obtain a cooling rate of 182 Btu/(hr x ft²). For a suit with a total area of 20 ft² this would be equivalent to a cooling rate of 3640 Btu/hr., which is considerably in excess of the goal of 3000 Btu/hr. Two special tests were devised to show the different behavior of the wicks and of the clothing systems. The first was called a "wick response test" and the second was called a "speed response test". The purpose of the "wick response test" was to show how the system reacted with a fixed quantity of water in the wick. The "speed response test" was devised to determine how rapidly the simulated skin temperature could be changed. Several tests were also made to study the temperature control possible with the system. It was found relatively easy to maintain the skin temperature at a preset value over a wide range of heat flow rates. For example, during one test with clothing system No. 3 and where the heat flow rate was varied from 53 to 150 Btu/(hr-ft²), the maximum variation of the skin temperature was ±2°F and the average fluctuation was less than ±1°F. A considerable difference in speed of response and operating characteristics of the three suits was noted. The differences are believed to be due to variations in the wick construction.

This phase of the work produced two worthwhile results: it proved the feasibility of this passive control system and it produced a piece of apparatus designed to test the cooling rates of composite clothing systems and the controllability of each composite.

Therefore, it is concluded from this part of the study that it is possible with the current state of technical knowledge to design a passive thermal system which will remove heat from a man in a vacuum environment at a rate in excess of 3000 Btu/hr without depending on sweating and his skin could be maintained relatively dry. Also, it would be possible to control the skin temperature within 1 or 2°F. over a wide range of metabolic outputs.

Additional experimental work should be carried out in which various wick designs could be studied. For reduced pressure operation, it would seem that the desired characteristics can be met by synthetic material which do not tie up relatively large quantities of water in the fiber.

An actual prototype protective clothing system using a wet wick and designed for reduced pressure operation should be constructed and tested under actual conditions.

B. PASSIVE THERMAL CONTROL SYSTEMS

1. Electroendosmosis

While the ability to utilize the latent heat of evaporation of water as a supplemental means of energy release is an important step forward in system-temperature adjustment, a far more significant achievement would be the development of a means for accurately controlling water evaporative loss from the system. Of the potentially practicable control-methods for moderating mass-transport processes within solids, undoubtedly the most attractive is the application of an electric field.

The use of an electric field to induce transport of fluids through solids is hardly a novel concept, although its practical utilization in devices or processes has been infrequently reported. The bulk transport of liquid through a microporous solid or capillary under the action of an externally impressed electrical potential gradient is known as the phenomenon of electroendosmosis.

If a fluid such as water is confined within a capillary or the pores of a porous solid, and if the electrostatic charges are immobilized on the solid surface, the condition of electrostatic neutrality requires that there be presented in the fluid an equal number of ions of charge opposite to that on the solid surface. As a consequence of this charge separation, the fluid phase is at an

electrical potential different from that of the solid within which it is confined. If an external electric field is now imposed upon the system, ions within the fluid are subjected to a force in the direction of the potential gradient; this force is transmitted by viscous shear to the fluid in which the ions are suspended. Consequently, both the ions and the fluid proceed to move at a constant velocity (the ions more rapidly than the fluid) whose magnitude is directly proportional to the field strength. This is illustrated in Figure 2. The magnitude of this electrically induced flow is dependent upon (a) the surface charge-density, (b) the degree of separation of immobilized surface charges from their mobile counter-charges, (c) the dielectric constant of that fluid, and (d) the fluid viscosity. Another important feature of this method is that the electroendosmotic flow velocity is independent of the pore or capillary size. Thus, an extremely fine-pore-texture medium can be employed which will exhibit virtually zero hydraulic permeability, yet will exhibit significant electroendosmotic permeability. This property will prove to be vital in developing a practical gas-barrier through which water may be readily transmitted via electrical means.

The possibility of utilizing the principle of electroendosmosis within a microporous or hydrous ionically-charged matrix as a means of electrically controlling the rate of transport of water from a space suit enclosure to outer space, for the purpose of thermal control of the suit environment, has been examined from physico-chemical, electrochemical, and materials technological standpoints. It has been deduced that this principle offers great promise as a means not only for transporting water into space at greater rates than are now achievable by simple diffusive mechanisms, but also for controlling water-transport rates over broad limits. By appropriate electrode design, it is believed possible not only to make such control continuous, but also to regenerate oxygen from water within the suit enclosure.

Calculations indicate that electrically induced water fluxes of between $400 - 700 \text{ gm/m}^2 - \text{sec}$ can be sustained with voltages across 2-mil sheet barriers of one volt. Minimum energy consumption under these conditions ranges from 3 to 30 watt-hours per gallon of water transported; actual energy requirements may be expected to be twice these values.

Surface-treated, microporous plastic sheet, polyelectrolyte gel-filled porous sheet, or homogeneous polyelectrolyte films appear to be promising candidates for the control layer in a suitably supported laminate.

A detailed derivation of equations and design characteristics is contained in Appendix B.

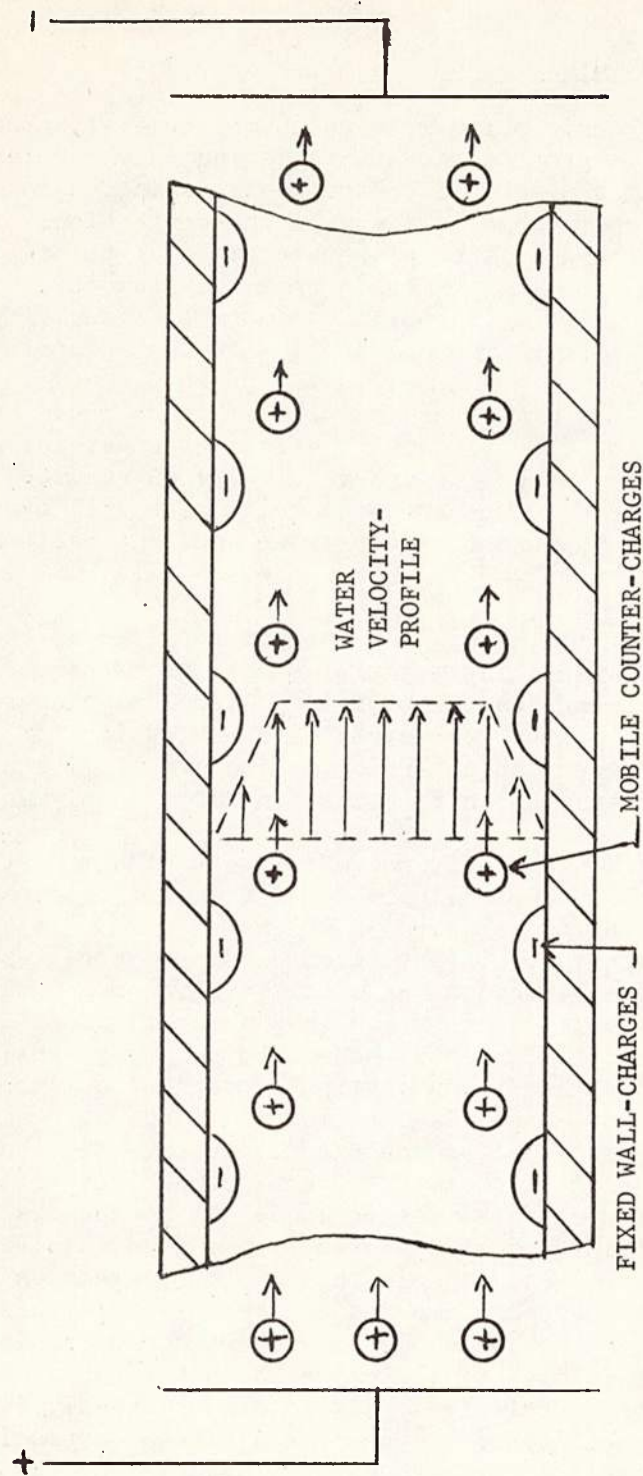


FIGURE 2. ELECTROENDOSMOSIS IN A CYLINDRICAL TUBE

2. Ionically Modulated Diffusion

A thin film of organic polymer in which molecular transport takes place via a diffusion process appears to be the only barrier material capable of giving a high moisture vapor transmission rate and still be relatively impermeable to air. Of the conventional film-forming polymers, those with a balance of reasonably high polarity and chain flexibility would be most suitable from the standpoint of maximizing both the driving force (solubility) and the diffusivity for activated water transport through the polymer. Nevertheless, since films much thinner than one mil are unreliable due to the high probability of pinhole formation, the maximum transmission rate which could be achieved under pervaporation conditions with existing commercial polymers one mil thick is less than 10% of the required 1000 gms/100 in² - 24 hrs. The transport rate of unwaterproofed cellophane will exceed this figure, but the porous nature of the polymer would make it unsuitable from the standpoint of very high air permeability.

An alternative barrier to the homogeneous polymer film is the composite structure. A film-forming material with high transport rates and good physical properties can be filled with well-dispersed particles of an even more moisture permeable material, which for various reasons may be an unsuitable barrier by itself, to give a composite with a higher transmission rate than the matrix polymer.

An ionically crosslinked, organic polymer with unusual moisture transmission characteristics (IOPLEX) has been developed by industry.* It is not water-soluble, but sorbs up to 50 weight percent moisture. Under pervaporative transport conditions (liquid water upstream-bone-dry air or vacuum downstream), Ioplex has a moisture vapor permeance (M.V.P.) of about 5000 gm-mils/24 hrs - 100 in², which is about 50 times higher than any other homogeneous, non-porous polymer, while being no more air-permeable than a conventional amorphous polymer. Ioplex can be fabricated into a self-supporting film, but such a film would not be sufficiently rugged, for space application. There are several factors which control the moisture vapor permeability of this type of composite. The shape of the particles making up the dispersed phase has a pronounced effect. When long fibers are used in place of spherical particles, a marked increase in the rate of permeation of the composite results, if they are compared at the same volume loading of particles. Methods have been developed, however, for preparing submicroscopic, fibrous particles of Ioplex which when incorporated into conventional polymers at relatively low loadings markedly increase the moisture permeability of the composite without appreciably altering the oxygen permeability or mechanical properties of the matrix polymer.

*IOPLEX - Tradename of Amicon Corporation

Tests were conducted on a composite of Ioplex and two polyester-type polyurethanes formulated by industry.

A polyester-based polyurethane elastomer was chosen as the matrix polymer because of its toughness and abrasion resistance and its comparatively high permeability characteristics. In spite of a high MVP of about 40 gm-mils/100 in² - 24 hrs, this polyurethane is not swollen appreciably by water, and its oxygen permeability is only about 10⁻⁸ CC (STP)/cm²-sec-atm. The polyurethane was filled with Ioplex powder at levels ranging from 20 to 40 weight percent. At the 20% loading the MVP of the composite was between two and three times that of the base polyurethane. At the 40% loading the composite MVP was 10 times that of the polyurethane (which is within a factor of two of the requirement). The oxygen permeabilities of the composites were comparable to the low polyurethane value.

The composites were also tested as the combination adhesive-and barrier-layer in a laminate consisting of a water absorbing and reinforcing fabric and thermally insulating fabric-foam sandwich. A detailed analysis of the laminates and their permeabilities has shown that at atmospheric pressure the fabric-foam layers offer significant resistance to moisture transport even though they are macroscopically porous. In theory the resistance of the fabric-and foam-layers should become negligible when stagnant air at atmospheric pressure is removed from the porous materials by making the water vapor transport measurements under simulated space (vacuum) conditions. These measurements were made and it was found that the polyurethane-Ioplex adhesive layer was, indeed, the sole barrier to water transport. Therefore, the aforementioned increase in MVP obtained with Ioplex as a filler in the unsupported films can also be obtained in the fully assembled laminate if the measurements are made under simulated space conditions.

There are several improvements in laminate construction which should allow the desired goal in MVP of 1000 gm-mils/24 hrs - 100 in² to be achieved. In the first place the base polyurethane resin in the barrier adhesive could be reformulated to give a material which is still tough and flexible but which would have an MVTR in excess of 100 gms/100 in² - 24 hrs.

The above-mentioned tests also disclosed that care must be taken in the way in which a multilayer laminate is assembled to optimize its MVTR. As many of the porous supporting and thermally insulating layers as possible must be kept on the low pressure (vacuum) side of the suit wall.

From other studies and the results of this test, it would seem probable that with improved dispersion techniques and improved matrix material the goal is within reach.

3. Studies in the Design of a High MVP Polyurethane

Polyurethanes, as a class of elastomers, are excellent candidates for application to a space suit system, since (1) they exhibit a permselectivity of water versus oxygen of a factor of 10,000 to 1, and (2) they have excellent mechanical properties. However, as has been stated previously, conventional polyurethanes are not capable of diffusing sufficient amounts of moisture to keep an astronaut in a comfortable environment.

Generically, polyurethanes are the reaction products of diisocyanates and glycols and polyols. The ultimate properties of the final polyurethane are unique functions of the detailed chemical architecture resulting from the specific choice of reactant type and stoichiometry. These reactants can be varied over extremely wide limits. This class of polymers essentially consists of block-type copolymers which allow a systematic and controlled variation of the structure of the "hard" and "flexible" units, each of which should exert a strong effect on permeability behavior. It was, therefore, the object of this area of study to determine which structural characteristics of a polyurethane system control moisture transport, in an attempt to exploit these findings to tailor a chemically homogeneous polyurethane membrane with an MVTR sufficient to provide passive thermal control of a space suit.

The work was divided into three areas: (1) a preliminary study of steady-state permeation in four samples, including a study of the effect of thickness on the MVP, (2) a study of characteristic structural parameters, and (3) a comprehensive study of the sorption of chemically characterized samples.

The early studies consisted of steady-state permeation studies of commercial samples. The tests were conducted in a controlled-temperature and-humidity chamber using a modified ASTM cup method to determine fluxes. Two of the samples were known by their trade name Estane*. Another sample was known as LD-550**, and the fourth sample was furnished by another commercial firm***. The latter also furnished three other samples with which some unsteady-state measurements were begun. Results of the steady state studies are contained in Table 1. These results showed an almost tenfold variation in MVTR from 26 to 190 gm-mil/100 in² - 24 hrs. for the different samples. Moreover, by separation of the specific permeability into its component factors, it was learned that the solubility of water was the same and small (~2%) in all four samples.

*Tradename of B.F. Goodrich

**Tradename of E.I. Dupont

***Mobay Chemical Company

TABLE 1

STEADY-STATE FLUX*

<u>Chamber Conditions</u>	<u>Estane 5740X100</u>	<u>Estane 5740X140</u>	<u>Dupont LD-550</u>	<u>Mobay Polyester</u>
(Dry Bulb Temp. 90°F.)				
40% R.H.	25.7	84	190	68
50%	----	60	158	62
60%	----	45	141	50
70%	----	--	---	39
70%	----	--	---	30

*Flux expressed in gm-mils/100 in² - 24 hrs.

(normalized for thickness)

Therefore, the observed permeabilities were proportional to the diffusion coefficient of water and controlled by the molecular flexibility of the polymer.

Through an examination of literature data and some steady-state atmospheric testing, it was observed that normalizing permeation rates for thickness by multiplying by the thickness was not strictly accurate. In order to correct the comparative data available, tests were conducted to determine a more exact relationship between the flux and the thickness. At the same time the existence of a relationship between the flux and the solvent or the substrate used for casting the film was tested.

Estane 5740 X 140 was dissolved with two different solvents and cast on two different substrates. The solvents and substrates were found by a trial-and-error process as the only ones readily available that gave a continuous, clear membrane. The solvents were tetrahydrofuran and cyclohexanone, and the substrates were glass and water. Neither solvent nor substrate variation had an apparent effect on the flux. For details, see Appendix D, Part 1.

It was found that the film was not the only barrier or resistance to permeation, but that the finite rate of evaporation of the water under the existing test conditions must also be accounted for in normalizing thin film data. For the polyurethane used, a linear relationship was found and is described by the formula

$$J = 1/(mL + b)$$

where J is the moisture vapor transmission rate, and L is the thickness. The parameters, m and b, are the reciprocal values for the normalized flux rate and the rate of evaporation of water, respectively.

Four types of well-characterized polyurethanes were received, each having a fixed composition of the hard unit of 3 moles MDI and 2 moles 1, 4 butanediol, while the soft structure of the four samples had the following composition:

1. Poly (1,4 butylene adipate)
2. Poly (1,4 butylene glycol)
3. Poly (propylene glycol)
4. Poly (ethylene glycol)

All prepolymers had a molecular weight of about 2000.

Little information was available as to the internal structure of the samples being studied (the chemical makeup was known); therefore, some structural analysis was conducted.

Four distinct transition regions common to the different polyurethane samples have been identified in the combined results from a rapid scanning calorimeter and thermomechanical analyzer. The transition (T_1) below 0°C. is the common glass transition. A transition in the region 60 - 90°C. (T_2) is tentatively identified with the disassociation of a secondary bonded network formed by interactions between the aromatic urethane segments. The transition at about 150°C. (T_3) is ascribed to allophonate bond disassociation. A final transition at 200 - 220°C. could arise from urethane bond disassociation but in at least one type of polyurethane it is due to the melting of birefringent regions present in small concentrations. The series of polyether based samples show increasing turbidity from polyethylene oxide to polytetramethylene oxide indicating the presence of regions of structure but there is no X-ray evidence for crystallinity in the unoriented samples. This domain structure, which has been characterized by preliminary low angle light scattering, must play an important role in determining the mechanical and permeability behavior of the polyurethanes. Finally, crystallization occurs on sample extension and undoubtedly governs the stress-strain behavior at higher elongations. Details of procedure, data and results are contained in Appendix D, Part 2.

One polyester type polyurethane has been extensively studied (sorption studies) and work on a polyether type was started. The hard structure of the polyurethane samples contained 3.2 moles di-phenylmethane-4,4' diisocyanate (MDI) and 2 moles of butanediol-1,4. The soft structure of the polyester was poly (1,4 butylene adipate) and the polyether was poly (1,4 tetramethylene glycol).

A gravimetric, sorption-desorption technique, employing a Cahn, continuous output electrobalance was used to study the diffusion and solubility behavior of the vapor in the samples. The diffusion coefficient was found to have a marked inverse dependence on the concentration with two-thirds of the effect taking place within 10% of the activity range. The sorption isotherms deviated positively from Henry's Law, possibly because of sorbent-sorbent interactions. A clustering of the water molecules within the polyurethane matrix was indicated by mathematical analysis. This in combination with a specific site sorption model would explain the inverse behavior of the diffusion coefficient. Little or no heat of mixing was observed in the process. An Arrhenius plot of the diffusion coefficient and solubility coefficient versus temperature indicated varying activation energies of diffusion and solubility.

The major difference in the reactions of the polyether versus the polyester based polyurethane was that the order of magnitude of the diffusion coefficient was 50% higher for the polyether. Otherwise, the results were similar (see Appendix D, Part 3).

To obtain a better understanding of the aspects of penetrant structure which govern the permeability of polymers to small organic molecules, detailed measurements were made on the unsteady-state sorption of ethanol vapor into the polybutylene adipate based polyurethane over a range of partial pressures using a quartz spring balance. The sorption isotherm was strongly concave upward, approaching Henry's Law behavior only for activities of less than 0.2. The heat of mixing was endothermic but quite small suggesting that the environment of ethanol in the polyurethane is energetically similar to the pure liquid. The diffusion coefficient at first decreases somewhat with increasing concentration and then increases about twofold to a plateau value. This behavior differs from the continuous and order of magnitude increase in D that occurs with increasing concentration of swelling penetrants. Further, many of the sorption-square root of time curves are anomalous. Some are S-shaped while for the initial pressure step there is a distinct break in the curve. This behavior is attributed to a process of diffusion with concurrent reaction. The immobilization of penetrant species may occur both through clustering and hydrogen bonding interactions of ethanol with the carboxyl groups of the polyester chain. An illustrative analysis suggests that the true diffusion coefficient may be tenfold higher than the apparent values ordinarily calculated.

III CONCLUSIONS AND RECOMMENDATIONS

At the present time, a semipassive, thermally controlled prototype space suit has been proven feasible and the state-of-the-art is such that it is possible for one to be made.

All other methods discussed need much work before they can become practical working systems. Electroendosmosis would be an excellent method with ionically modulated diffusion considered second best.

Because enough work has not been done in the design of the optimum polyurethane, the diffusion method is the most remotely probable.

ACKNOWLEDGMENT

The authors wish to acknowledge the contributions of the following people: Dr. J. H. Saunders, Director of Research at the Mobay Chemical Company, Dr. Stuart Clough, Research Chemist, Mr. Alfred Allen and Mr. John Nystrom, Research Chemical Engineers.

APPENDIX A

EXPERIMENTAL STUDY OF A PASSIVE
THERMAL CONTROL SYSTEM

CONTENTS

	<u>Page</u>
I Experimental Equipment	18
II Operating Procedure	23
III Calculated Heat Flow Rate	23
IV Results	25
V Reliability of Results	29

LIST OF FIGURES

Figure

A-1 Schematic Diagram of Apparatus	19
A-2 Complete Apparatus with Outer Pipe Removed	20
A-3 Inner Pipe and Measuring Devices	21
A-4 Assembled System	22
A-5 Heat Flow Rate	27

LIST OF TABLES

Table

A-1 Summary of Reduced Pressure Tests	26
---------------------------------------	----

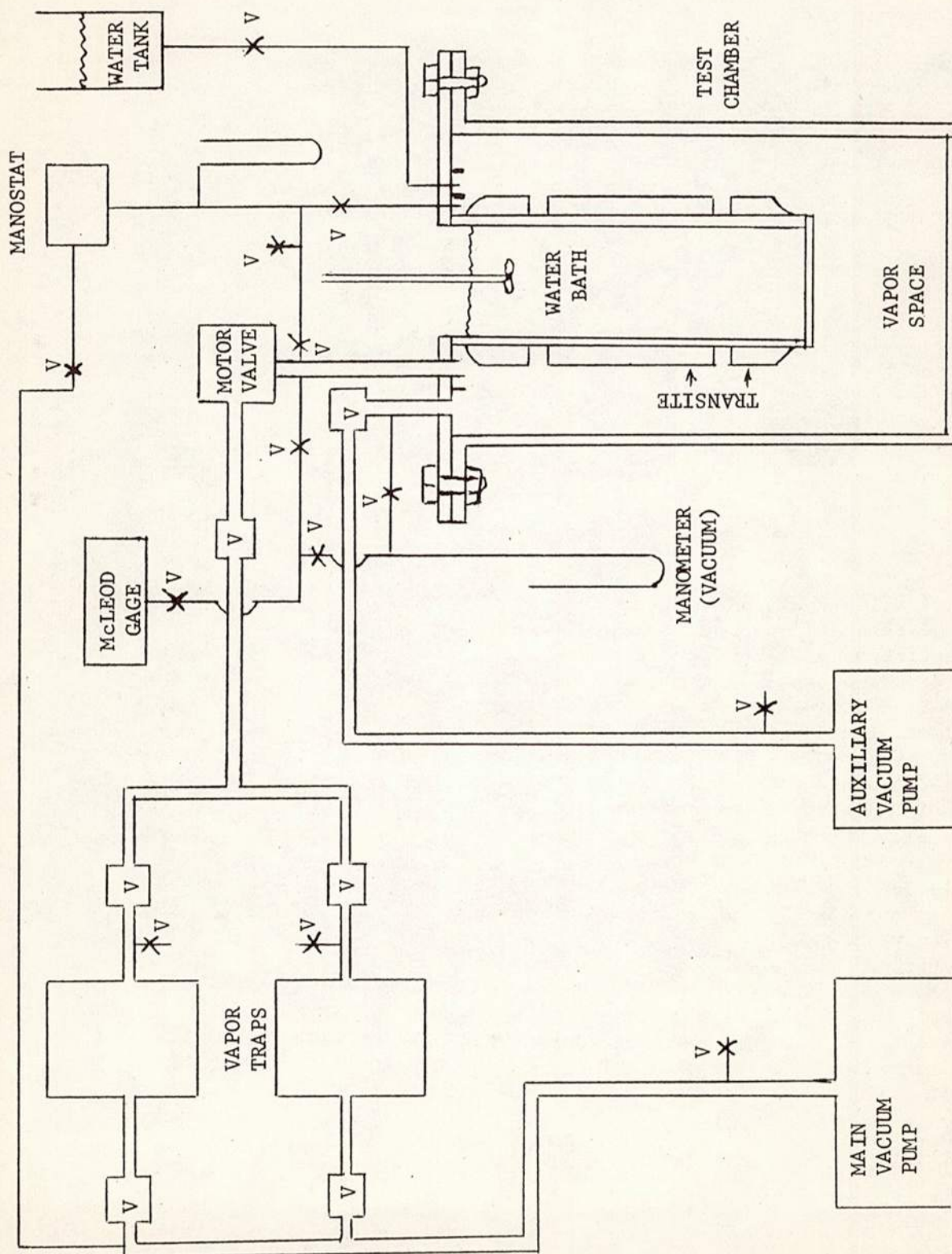
I EXPERIMENTAL EQUIPMENT

A schematic diagram of the equipment used in this investigation is shown in Figures A-1. The equipment (Figures A-2, A-3, A-4) consisted of a test chamber, two vacuum pumps, two vapor traps, a motor-operated control valve, vacuum or pressure measuring instruments, temperature control and measuring instruments, and various small valves and piping.

The test chamber consisted of an annular space formed by two concentric brass pipes. Each pipe was sealed off by being welded to a disc or head at one end and to a flange at the other end. The flanges were bolted together with a gasket between them to form the test chamber. The outer pipe was a standard 16-inch pipe and the inner pipe was a standard 8-inch pipe. A transite pipe (asbestos cement) was mounted over the inner pipe and served as the simulated skin surface. The temperature drop through the transite pipe, measured with a differential thermocouple, was used as the basis for calculating the rate of heat flow. The transite pipe was divided into three sections to reduce longitudinal heat transfer. The center section was one foot long and served as the test section. The total surface area of the transite was 3.8 square feet. Eleven thermocouples were installed to the surface. Each thermocouple consisted of three junctions connected in parallel. Heat was supplied by an electrically heated hot water bath inside the inner pipe. The water temperature for most tests was controlled by a mercury in glass thermo-regulator.

The motor-operated valve in the vacuum line from the vapor space controlled the pressure in that space and thus controlled the rate of water vaporization from the wet wick. It was operated by a potentiometric thermo-regulator. In an actual operation the pressure control valve would be activated by the skin temperature, but for steady state tests it was found that more uniform operations resulted when the valve was activated by one of the wick thermocouples. In several temperature control tests, however, the control valve was activated by the simulated skin temperature.

Two other potentiometers were used to measure temperatures. One, a 24-point Honeywell-temperature recorder, was used to record the E.M.F. from all the thermocouple junctions in the system. The other potentiometer was a two-pen Moseley strip-chart recorder. Generally, one pen was used to measure the temperature of the outer surface of the transite (simulated skin temperature) and the other to measure the temperature drop through the asbestos cement from which the rate of heat flow was calculated. However, by using a thermocouple selector switch, it was possible to use the more sensitive strip chart recorder to measure and record other key temperatures. Full scale range on the strip chart recorder was adjustable. Generally it was used with full scale set at 1 or 2 millivolts. At maximum sensitivity each division on the chart was less than 0.5°F and it was possible to estimate temperatures to approximately 0.1°F .



V = VALVE

FIGURE A-1. SCHEMATIC DIAGRAM OF APPARATUS

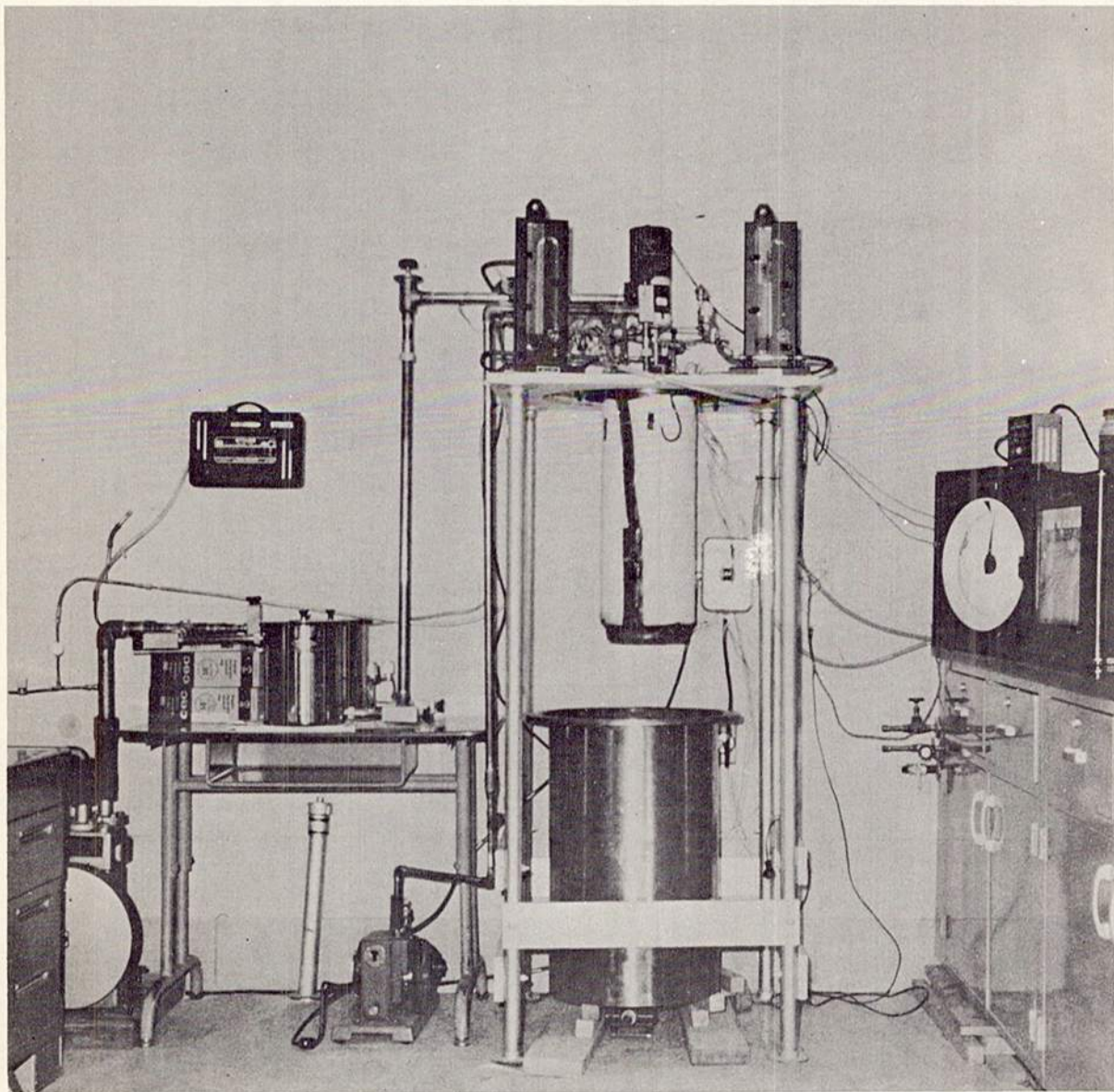


Figure A-2. COMPLETE APPARATUS WITH OUTER
PIPE REMOVED

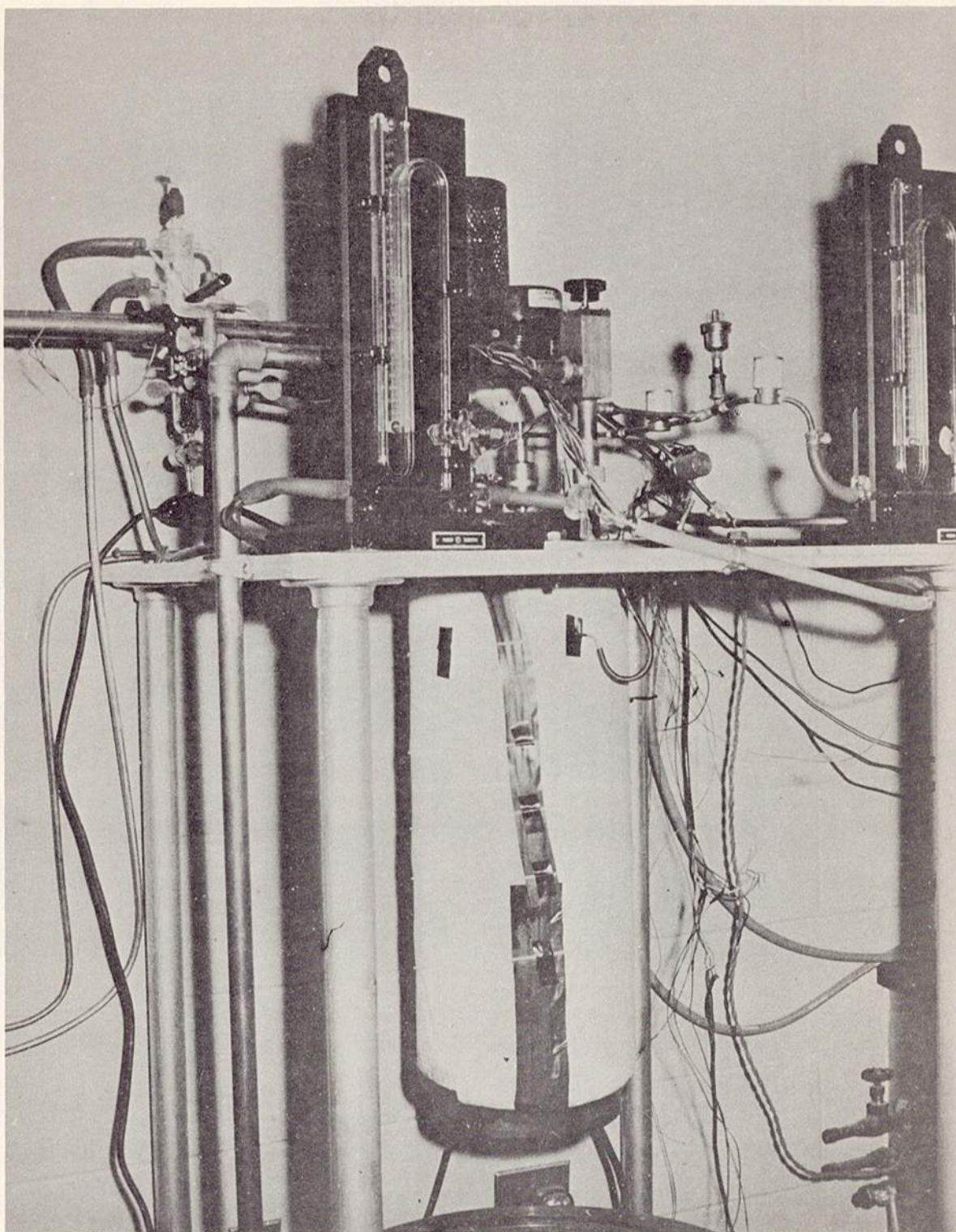


Figure A-3. INNER PIPE AND MEASURING DEVICES

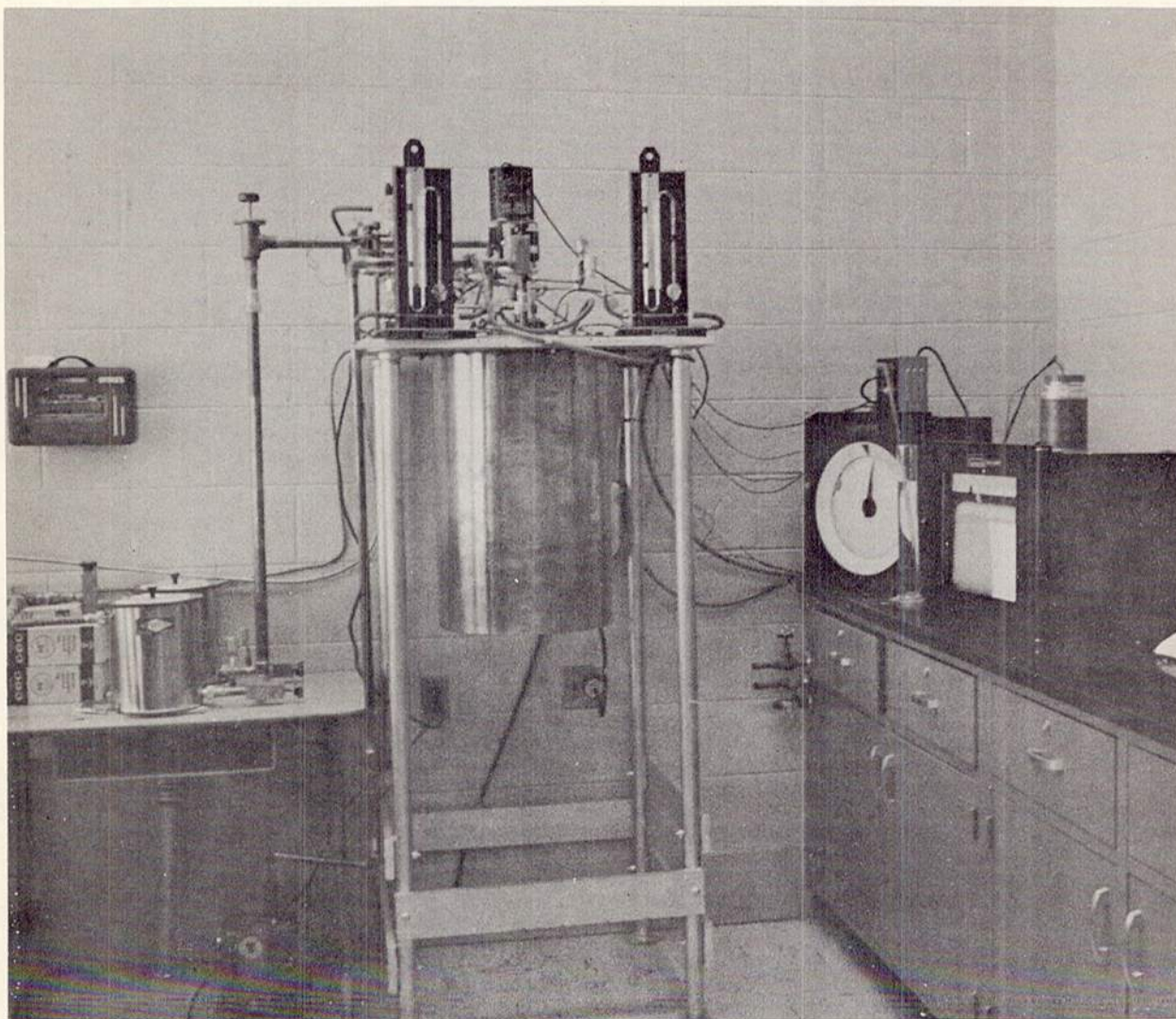


Figure A-4. ASSEMBLED SYSTEM

The simulated clothing systems were mounted over the transite skin simulator. The impermeable membrane was cemented and clamped to projections on the flange and to the lower portion of the inner pipe. The outer brass pipe served as the outer impermeable membrane. Figures A-2 and A-3 show the equipment with the outer pipe dismantled and the impermeable membrane in place over the transite. Figure A-4 shows the equipment assembled with the outer pipe bolted in place.

II OPERATING PROCEDURE FOR REDUCED PRESSURE TESTS

Before conducting any experimental tests the system was leak tested, both between the entire system and the atmosphere, and between the air gap and vapor space.

In carrying out a test, the water bath heater and stirrer were turned on and the bath was heated to the desired temperature. The vapor space and air gap were slowly evacuated with a bypass valve between the two open so that the pressures would be equalized. When the pressure reached 180 mm of Hg (3.5 psi) the bypass valve was closed and full vacuum was applied to the vapor space. The air gap pressure was maintained at approximately 180 mm of Hg for most tests. Originally, a manostat was planned for pressure control of the air gap. However, the glass manostat broke and it was found that manual control of the pressure was not difficult as the air gap pressure changed very slowly. Ice was put into one of the vapor traps. The main vacuum pump was a ballast pump which could handle up to 25 mm of Hg partial pressure of vapor but the pumping speed was increased if some of the vapor was condensed and separated before the pump. In three of the runs where very high pumping speeds were required, dry ice and acetone were used in the traps. The controller operating the automatic control valve was set at the estimated required wick temperature and water was allowed to flow into the wick. Sufficient water was added so that the six wick thermocouples were nearly the same. The water vaporized from the wick and cooled it very rapidly. The simulated surface temperature also cooled rapidly. When the wick temperature reached its set point the motor valve closed and vaporization stopped. The temperatures then started to rise until the control valve reopened. The temperature set point for the valve was adjusted until the simulated skin temperature was maintained at the desired value. After conditions in the system had been constant for approximately 30 minutes, the temperatures were recorded and the run ended.

III CALCULATED HEAT FLOW RATE

The experimental rate of heat flow was determined from the temperature drop across the transite. The rate of heat flow through the transite is given by:

$$\frac{q_t}{A} = \frac{k_t \Delta t}{L} \quad A-1$$

where:

- q_t = heat transfer through the transite
- A = area, sq. ft.
- k = thermal conductivity of transite, 5.5(Btu x in)/(hr. x sq.ft. x °F)
- L = thickness of transite, 0.4 inches
- Δt = temperature difference between inner and outer surface, °F

The theoretical rate of heat flow through the air gap from the simulated skin surface was calculated and compared with the experimentally measured rate through the transite. Heat, leaving the simulated skin surface, will be transferred through the air gap spacer to the inside wick surface by radiation, conduction and by natural convection. The total heat transferred across the air gap will be conducted through the wick where it will be removed by vaporization of the water from the outer wick surface. Thus:

$$q_w = q_R + q_c + q_{NC} \quad A-2$$

where:

- q_w = heat transferred through wick
- q_R = radiant heat transfer
- q_c = conductive heat transfer
- q_{NC} = heat transfer due to natural convection

In these calculations it was assumed that convection in the spacing material would be negligible and that the temperature drop through the wick will be small and the wick temperature would be uniform.

The rate of energy transfer by radiation from the simulated skin surface to the wet wick may be approximated by:

$$\frac{q_R}{A} = (\epsilon) 0.173 \left[\left(\frac{T_s}{100} \right)^4 - \left(\frac{T_w}{100} \right)^4 \right] \quad A-3$$

where:

- ϵ = emissivity of skin surface
- T_s = simulated skin temperature, °R
- T_w = wick temperature, °R

In using Equation A-3, it was assumed that the wet wick behaved as a black body and the skin surface as a grey body. The emissivity was assumed to be 0.95. The air gap size has no effect on the rate of radiation.

Conduction through the spacer material may be calculated by:

$$\frac{q_c}{A} = \frac{k_m(T_s - T_w)}{L} \quad A-4$$

where:

k_m = thermal conductivity of spacer (Btu x inch)/
(hr. x sq. ft. x °F)
 L = thickness in inches

Two different thickness of spacer materials was used. The first, used only in Suit No. 1, was a 0.285 inch thick polyethylene-saran spacer, and the second, used in Suit numbers 2 and 3, was a 0.10-inch-thick polyethylene-saran spacer. The thermal conductivities of both thicknesses were determined and supplied. These were 0.27279 for the 0.285-inch spacer and 0.29196 for the 0.10-inch spacer. In calculations for Suits 2 and 3, the thickness of the cotton shirt-ing of 0.01 inch was added to the spacer thickness.

IV RESULTS

The results of the reduced pressure tests are summarized in Table A-1. Both the calculated and experimentally measured heat flow rates for each of the three clothing systems are listed. Also listed for each run are the simulated skin temperature t_s , the wick temperature, t_w , the condition of the wick and the air gap pressure. Figure A-5 shows the calculated and experimentally measured cooling rates for a simulated skin temperature of 91°F as a function of wick temperature.

The agreement between the calculated and measured cooling rates was very good. With a simulated skin temperature of 91°F, it was possible to obtain a cooling rate of 182 Btu/(hr. x sq. ft.). For a suit with a total area of 20 sq. ft. this would be equivalent to a cooling rate of 3640 Btu/hr., which is considerably in excess of the goal of 3000 Btu/hr. Suits No. 2 and 3 gave essentially the same heat flow rates for the same wick and skin temperature. This was as expected since they both contained the same spacing material for the air gap.

A considerable difference in the speed of response and operating characteristics of the three suits was noted. Suit No. 2 required considerably more water to wet the wick uniformly and responded to temperature change more slowly than did either of Suits No. 1 or 3. Suit No. 3 required the least water and reacted most rapidly to temperature changes. Suit No. 2 required over 1000 ml. of water to wet the wick uniformly. These differences, it is believed, are due

TABLE A-1

SUMMARY OF REDUCED PRESSURE TESTS

RUN NO.	SUIT NO.	t_s °F	t_w °F	WICK	AIR GAP PRES mm. Hg	COOLING RATE	Btu/(hr' x sq ft)
						Measured	Calculated
4	1	118.2	110.9	dry	0	18	---
6	1	91.5	80.0	wet	180	33	22
7	1	90.9	64.0	wet	173	48	52.5
8	1	90.9	52.0	wet	174	69	67.5
9	1	91.2	65.4	wet	187	41	45
10	1	91.1	73.4	wet	186	24	34
11	1	95.3	69.4	wet	177	54	54
12	1	95.5	81.8	wet	180	37.5	25
13	1	91.0	86.3	dry	0	13	---
14	1	90.9	85.5	dry	180	16	11
15	2	92.0	91.6	dry	0	6.5	---
16	2	91.0	77.4	wet	180	54	50
17	2	91.0	68.5	wet	180	71	82
18	2	91.6	61.5	wet	180	115	108
19	2	116.0	113.3	dry	180	23.5	14.5
20	2	104.0	102.3	dry	180	12	8
21	2	91.5	30.5	wet	180	39	39
22	2	103.0	87.3	wet	180	60	60
23	2	95.7	79.3	wet	180	56	62
24	2	91.2	46.5	wet	180	159	161
25	2	95.8	44.5	wet	180	172	189
26	2	91.4	40.0	wet	180	182	184
30	3	118.4	114.0	dry	180	24	17
31	3	103.0	91.4	wet	180	64.5	42
32	3	90.8	80.7	wet	200	46	39
33	3	92.0	71.2	wet	190	79.5	72
34	3	90.9	65.8	wet	185	110	92

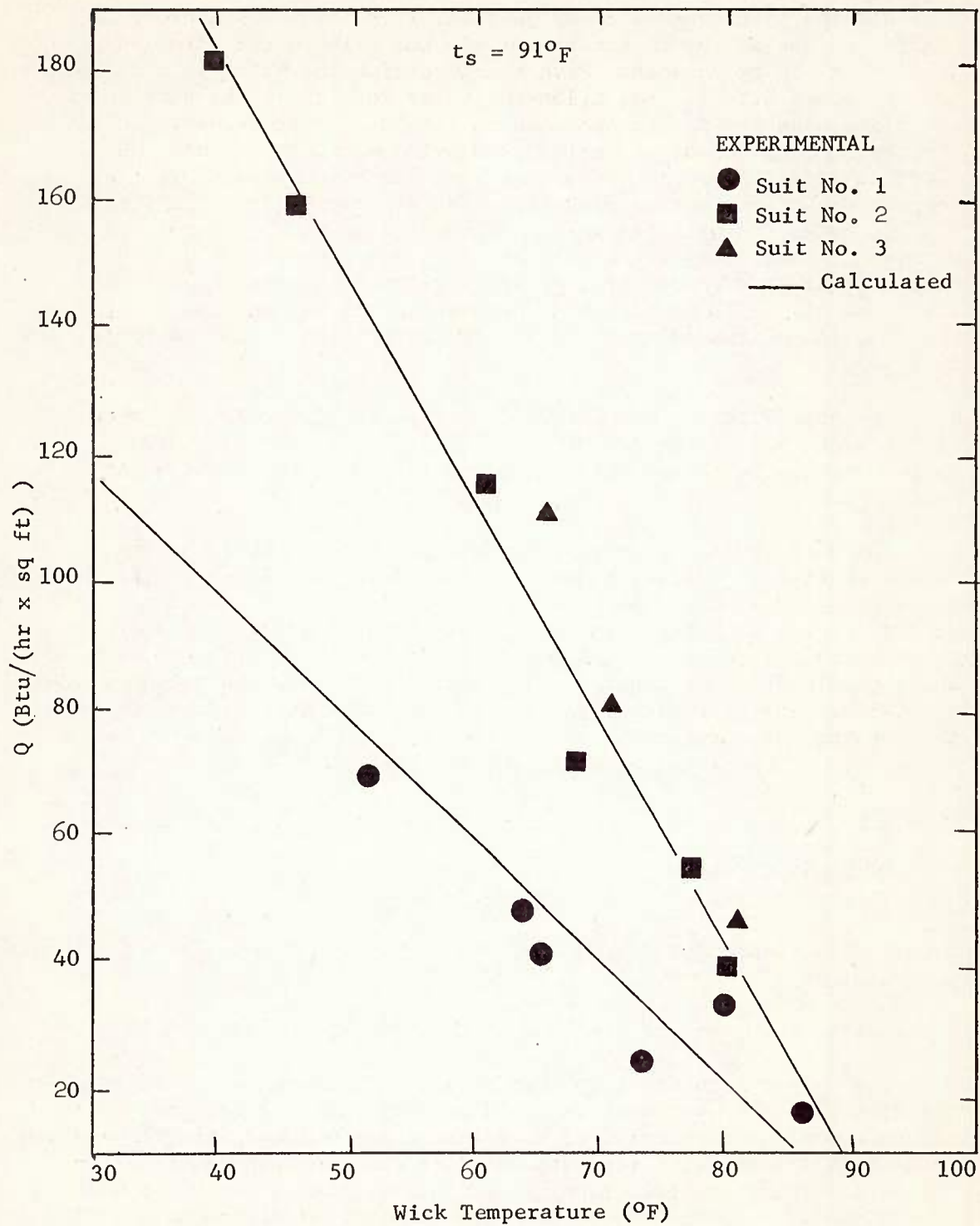


FIGURE A-5. HEAT FLOW RATE

to the differences in wick construction of the three suits. The multilayer cotton wick of Suit No. 2 required considerably more water than did the thin paper wick of Suit No. 1 or the nylon wick of Suit No. 3. Also the cotton fibers did not release the water as readily as the nylon wick. With a cotton wick the water is absorbed in the fibers but with the nylon the water remains on the surface of the fiber. An interesting phenomenon was noted that shows the difference in behavior of the cotton and nylon wick. When water was first added to the system after the wick had been pumped dry, the temperature of the cotton wick increased sharply, before dropping. In some cases the wick temperature increased to above the bath temperature and in one test the temperature rise was approximately 20°F. This initial rise in temperature was negligible or non-existent with the nylon wick. It was assumed that the phenomenon was due to the condensation of the water vapor and its absorption in the cotton fibers.

Two special tests were devised to show the different behavior of the wicks and of the clothing systems. The first was called a "wick response test" and the second was called a "speed response test."

The purpose of the "wick response test" was to show how the system reacted to a fixed quantity of water in the wick. The bath was controlled at 120°F and the system was first evacuated completely to dry out the wick. Air in the gap was controlled at 180 mm of Hg pressure. Then, exactly 100 ml. of water was added to the wick while continuing to evacuate on the vapor space with the vacuum valve open wide. The response of the system was noted and the results of the test on the three suits are listed.

	<u>Suit No. 1</u>	<u>Suit No. 2</u>	<u>Suit No. 3</u>
Maximum Cooling Rate Btu/(hr. x sq. ft.)	82.5	59.0	190
Lowest skin temperature reached, °F	107	111	89

The initial skin temperature in each case was approximately 117°F.

The "speed response test" was devised to determine how rapidly the simulated skin temperature could be changed. The test consisted of measuring the time required to reduce the simulated skin temperature from 103°F to 96°F with the bath at 112°F and the time required for the skin temperature to return to 103°F after the vacuum valve had been closed. A comparison of the time required by different clothing systems to this standard test would give an indication of their

relative response speeds to changing conditions. Only Suits No. 2 and No. 3 were subjected to this test. Suit No. 2 changed from 103°F to 96°F in 19 minutes and required 40 minutes for the temperature to return to 103°F. Suit No. 3, on the other hand, only required 4.5 and 22.5 minutes, respectively, for the same tests. This would clearly indicate the superiority of Suit No. 3 in the ability to adjust to rapid changes of conditions even though the steady state heat flow rates were approximately the same for both.

Several tests were made to study the temperature control possible with the system. Temperature control was obtained by the motor-operated valve in the vacuum line. By opening and closing this vacuum valve, the heat flow rate from the system was varied. For the steady state runs, the motor valve was activated and controlled by the wick temperature. However, for the temperature control runs the valve was operated by the simulated skin temperature. It was found relatively easy to maintain the skin temperature at a preset value over a wide range of heat flow rates. During one test with Suit No. 3, the skin temperature control was set at 91°F and the heat flow rate was varied from 53 to 150 Btu/(hr. x sq. ft.). In this test the skin temperature did not vary by more than 2°F, and most of the time the variation was less than 1°F.

The heat flow rates were only slightly dependent on the air gap pressure. The heat flow rate was increased by decreasing the air gap pressure. This is contrary to what would be expected and it is believed to be due to variation in the thickness of the gap with the variation in pressure. In a test made with Suit No. 3, the heat flow at a gap pressure of 90 mm of Hg was 127 Btu/(hr. x sq. ft.). When the pressure was increased to 200 mm of Hg, the heat flow decreased to 110 Btu/(hr. x sq. ft.). The effect of pressure on the cooling rates of Suits No. 1 and No. 2 was less than that of Suit No. 3.

V RELIABILITY OF RESULTS

The experimental heat flow rates were calculated from the measured temperature drop through the asbestos cement (transite) pipe and the reported thermal conductivity. While the good agreement of the heat flow through the transite and the calculated heat flow through the air gap seemed to indicate that the method used and measurements were reliable, a completely independent check of the results seemed desirable. This was done by making an overall energy balance on the equipment.

The total energy into the system came from the electrical hot water heater and from the water stirrer. The "energy out" consisted of the heat transferred through the transite pipe and the loss from the water surface and top flange. A wattmeter was installed in the electrical line to the heater. The total heat transferred through the

transite pipe could be calculated from the temperature drop measurements since the total surface area of the transite was known (3.8 sq. ft.). The heat loss from the water and top surface was neglected. This left only the heat input from the stirrer unknown.

A special test was made to determine the rate of energy added to the system from the stirrer. The bath temperature was lowered to slightly below room temperature. Under this condition the direction of the heat flow was from the surroundings into the bath. The stirrer was turned on and the rate of temperature rise was measured when the temperature drop through the transite was zero, indicating no heat flow. The test was repeated with a measured energy input into the electrical heater in addition to the stirrer. From the results of these tests it was possible to calculate the energy input from the stirrer.

$$q_s = M_c \Delta t_1 \quad A-5$$

$$q_s + q_e = M_c \Delta t_2 \quad A-6$$

where:

- q_s = energy input of stirrer
- q_e = energy input of heater
- M_c = heat capacity of system
- t_1 = rate of temperature rise, stirrer alone
- t_2 = rate of temperature rise, stirrer and heater

Dividing equation A-5 by A-6 gives

$$\frac{q_s}{q_s + q_e} = \frac{\Delta t_1}{\Delta t_2} \quad A-7$$

From the results of these tests it was found that the stirrer heat input, q_e , was 50 Btu/hr.

The overall energy balance was applied to several test runs. The "energy in", which was the sum of the heat added by the stirrer and the electrical heater was compared to the "energy out", which was the total heat flow through the transite. The results are given below:

RUN	ENERGY IN Btu/hr.	ENERGY OUT Btu/hr.	ENERGY OUT ENERGY IN
6	173	125.5	0.73
7	220	182	0.83
8	340	262	0.77
9	190	156	0.82
10	125	91	0.73
11	220	205	0.93
12	180	143	0.79
		Average	0.80

Since the heat loss from the top surface of the equipment was neglected, the overall energy balance was considered a very satisfactory check of the measured heat flow through the transite pipe.

APPENDIX B

ELECTROENDOSMOSIS AND WATER TRANSPORT

CONTENTS

	<u>Page</u>
I Theory of Electroendosmosis	34
II Current and Power Requirements for Electroendosmotic Water Transport	39
III Electrochemical Processes in Electroendosmosis	40
IV Design Requirements	43
V Bibliography	46

LIST OF FIGURES

Figure

B-1	Electroendosmosis in a Cylindrical Tube	35
B-2	Electroendosmotic Transport in a Homogeneous Polyelectrolyte Gel	38
B-3	Electroendosmosis with Electrode Reactions Generating H_2 and O_2	42
B-4	Schematic Cross Section of Idealized Laminate	45

I THEORY OF ELECTROENDOSMOSIS

If a fluid such as water is confined within a capillary or the pores of a porous solid, and if electrostatic (i.e., ionic) charges are immobilized on the solid surface, the condition of electrostatic neutrality requires that there be present in the fluid an equal number of ions of charge opposite to that on the solid surface. As a consequence of this charge-separation, the fluid phase is at an electrical potential different from that of the solid within which it is confined. If an external electric field is now imposed upon the system, ions within the fluid are subjected to a force in the direction of the potential gradient; this force is transmitted by viscous shear to the fluid in which the ions are suspended. Consequently, both the ions and the fluid move at a constant velocity (the ions more rapidly than the fluid) whose magnitude is directly proportional to the field strength. This is illustrated schematically in Figure B-1.

The magnitude of this electrically induced flow is dependent upon (a) the surface charge-density, (b) the degree of separation of immobilized surface charges from their mobile counter-charges, (c) the dielectric constant of the fluid, and (d) the fluid viscosity. The charge density and charge-separation are reflected in the so-called "electrokinetic" or "zeta" potential between the phases. Application of electric field-theory and the Boltzman principle to this system yields the following simple expression for the electroendosmotic flow velocity in a capillary or porous plug of arbitrary geometry:

$$\bar{U} = \frac{D \bar{\rho} (dE/dl)}{4 \pi \eta} \quad \text{B-1}$$

where:

- D = fluid dielectric constant
- $\bar{\rho}$ = Zeta potential, volts
- dE/dl = applied potential gradient, volts/cm
- η = fluid viscosity, poises
- \bar{U} = electroendosmotic velocity, cm/sec.

Equation B-1 is dimensionally correct when voltages are expressed in electrostatic c.g.s units (1 stat volt = 300 Int. volts).

An unusual and critically important property of Equation B-1 is that it contains no quantities relating to the pore structure of the medium which confines the fluid. This means that the electroendosmotic flow velocity is independent of the pore- or capillary size. Thus, an extremely fine-pore-texture medium can be employed which will exhibit virtually zero hydraulic permeability, yet will exhibit significant

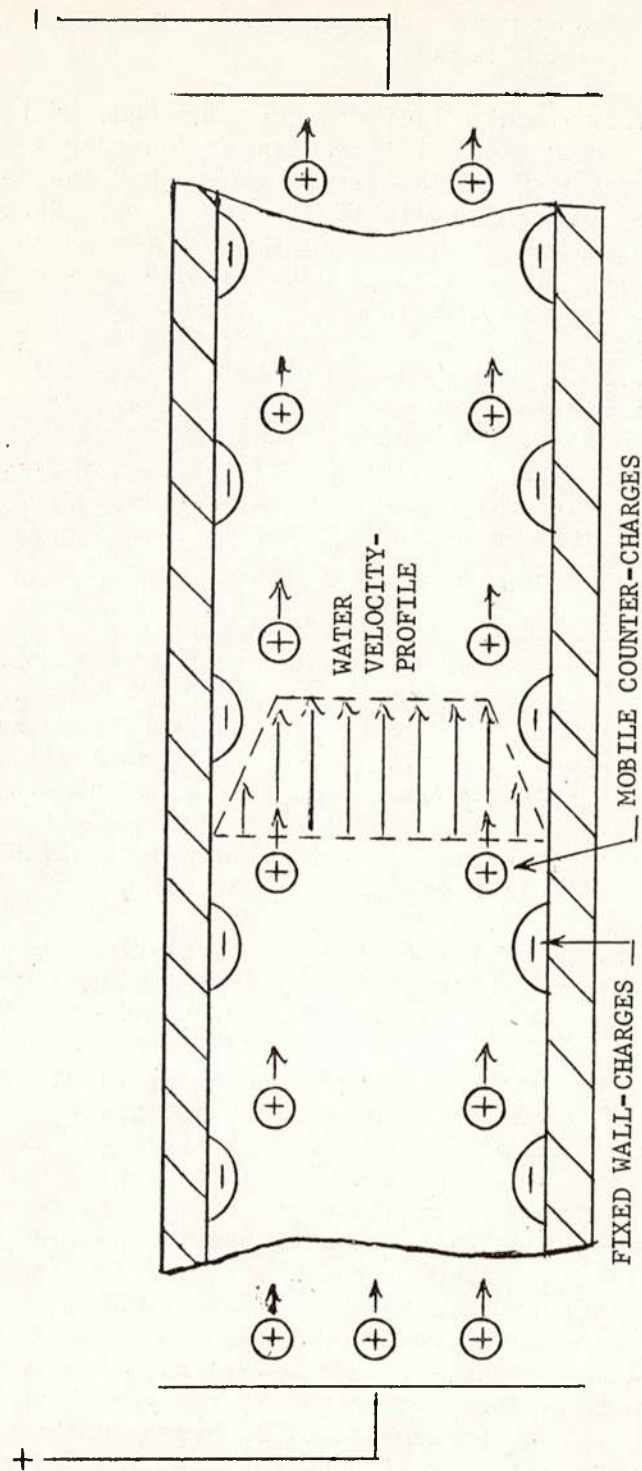


FIGURE B-1. ELECTROOSMOSIS IN A CYLINDRICAL TUBE

electroendosmotic permeability. This property will prove to be vital in developing a practicable gas-barrier through which water may be readily transmitted via electrical means.

A trial calculation will readily indicate the magnitude of flow which may be induced by a modest potential gradient. Consider a 2-mil (50 micron) flat sheet of material of porosity of 50%. Let the zeta potential for the system be 100 millivolts (a normal value). For water, $D = 80$; $\eta = 0.01$ poise. Let a voltage of 1.0 volt be impressed across the sheet. From Equation B-1, \bar{U} is calculated to be 0.14 cm/sec. The mass-flux of water through the sheet is thus $0.07 \text{ gm/sec} \times \text{cm}^2$, or $700 \text{ gm/m}^2 \times \text{sec}$. By way of comparison, the maximum rate at which water could be transmitted by molecular diffusion through such a sheet (assuming a diffusion coefficient for water of $10^{-5} \text{ cm}^2/\text{sec}$, an upstream concentration of water of 0.5 g/cc, and zero concentration downstream) is roughly $10^{-3} \text{ gm/sec} \times \text{cm}^2$, or one-seventieth of the electroendosmotic transport rate. It is thus obvious that electrical modulation of water-transport within a charged solid is potentially an extremely powerful tool for water-permeation control.

The direction of electroendosmotic fluid transport is always toward the electrode whose sign-of-charge is the same as that of the solid surface comprising the medium. Thus, by reversing the polarity of the electrodes, one can reverse the flow-direction. This renders it possible not only to greatly accelerate fluid transport in the normal diffusion-direction, but also to block flow virtually completely by "bucking" the electroosmotic flow against the normal diffusive or hydraulic flow. Hence, one can utilize the impressed potential as a precisely controllable "valve" for adjustment of water-transport over wide limits.

As mentioned above, the magnitude of the zeta potential is governed by the surface charge density on the confining pore-walls, and the separation of mobile and fixed charges. The former parameter is determined by the chemical composition of the solid medium (a highly ionic polymeric material being among the most desirable); the latter, by the nature of the counterions and the concentration of extraneous electrolyte in the fluid. For maximum electroendosmotic efficiency, it is important that the concentration of spurious ionic species be kept to a minimum - that is, there should be no extraneous electrolyte within the aqueous phase. The reason for this is simply that extraneous electrolyte not only does not contribute to fluid-drag, but also "screens off" the surface-charge on which the electroendosmotic process depends. Furthermore, extraneous electrolyte contributes to the electrical conductance of the system, thereby increasing the amount of current (and power) required for effective water-transport. Fortunately, by employing an extremely highly charged ionic matrix as the solid medium, Donnan exclusion prevents the intrusion of extraneous electrolyte into the pore fluid, thereby minimizing this undesirable complication.

The classical model of electroendosmosis, as expressed in Equation B-1, is applicable under conditions where the mobile counter-charges on which the impressed potential operates are confined to a layer near the pore-wall which is thin compared to the pore diameter. This, in effect, means that the analysis is applicable only to porous media in which the pore-diameters are of the order of 2000A or greater. In polymeric ion-exchange matrices, which would appear to be choice for the intended application, the "pore" sizes are far smaller than this, and another model must be employed to estimate electroendosmotic flow velocities in such media.

The model employed in this case is that of a three-dimensional, charged molecular network in which ions of opposite charge to those of the network are homogeneously distributed within the interstitial fluid. When a potential gradient is impressed across this system, the ions within the fluid are caused to migrate, carrying with them (by viscous drag) part of the fluid. This is illustrated in Figure B-2.

The ion-flux (ions/cm²sec) through the network is directly proportional to the electric current density, i.e.,

$$v_i C_i Z F = i \quad \text{B-2}$$

where:

$$\begin{aligned} v_i &= \text{mean ion-velocity, cm/sec} \\ C_i &= \text{mean ion-concentration meq/cc} \\ Z &= \text{ion valency} \\ F &= \text{Faraday equivalent, } 96.5 \text{ constants/meq.} \\ i &= \text{current density, amps/cm}^2 \end{aligned}$$

The water-flux through the network is directly proportional to the ion-flux; i.e.,

$$\bar{v}_{\text{OSMOTIC FLUX}} = \eta v_i C_i = \frac{\eta i}{Z F} \quad \text{B-3}$$

where: η = number of molecules of water transported per ion. Hence, the electroendosmotic water flux through the matrix is given by:

$$\bar{v}_{\text{OSMOTIC FLUX}} = \frac{\eta i}{Z F} = \frac{\eta \lambda \Delta E}{Z t F} \quad \text{B-4}$$

where: λ = specific conductance of the matrix, (ohm⁻¹ cm⁻¹), t = film thickness

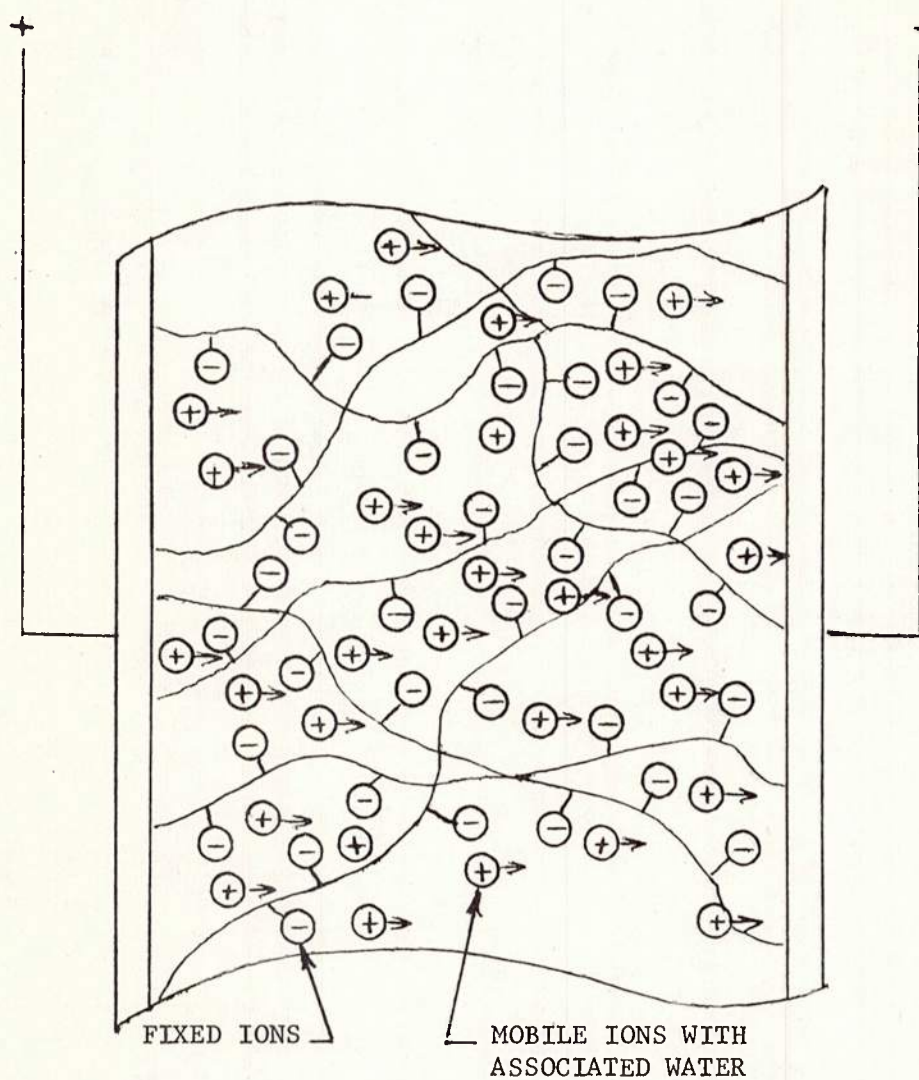


FIGURE B-2. ELECTROENDOSMOTIC TRANSPORT IN A HOMOGENEOUS POLYELECTROLYTE GEL

For a typical ion-exchange resin matrix,

$$C_i = 3 \text{ meq/cc}$$

$$Z = 1.0$$

$$n = 10 \text{ mmol H}_2\text{O/meq} = 0.2 \text{ gm/meq}$$

$$\lambda = 10^{-2} \text{ mho/cm.}$$

Whereupon, for a 2 mil-membrane and 1-volt impressed potential, $0.4 \text{ gm/cm}^2 \times \text{sec}$, or $400 \text{ gm/m}^2 \times \text{sec}$. This is only one half of the flux predicted from the classical electroendosmosis model, but is still 35 times the rate of transport achievable by normal diffusion. It is thus deduced that, even under unfavorable circumstances for water-transport within a charged matrix, substantial water-fluxes can be induced by application of modest potentials across relatively thin membranes.

II CURRENT - AND POWER REQUIREMENTS FOR ELECTROENDOSMOTIC WATER TRANSPORT

According to Equation B-1, the electroendosmotic flow rate is dependent only on the potential gradient across the matrix. The electric current flowing through the matrix, however, is directly proportional to the potential gradient across the matrix, and the matrix-conductance. By way of example, if the specific conductance of the medium is $10^{-3} \text{ ohm}^{-1} \text{ cm}^{-1}$, a one-volt potential across a two-mil film will induce a current of 200 ma/cm^2 ; the corresponding power requirement is 0.2 watts/cm^2 , or (from Equation B-1) roughly 3 watt-seconds per gm of water transported. One kilowatt-hour of electrical energy is thus capable of transmitting $1.2 \times 10^{16} \text{ gm}$ of water - roughly 300 gallons.

Using the model of Equation B-4, a one volt potential impressed across a two-mil film of conductance $10^{-2} \text{ ohm}^{-1} \text{ cm}^{-1}$ will induce a current of 2.0 amps/cm^2 . The corresponding power requirement in this case is 2.0 watts/cm^2 , or 30 watt-seconds/gm of water. One kilowatt-hour of electrical energy will thus transport 120,000 gm, or 30 gallons of water.

Since, for either model, the water-transport rate is proportional to the impressed voltage while the power requirement is proportional to the square of the voltage, it is evident that energy can be conserved by maximizing membrane-area and minimizing voltage to achieve the desired water-transmission level. Similarly, by reducing membrane-thickness, impressed voltage can be reduced without loss in water-transport rate, but with significant power saving.

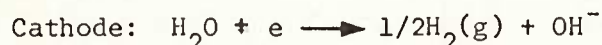
It is informative to estimate, for the two models developed above, the "refrigeration efficiency" of the electroendosmotic system, in terms of calories of thermal energy removed from the system per calories of electrical energy supplied. In the first case, the figure is roughly 700; in the latter, 70. Either figure is very large when compared to, say, thermoelectric refrigeration efficiencies.

III ELECTROCHEMICAL PROCESSES IN ELECTROENDOSMOSIS

The ion-transport process which is essential to electroendosmotic water-transport must in some manner be sustained as long as an electrical potential is applied to the system. This requires that the matrix material be confined between electrodes which will allow (at the upstream boundary of the matrix) the generation of ions from neutral species, and (at the downstream boundary) the discharge of ions and elimination of resulting neutral species. In other words, an electroendosmotic system must also function as an electrochemical cell.

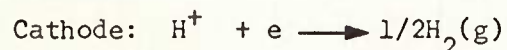
In such a system, the supply of ions may come from either (a) the electrode materials themselves, or (b) the transported fluid. The former alternative is in all likelihood unacceptable for an isolated system, since the process must terminate when one or the other electrode is electrolytically consumed. The latter alternative, is however, both feasible and attractive for the case at hand: that is, one bounds the matrix with noble-metal electrodes, and allows electrolysis of water to supply the necessary ion-carriers. Two possibilities exist:

a. A cationic (positively charged) matrix is employed, and hydroxyl ions serve as the counterions and charge-carriers. In this case, water is transported from cathode to anode, and if noble-metal electrodes are used, the electrode reactions are:



Thus, hydrogen gas is liberated at the upstream electrode, and oxygen and water at the downstream electrode.

b. An anionic (negatively charged) matrix is employed, and hydrogen ions serve as the counterions and charge carriers. In this case, water is transported to the cathode, and the electrode reactions are:



Thus, hydrogen gas is liberated at the downstream electrode, and oxygen at the upstream electrode.

Of these two possibilities, the latter is by far the most attractive: for in this case, hydrogen gas is discharged at the external surface of the barrier, while oxygen is liberated within the enclosure. In this fashion, a significant fraction of the water to be removed from the system is converted into oxygen which is conserved. Another important plus factor in this arrangement is the fact that much thermal energy within the system is discharged to the surroundings in the form of the latent heat of combustion of gaseous hydrogen.

A possible disadvantage of utilizing hydrogen-ions as charge-carriers may lie in the observation that the hydrogen ion possesses high mobility, and may thus be relatively inefficient for transporting water by viscous drag. Whether this potential limitation is likely to offset the numerous advantages attributable to hydrogen ion as a carrier must be determined by experiment.

It should be clearly pointed out that the electroendosmotic flow relations of Equations B-1 and B-4 have been derived on the basis of potential gradients measured within the matrix, and not the potential differences across the bounding electrodes. If the electrode-processes take place reversibly, then the driving potential for electroendosmosis, ΔE , is related to the impressed potential, E by the simple relationship

$$\Delta E = \Delta E_o - \Delta E_e$$

Where ΔE_e is the reversible electrochemical cell-potential for the system. For the electrolysis of water from 3N acid solutions, $\Delta E_e \cong 1.3v$. Thus, to sustain a one-volt drop across the matrix, a potential of 2.3 volts must be impressed across the electrodes. This naturally increases the power-requirements to produce a given water-transport rate, although this excess power is effectively utilized in oxygen generation, and elimination of sensible heat in the form of latent energy in gaseous hydrogen. A schematic sketch of this system is shown in Figure B-3.

It is obvious that, for the most efficient use of electrical energy in this process, it is necessary to select, as electrode-materials, those which permit ion-discharge at potentials as close to the reversible potentials as is possible. This, in effect, requires electrodes with low overvoltages with respect to the particular ionic species to be discharged. Since, unlike primary batteries or fuel cells, the electroendosmotic system must be designed to operate with comparable efficiency irrespective of the direction of the impressed potential, electrode materials must be chosen carefully, with this requirement in mind.

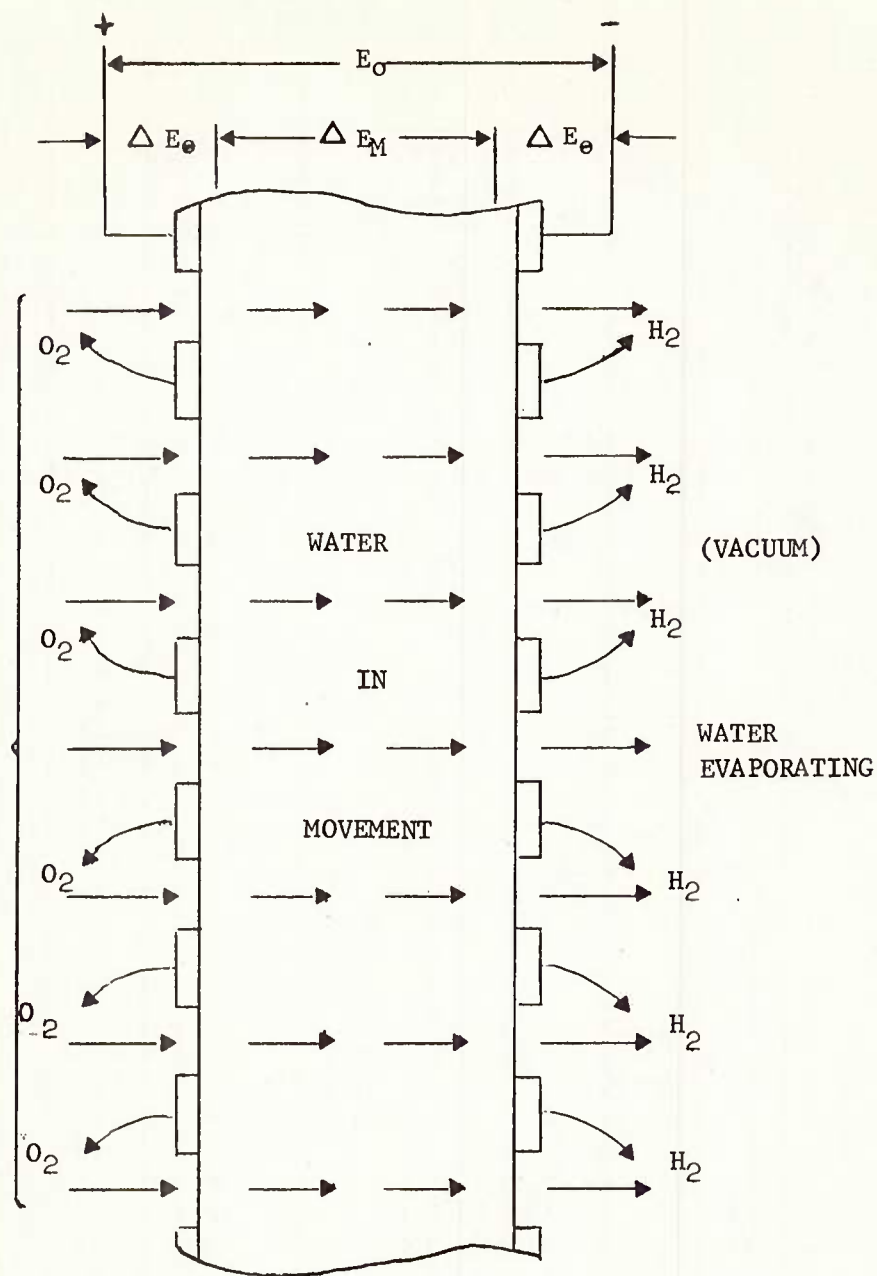


FIGURE B-3. ELECTROENDOSMOSIS WITH ELECTRODE REACTIONS GENERATING H_2 AND O_2

IV DESIGN REQUIREMENTS

For its successful embodiment into an enclosure to be utilized in space, an electrically modulated moisture-loss-control barrier must be built into a system which also possesses the physical, mechanical, and thermal requirements of a barrier to the hostile external environment. Such a barrier must be (for a space suit) flexible, mechanically strong, gas (air)-impermeable, a thermal insulator, and resistant to abrasion and penetration by micro-meteorites or sharp objects. At the same time, the structural components of the barrier must be sufficiently permeable to water vapor that they will not provide such resistance to water-transport as to render the modulating component ineffectual as a control device.

It is evident that a multilayered laminated structure can provide the best balance of properties for this purpose. Strength, coupled with flexibility and toughness, can be imparted by woven fabrics or felts; at the same time, these types of materials possess sufficient porosity and gas-permeability to eliminate their contributing significantly to the overall moisture-transport resistance of the laminate. The external (space-side) of the laminate should, in all likelihood, be composed of a thin sheet of aluminized, open-cell elastomeric foam to provide both low radiative absorptivity, and low thermal conductivity, as well as negligible resistance to water-vapor escape.

The modulating, moisture-transmissive, electrically conductive, gas-impermeable barrier must possess special properties and meet rather rigid requirements. Three alternative structures may be envisioned:

1. A thin, flexible, microporous (mean pore size of ca. 0.1 microns, maximum pore size not greater than 0.5 microns) sheet whose pores are readily water-wettable, and whose pore-surfaces contain ionizable strongly acidic groups. Such a structure might be prepared from a porous vinyl, urethane, or polyolefin film whose internal surfaces have either been chemically sulfonated, or coated with a thin layer of sulfonate-bearing polymer. Such a structure will always operate with its pores completely filled with water, whence air-leakage from inside the enclosure will be confined to diffusive transport in the solution within the pores.

2. The same porous sheet structure of (1), but with the pores filled with a highly hydrated, ionized polymeric gel. Such a composition will minimize the possibility of air-leakage through occasionally gas-filled pores, and may allow the use of a porous matrix with less rigidly controlled pore-size and pore-size distribution.

3. A thin, homogeneous, polyelectrolyte (ion-exchange) film which is tough and flexible over wide ranges in moisture-content, and can be readily adhered to other laminate components without significant interference with its moisture-transmissivity.

Any one of these three structures would then be coated on both sides with suitable electrode-metal, in an extremely thin, porous layer. Such coatings (e.g., of gold, platinum, palladium) could be deposited by vacuum-or electroless chemical plating techniques. The resulting metallized film would then be laminated between and bonded to the structural membranes. A schematic view of the final laminate is shown in Figure B-4.

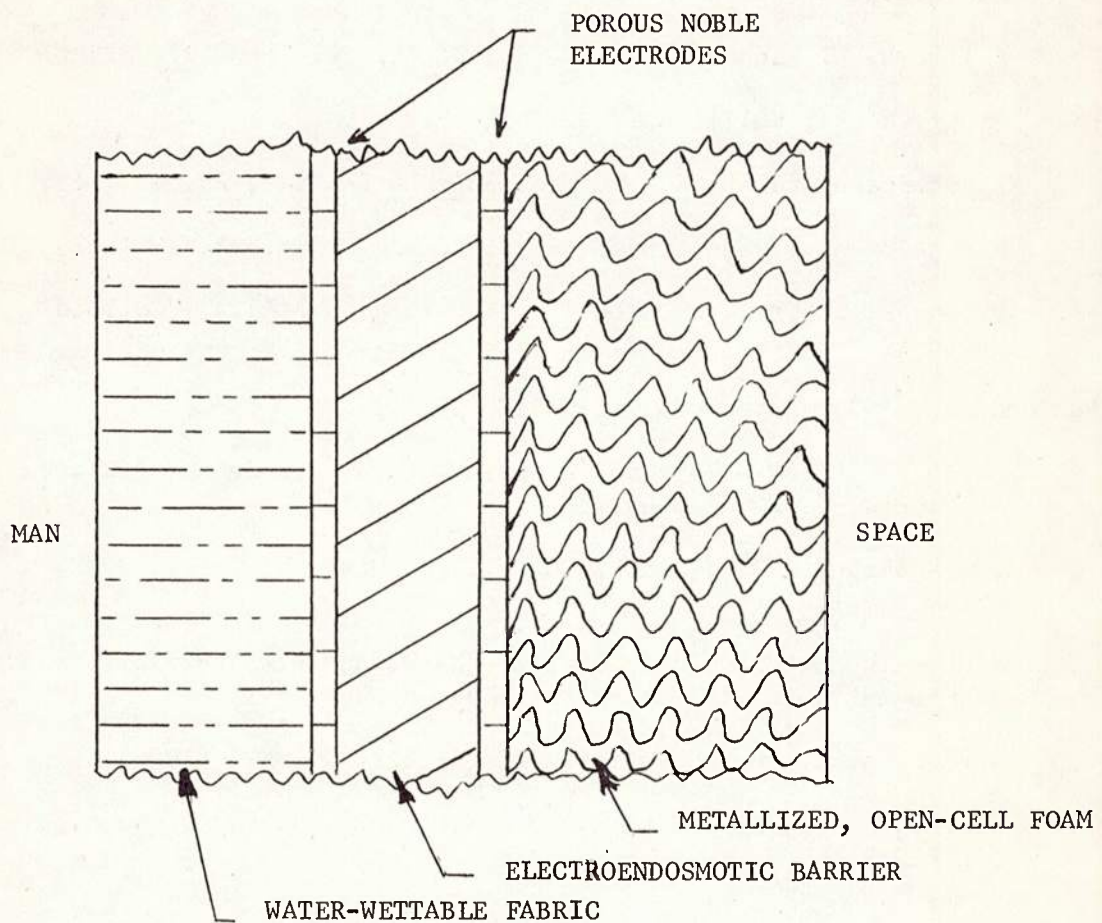


FIGURE B-4. SCHEMATIC CROSS SECTION OF IDEALIZED LAMINATE

V BIBLIOGRAPHY

- B-1. Freundlich, H. and Rona, P., Sitz-ber preuss Akad. Wiss. Physik math. klasse 20, 397 (1920).
- B-2. Helmholtz, H., Wied. Ann. 7, 337 (1879).
- B-3. Hellmuth, E., and Mueller, F. H., Z. Physik. Chem. 37, 328 (1963).
- B-4. Kruyt, H. R., Kolloid-Z., 22, 81 (1918).
- B-5. Lakshminaraganaiah, N., Current Science (India), 28, 321 (1959).
- B-6. Michaels, A. S. and Lin, C. S., Ind. Eng. Chem. 47, 1249 (1955).
- B-7. Overbeek, J. ThG., Chapter V in Kruyt, H. R. (Ed.), "Colloid Science," Vol. I, p. 195, Elsevier Publ., Amsterdam, 1952.
- B-8. Quincke, G., Pogg. Ann. 113, 513 (1861).
- B-9. Reuss, F. F., Memoires de la Societe Imperiale de Naturalistes de Moscow, 2, 327 (1809).
- B-10. Tombalakian, A. S., Burton, H. J., and Graydon, W. F., J. Phys. Chem. 66, 1006 (1962).
- B-11. von Smolnchowski, M., in Graetz, "Handbuch der Electrizaritat und des Magnetismus II," Leipzig (1914); p. 366.
- B-12. Wiedemann, G., Pogg. Ann. 87, 321 (1852); 99, 177 (1856).
- B-13. Winger, A. G., Ferguson, R., and Kunin, R., J. Phys. Chem. 60, 556 (1956).

APPENDIX C

EVALUATION OF "IOPLEX" FOR IONICALLY

MODULATED DIFFUSION

CONTENTS

	<u>PAGE</u>
I <u>BACKGROUND</u>	50
II <u>EXPERIMENTAL</u>	50
A. Adhesive Dope Preparation	50
B. Laminate Preparation	51
C. Unsupported Polyurethane - Adhesive Films	51
D. MVTR Measurements at Atmospheric Pressure	51
E. Oxygen and Water Vapor Transmission Measurements under High Vacuum	53
III <u>RESULTS</u>	53
IV <u>DISCUSSION</u>	57
A. Properties of the Unmodified Adhesive - Barrier Layer	57
B. Increased MVTR of Ioplex-Loaded Polyurethanes	62
C. Moisture and Oxygen Permeabilities of Laminate Structures	63
V <u>CONCLUSIONS</u>	67
VI <u>REFERENCES</u>	69
Information Sheets for Ioplex	70

LIST OF FIGURES

<u>FIGURE</u>		<u>PAGE</u>
C-1	MEASUREMENT OF MOISTURE VAPOR TRANSMISSION RATES AT ATMOSPHERIC PRESSURE	52
C-2	VACUUM PERMEAMETER	54
C-3	MOISTURE VAPOR PERMEANCE OF UNSUPPORTED POLYURETHANE COMPOSITES	56
C-4	MOISTURE VAPOR TRANSMISSION RATES IN LAMINATES MEASURED AT ATMOSPHERIC PRESSURE	59
C-5	MVT OF "IOPLEX"/PLASTIC COMPOSITES	74

LIST OF TABLES

<u>TABLE</u>		
C-1	MOISTURE VAPOR PERMEANCE FOR POLYURETHANE- ADHESIVE FILMS CONTAINING VARYING AMOUNTS OF IOPLEX	55
C-2	ATMOSPHERIC PRESSURE MOISTURE VAPOR TRANSMISSION RATES FOR CLOTH/ADHESIVE/IOPLEX/FOAM-NYLON LAMINATES	58
C-3	VACUUM PERMEAMETER RESULTS FOR OXYGEN AND WATER VAPOR TRANSPORT	60
C-4	COMPARISON OF LAMINATE AND UNSUPPORTED FILM RESULTS	66
C-5	MVT OF "IOPLEX"/PLASTIC COMPOSITES	

I BACKGROUND

Amicon has prepared samples of Ioplex-filled composites to be evaluated as improved (higher MVTR) barriers for pervaporative cooling of space suits. A multilayer suit wall containing an interior reinforcing and moisture sorbing fabric layer and an external thermally insulating foam layer is currently under investigation for use in the Apollo space suit. It was proposed that Amicon fabricate a series of Ioplex filled resins which could serve the dual function of barrier and adhesive layer between the fabric and foam. Because of their excellent adhesive properties, high tear and abrasion resistance and inherently high MVTR compared to most polymers, polyurethane elastomers were to be evaluated as the matrix polymer for the adhesive layer.

To demonstrate that controlled moisture permeability could be imparted to a composite, MVTR as a function of Ioplex loading in the adhesive was to be determined. MVTR measurements on the composites were to be made at 35°C and atmospheric pressure under the driving force obtained with 100% relative humidity (R.H.) on one side of the composite and 50% R.H. on the other. To demonstrate the negligible effect of Ioplex loading on the gas transport through the adhesive layer, oxygen permeabilities of the composites were to be determined in a manometric, high vacuum permeameter with 10 psia oxygen pressure upstream of the laminate and 10^{-6} to 10^{-2} mm Hg pressure downstream. To better simulate moisture transport under pervaporation conditions in space, MVTR data were also to be obtained in the high vacuum permeameter.

II EXPERIMENTAL

A. Adhesive Dope Preparation

Two polyester-type polyurethane elastomers were employed in adhesive formulations. These were the thermoplastic, solvent soluble Estanes 5740 and 5703*. The former is a high molecular weight, tough rubber and the latter is a lower molecular weight, tacky gum. Combinations of the two polymers in the weight ratios of 65/35 and 75/25 (5703/5740) were used to give the desired toughness and tack. While both formulations gave adhesive layers with acceptable properties as far as could be determined by visual inspection, the former was somewhat tougher and the latter a somewhat better adhesive. These elastomers were dissolved in a mixture of solvents (94 parts tetrahydrofuran, 4 parts dioxane) to give a dope containing about 20% total solids. Dioxane was used in the mixture to control (reduce) the rate of solvent evaporation from the adhesive.

*Tradename of B.F. Goodrich

For formulations containing Ioplex, the powder was blended into the above dope in a blender. Depending on the Ioplex loading, varying amounts of the mixed solvent were added to maintain the desired viscosity in the final dope formulation.

B. Laminate Preparation

The dope prepared above was cast onto a Teflon-coated fabric to give a layer of adhesive which after drying would be about 1.5 mils thick. Solvent was allowed to evaporate at room temperature until the dope was quite viscous and tacky. Cotton fabric and a urethane foam-nylon fabric laminate (foam side down) were placed side by side on the tacky adhesive and the sandwich of fabrics and adhesive was stripped from the Teflon-coated supporting sheet. A completed laminate was obtained by folding the assembly so that the adhesive was pressed together. This procedure gave a structure consisting of cotton fabric/adhesive/urethane foam-nylon fabric. This procedure evolved when it was found that the adhesive could not be coated directly onto the foam or fabric because of excessive penetration into these porous substrates.

C. Unsupported Polyurethane-Adhesive Films

To determine the influence of the laminate structure on MVTR, Ioplex-filled and unfilled samples of unsupported polyurethane-adhesive film were studied. These were prepared by casting the adhesive dope discussed in Section A above onto the Teflon-coated glass and allowing the solvent to evaporate.

D. MVTR Measurements at Atmospheric Pressure

Moisture vapor transmission rates were measured using the cup method described in ASTM E-96-63T. Figure C-1 is a sketch of the cup configuration and the manner of laminate mounting. The exposed laminate area is 11.3 cm². As can be seen from this figure, the measurements have been made at 35°C with a driving force of 100% to 50% R.H. Transmission rates were determined by periodically weighing the cup and computing the weight loss per unit time per unit area. MVTR data are reported in the units of gms/100 in² 24 hrs. While the barrier adhesive layer as cast was 3-mils thick, it will be shown later that the effective thickness of the barrier is less than this, so no attempt was made to normalize the MVTR data for the laminates with respect to thickness when reporting it in the Results Section. For the unsupported film the results were normalized and reported as moisture vapor permeance (MVP) in gm-mils/100 in² 24 hrs.

With the high MVTR materials such as those under investigation, there is a possibility that diffusion of water vapor to or away from

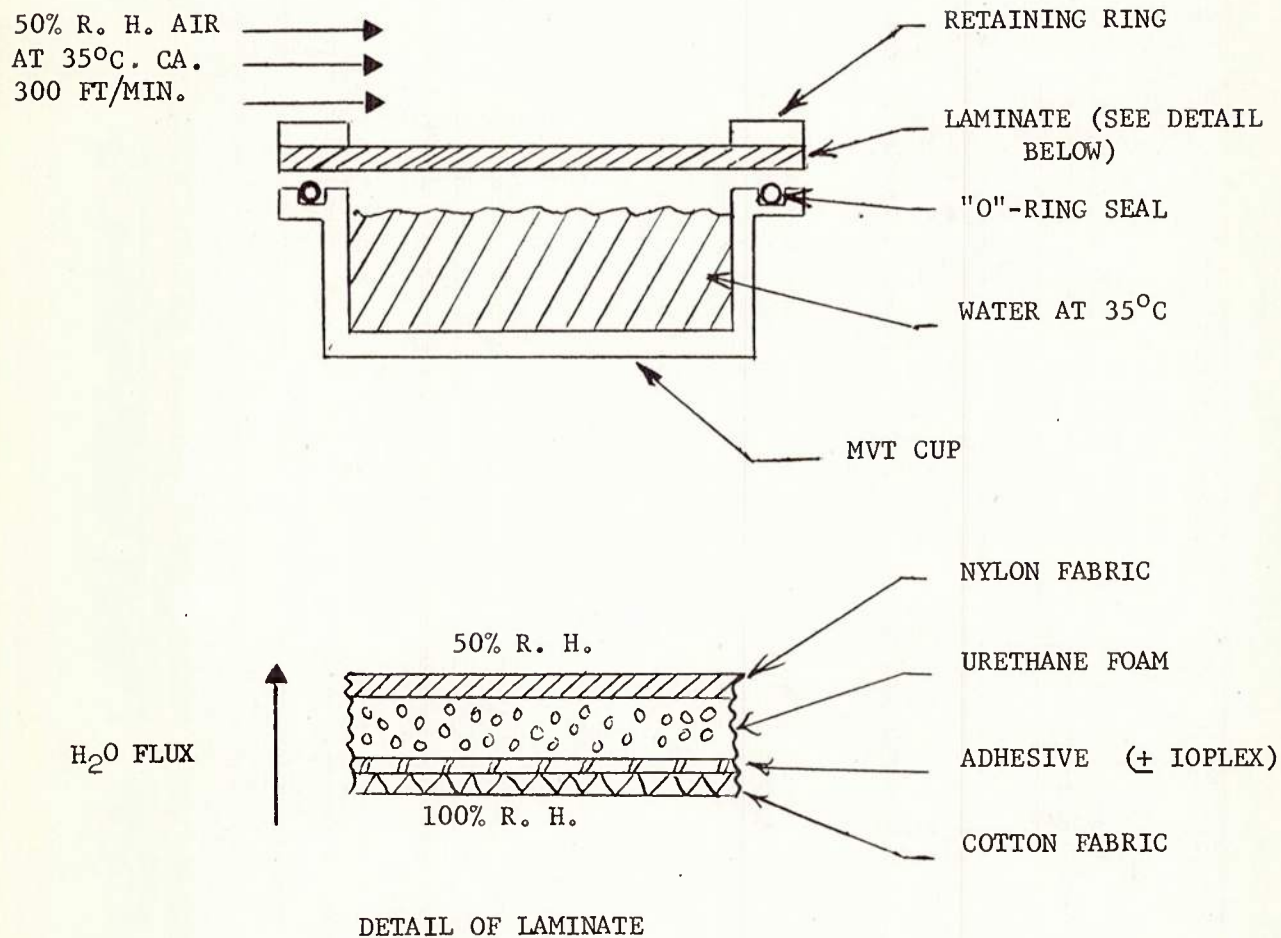


FIGURE C-1. MEASUREMENT OF MOISTURE VAPOR TRANSMISSION
RATES AT ATMOSPHERIC PRESSURE

the sample could control the weight loss from the cup. Evaporation rates on a cup containing no sample indicate MVTR's as high as 1000 gms/100 in²-24 hrs. can be reliably measured under the above humidity driving force.

E. Oxygen and Water Vapor Transmission Measurements Under High Vacuum

Figure C-2 is a sketch of the vacuum permeameter used for this study. The laminate was mounted in the permeability cell using Silastic RTV as a gasketing and sealing material. This sealing procedure was found to be necessary because of the porous nature of the laminate. The temperature of the cell and laminate were controlled by immersing the cell in a constant temperature bath. The exposed laminate area when mounted in the cell was 31.7 cm².

At the start of a measurement the system was evacuated to 10⁻⁵ mm Hg. For the determination of oxygen transmission rates, the gas was introduced to the upstream side of the laminate at a pressure of 10 psia. The pressure in the initially evacuated portion of the system downstream of the laminate was monitored in the range of 1 to 500 μ Hg on a recording Decker differential pressure sensor. From a plot of downstream pressure versus time the oxygen transmission rate was determined, knowing the downstream volume of the system and applying the perfect gas law. The data are reported as permeability constants with the units cc(STP)-cm/cm²-sec-atm. With oxygen, the adhesive barrier layer is the sole gas transmission rate controlling portion of the laminate, and therefore the permeability was normalized with respect to barrier (adhesive) thickness.

For moisture transmission measurements the same equipment was used with a modified operating procedure. The calibrated sample tube in Figure C-2 was filled with water. This tube and the cell containing the laminate were immersed in a constant temperature bath to saturate the upstream portion of the system with water vapor at the laminate temperature. The system downstream of the laminate was attached to a vacuum train which maintained the pressure in this part of the system less than 10⁻⁴ mm Hg while water vapor was permeating the laminate. The MVTR was determined by monitoring the drop in water level in the calibrated sample tube as a function of time.

III RESULTS

Table C-1 shows the MVP results for unsupported polyurethane-adhesive films as a function of Ioplex loading when the measurements were made at atmospheric pressure under a driving force of 100% to 50% relative humidity. These results are shown graphically in Figure C-3. Similar results on the complete laminate structures, except

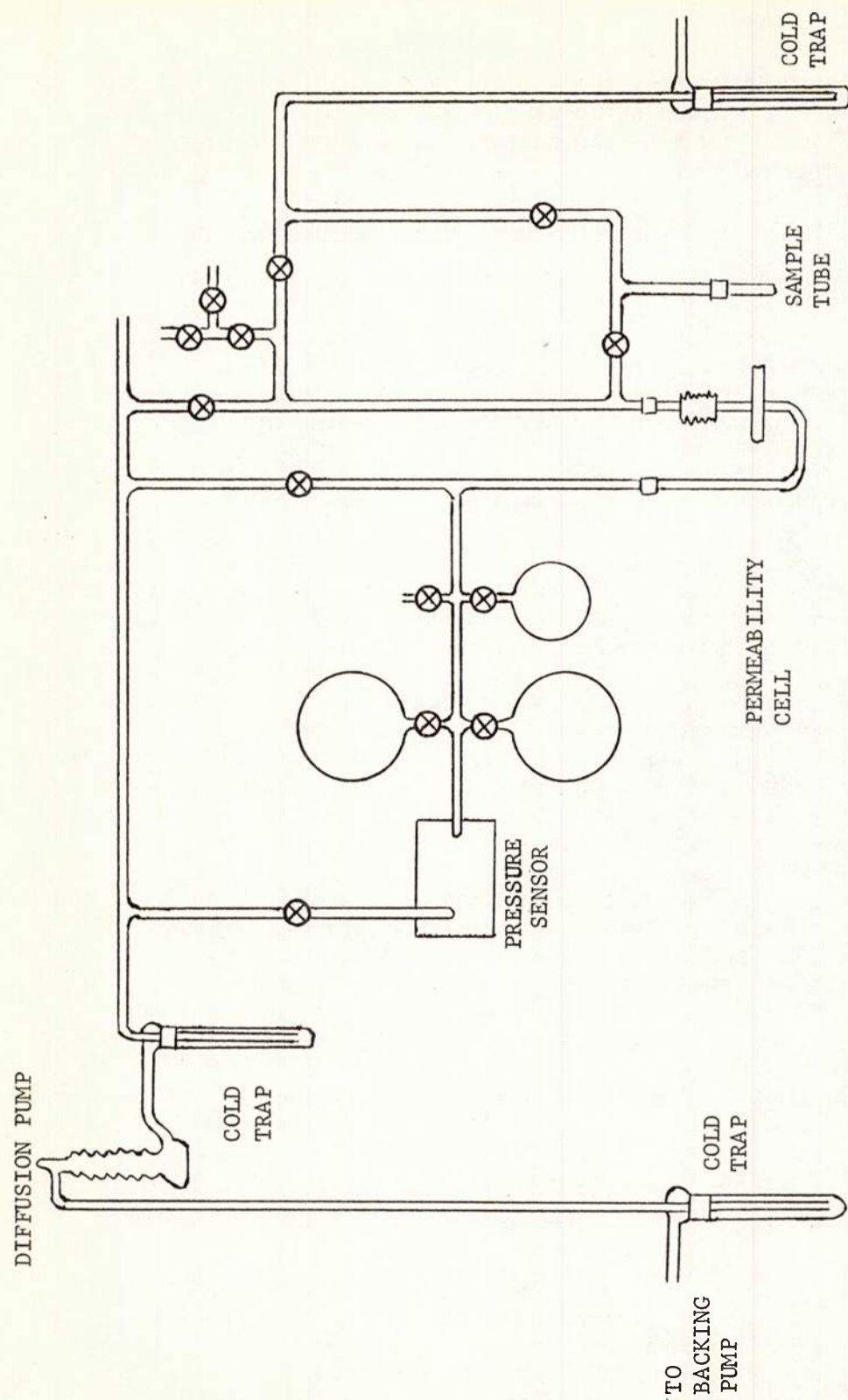


FIGURE C-2. VACUUM PERMEAMETER

TABLE C-1

MOISTURE VAPOR PERMEANCE FOR POLYURETHANE-ADHESIVE
FILMS CONTAINING VARYING AMOUNTS OF IOPLEX

A. Adhesive System: 75/25 Estane 5703/5740

Ioplex Content (Wt. %) MVP (gm-mil/100 in²-24 hrs)*

0	47
20	108
30	228
40	400

B. Adhesive System: 65/35 Estane 5703/5740

Ioplex Content (Wt. %) MVP (gm-mil/100 in²-24 hrs)

0	53
20	164
30	266
40	416

*Driving Force: 100% R.H. 50% R.H.

Total pressure: atmospheric

Temperature: 35°C

Original film thickness: ca. 1.5 mils

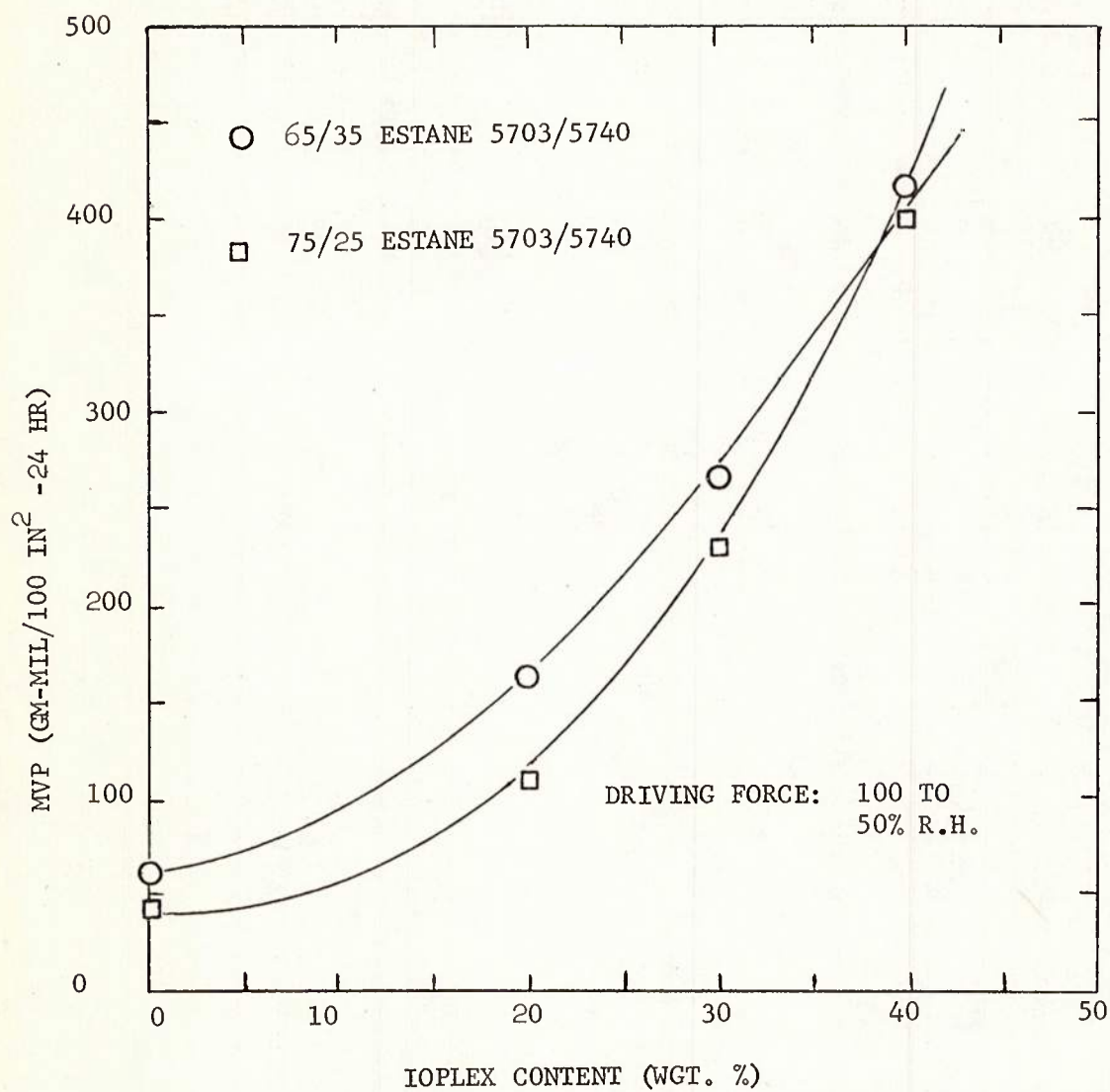


FIGURE C-3. MOISTURE VAPOR PERMEANCE OF UNSUPPORTED POLYURETHANE COMPOSITES

those reported as unnormalized MVTR are shown in Table C-2 and Figure C-4. Table C-3 shows the oxygen permeabilities and MVTR's of unsupported films and laminates obtained with the vacuum permeameter.

IV DISCUSSION

A. Properties of the Unmodified Adhesive-Barrier Layer

A thermoplastic-polyurethane was chosen as the base resin to be employed in the barrier-adhesive layer of the suit wall laminate because of the high MVTR, relatively low air permeability and toughness of this type of elastomer. The results in Tables C-1, C-2 and C-3 attest to the soundness of this choice as far as the permeability criteria are concerned. The oxygen permeability constant of the film without Ioplex given in Table C-3 is about one-twentieth the value reported for natural rubber and is comparable to that for butyl rubber, an elastomer noted for its low gas permeability. The MVP data recorded in Tables C-1 and C-3 for the unmodified adhesive films are very high and exceeded only in polymers such as plasticized ethyl cellulose and cellulose triacetate. These findings agree with the limited permeability data reported elsewhere for urethane elastomers (C-7).

The specific adhesive formulated from the two Estanes does not have a pronounced effect on the MVTR as seen from the data in Tables C-1 and C-2. This is not surprising, since the main difference between Estane 5703 and 5740 is molecular weight, a property which does not markedly affect permeability after a rather low minimum value is exceeded. The ratio of MVP to oxygen permeability in the above polyurethanes is about 10,000 when expressed as a dimensionless ratio of permeability constants (flux rate through the polymer per unit of pressure gradient across the polymer) and when moisture and oxygen permeabilities have been independently determined. In the present space unit application this ratio must be high when simultaneous moisture and oxygen transport is taking place. The ratio noted for the polyurethanes is indeed very high. For example, the ratio is less than 25 in most elastomers and it is exceeded or matched only by highly polar polymers which undergo extensive swelling in water. However, besides being weakened appreciably by swelling, the ratio of simultaneous moisture to oxygen permeability in such polymers is usually dramatically reduced. This is due to the strong plasticizing effect of water on the polymer which markedly increases the diffusivity of oxygen over the value determined in the dry polymer. It is expected, however, that the moisture permselectivity of polyurethanes remains very high even when water and oxygen transport are taking place simultaneously, and, therefore, should be suitable as the barrier-adhesive in the present application.

TABLE C-2

ATMOSPHERIC PRESSURE MOISTURE VAPOR TRANSMISSION

RATES FOR CLOTH/ADHESIVE

IOPLEX/FOAM-NYLON LAMINATES

<u>Adhesive System</u>	<u>Ioplex (Wt. %)</u>	<u>MVTR (gm/100 in²-24 hrs)*</u>
None	0	143
75/25 Estane 5703-5740	0	54
"	20	72
"	30	88
"	40	92
65/35	0	54
"	20	77
"	30	99
"	40	109

*Driving Force: 100% R.H. 50% R.H.
Laminate thickness: ca. 100 mils
Total Pressure: atmospheric
Temperature: 35°C

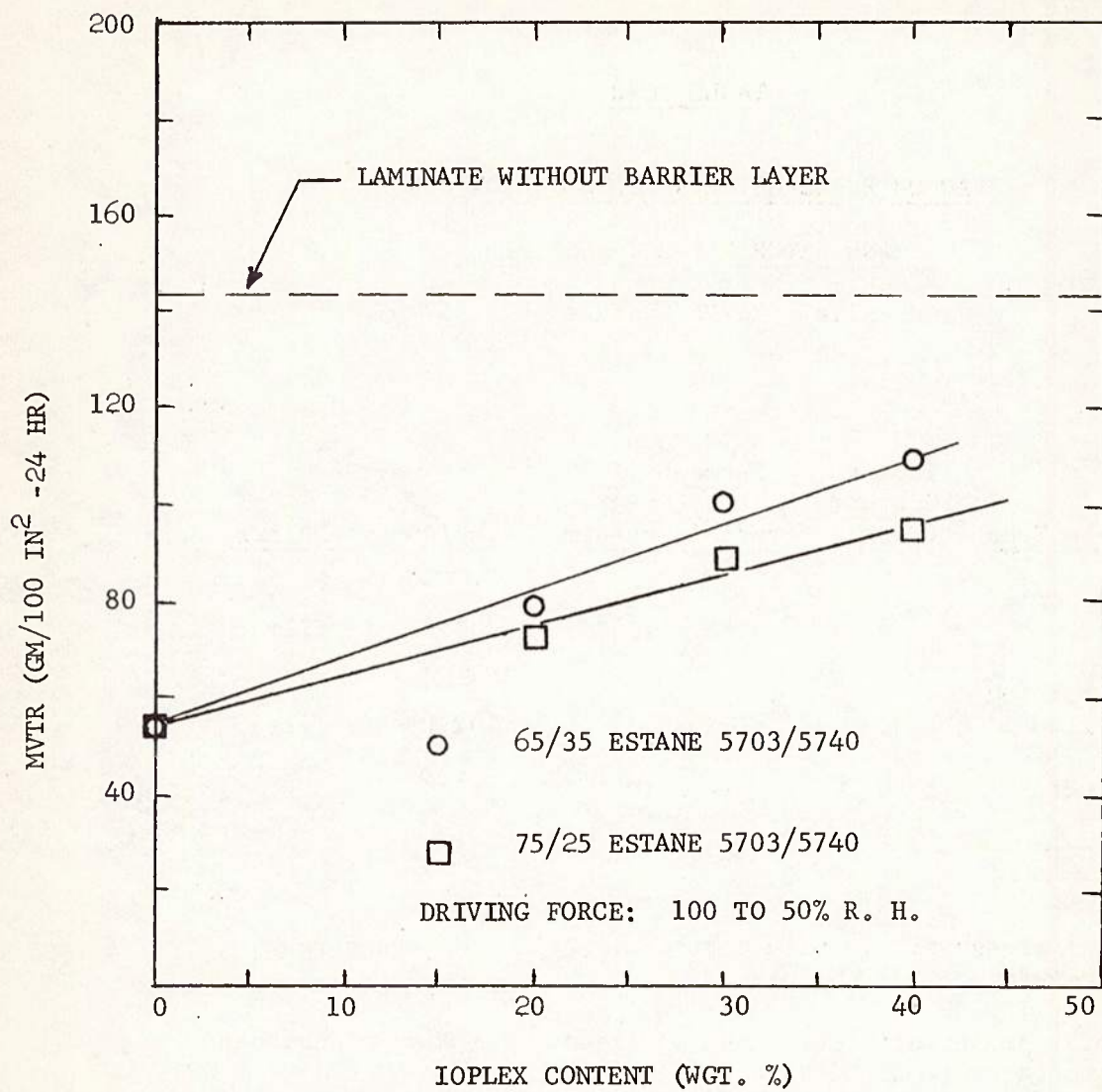


FIGURE C-4. MOISTURE VAPOR TRANSMISSION RATES IN LAMINATES MEASURED AT ATMOSPHERIC PRESSURE

TABLE C-3

VACUUM PERMEAMETER RESULTS FOR OXYGEN
AND WATER VAPOR TRANSPORT

Adhesive: 75/25 Estane 5703-5740

<u>Sample Type</u>	<u>Ioplex Content (Wt. %)</u>	<u>Oxygen Permeability* (cc (STP) - cm/cm²-sec-atm</u>	<u>MVTR** (gm/100 in²-24 hrs)</u>
Unsupported film	0	1.5×10^{-8}	40 (1-mil film)
Unsupported film	20	1.1×10^{-8}	102 (1-mil film)
Laminate	0	1.4×10^{-8}	65
Laminate	20	ca. 10^{-8}	97

*Total pressure: 10 psia upstream; 0.01 mmHg downstream
 Temperature: 23°C

**Total pressure: ca .42mmHg upstream; 0.1 mmHg downstream
 Temperature: 35°C

MVTR for unsupported film reported on 1-mil basis and therefore
 is equivalent to MVP

Polyurethanes are prepared by reacting di-isocyanates with relatively high molecular weight polyether and polyester prepolymers. The isocyanate reactions lead to highly polar urethane and related linkages; however, the prepolymers contain linkages which are considerably less polar. This leads to a matrix which on a micro-scale is heterogeneous with respect to polarity. When brought into contact with water, the regions which are rich in urethane linkages would like to imbibe moisture, but the adjoining regions which are rich in prepolymer and lower in polarity restrain the polymer from swelling extensively. If the polymer is not swollen appreciably by water, the oxygen permeability should be comparable to that of the dry polymer. However, if the polyurethanes are not swollen appreciably by water, why do they exhibit such high moisture permeabilities? The answer to this seems to lie in a recently proposed model for moisture transport in moderately polar polymers (C-5). In this model which has undergone considerable refinement since its original inception (C-3, C-4), water is envisioned to move through the polymer by a highly ordered diffusion process involving hydrogen bonding with polar groups on the polymer chain in much the same way self diffusion in water takes place. This model is akin to that proposed in the Introduction for moisture transport through Ioplex. Accordingly, a polymer such as a polyurethane can support rapid "alignment-type" diffusion of water without having to be so highly polar that the polymer swells extensively and loses its permselectivity.

In spite of the fact that the polyester-polyurethanes used here did not swell appreciably when brought into contact with water, the water permeability constant was found to be slightly dependent on the humidity driving force for water transport. If the permeation process were ideal (C-6), MVP would be directly proportional to the humidity driving force across the film, but, as can be seen from the first entries in Tables C-1 and C-3, this is not the case. The MVP for R.H. equal to 50% is about the same as the MVP for R.H. equal to 100%. This is a common occurrence in systems where there is a specific interaction such as hydrogen bonding between the polymer and the permeating species. It is a reflection of a higher average diffusivity for water in a polymer in which moisture is in contact with both sides of the barrier, and thus the average moisture activity within the film is higher than in the case where one side of the film is maintained essentially free of moisture due to being in contact with a vacuum. The practical implication of this finding is that candidate materials for the present application must be evaluated under simulated space conditions or misleading results will be obtained. This consideration takes on added significance later when the data for the laminates are discussed.

All things considered, it would still appear that polyurethane elastomer is a very good choice for the adhesive matrix in the present

study. It is nonetheless clear that a marked increase in this permeability is required to obtain a satisfactory barrier for pervaporative cooling of a space suit. Incorporation of Ioplex into the barrier will be shown to markedly improve its moisture vapor permeability, but there are also modifications to the base polyurethane that can be made to further improve it as a barrier matrix material. For instance, certain polyether-based polyurethanes are more moisture permeable than the polyester-based polymers used in this study. Values of MVP as high as 100 gm-mil/100 in²-24 hrs. for a driving force of 100 to 0% R.H. have been reported for such resins (C-7). Further optimization is no doubt possible. A reduction in the pre-polymer chain length would also increase the MVP, although a balance must be made between this and excessive swelling and loss of strength in contact with moisture. In all likelihood a polymer could be formulated with an MVP significantly in excess of the value of 100 quoted above which would still be relatively impermeable to oxygen.

Before moving on to the work on the Ioplex filled composites, a comment should be made concerning the absolute magnitude of the oxygen permeability of the polyurethane elastomers. In spite of the fact that 10^{-8} cc(STP cm/cm²-sec-atm) is a relatively low permeability for an amorphous elastomeric polymer, it still would permit a loss of about 0.3 lbs. of oxygen/hr from a space suit in which the barrier area was 20 ft², the thickness was 1-mil, and the oxygen pressure drop across the suit wall was 10 psia. This is not an inconsequential "leak" from the suit.

B. Increased MVTR of Ioplex-loaded Polyurethanes

Incorporation of powdered Ioplex into the polyurethanes adhesive formulations yields composites of markedly increased MVP or MVTR as seen from the data in Tables C-1 and C-3. The data in Table C-1 are plotted in Figure C-3 and here it can be seen that the MVP increases rapidly with increasing Ioplex loading.

An indication of the effectiveness of Ioplex in this role is obtained from the following considerations. The MVP of Ioplex is approximately 5000 gm-mil/100 in²-24 hrs. for a driving force of 100 to 0% R.H. If Ioplex powder were incorporated in the composite as discrete spherical particles which were small relative to the composite thickness, the water flux, J , through the composite would be given by

$$J = [v_I/\bar{P}_I + v_u/\bar{P}_u]^{-1} \cdot \Delta p/L \quad C-1$$

where V is volume fraction, \bar{P} is the moisture permeability constant, $\Delta p/L$ is the moisture vapor pressure gradient across the composite and the subscripts I and u refer to the Ioplex and polyurethane phases, respectively. In this model it has been assumed for simplicity that water permeation through both Ioplex and polyurethane is an ideal process characterized by a constant diffusivity in each phase. Furthermore, random distribution of the dispersed Ioplex phase has been assumed. Since Ioplex is considerably more permeable to water than is polyurethane, Equation C-1 reduces to the simple relationship that the MVP of the composite is equal to the MVP of the base polyurethane divided by the volume fraction of polyurethane in the composite. Thus 20% Ioplex should increase the MVP of the composite by 20%. The observed increase is over a factor of two indicating, as noted earlier, that the Ioplex phase is composed of highly anisometric particles and not spheres, and as such is very effective in increasing the MVP of a composite.

Since completing the experimental work on this project, techniques have been perfected which give a sixfold increase in permeability to a PVC composite loaded with 15% Ioplex. This represents a considerable improvement over the already encouraging results reported here and takes on added significance when taken in the light of the results in Table C-1 and the MVTR requirements for pervaporative cooling previously cited. At a 40% loading of Ioplex (at which point the parent properties of the polyurethane begin to suffer significantly), the MVP of the unsupported film is within about a factor of two to three of that required for space suit cooling. It seems probable that the new and improved dispersion techniques could yield unsupported composites with the necessary MVP of about 1000 gm-mil/100 in²-24 hrs. at an Ioplex loading of less than 40%.

Of course, the above encouraging results would be of little value if they had been obtained at the sacrifice of a greatly elevated oxygen permeability. The results in Table C-3 indicate that this is not the case, however. The film containing 20% Ioplex was, if anything, less permeable to oxygen than that containing no Ioplex. It must be emphasized that these results were obtained for oxygen transport alone and not with simultaneous oxygen and moisture transport. Ioplex, however, does not swell appreciably in water. It will be recalled that its high MVP is the result of a special "alignment-type" diffusion of water through the polymer and is not due to excessive water plasticization of the matrix. It would, therefore, not be expected to markedly increase the oxygen permeability of the composites. Industry will soon be in a position to make oxygen transport measurements in the presence of moisture and the above point could be confirmed when further work is merited.

C. Moisture and Oxygen Permeabilities of Laminate Structures

Results for the laminates prepared from fabric, foam and polyurethane adhesive (with and without Ioplex) are shown in Tables C-2

and C-3, and Figure C-4. It can be seen from these data that the qualitative conclusions are similar to those already made. Loading Ioplex into the adhesive layer increased the MVTR without increasing the oxygen permeability. At first glance, however, it appears as if the barrier is less permeable in the laminate than it is as an unsupported film. The increase in MVTR with Ioplex loading, as shown in Figure C-4, is not as marked as the results in Figure C-3 indicated. The reason for this behavior became clear when the total resistance to water transport through the laminate is analyzed as several resistances operating in series.

The MVTR for the cloth and foam structure containing no barrier-adhesive layer has been measured and found to offer significant resistance to moisture transport (see Table C-2). The moisture permeability of the laminating porous materials is only about three times that of the adhesive layer when the latter contain no Ioplex. In spite of the fact that these materials are composed of inter-connected macroscopic pores, the stagnant air in these pores, their tortuosity and the restricted area available for flow all contribute to the observed resistance to moisture transport. While the apparent MVTR of the fabrics and foams is somewhat higher than any of the other reported data, it should be recalled that it does not exceed the capabilities of the measuring device.

The MVTR for the barrierless laminate can be combined with the data for the laminate containing the adhesive layer in order to estimate the thickness of the adhesive layer in the finished laminate. This type of calculation will provide an internal check on the consistency of the data and the ability to relate the performance of the unsupported films to the performance of the adhesive layer in the laminate.

If for simplicity it can again be assumed that the permeation process through the laminate is ideal and consists of two series resistances, the following relationship applies:

$$\frac{1}{[\text{MVTR}] \text{ complete laminate}} = \frac{1}{[\text{MVTR}] \text{ barrierless laminate}} + \frac{1}{[\text{MVTR}] \text{ barrier C-2}}$$

provided all measurements are made under the same condition of driving force and temperature. Furthermore,

$$\frac{1}{[\text{MVTR}] \text{ barrier}} = \frac{1_{\text{app}}}{[\text{MVP}] \text{ unsupported film}} \quad \text{C-3}$$

where l_{app} is the apparent thickness of the barrier layer in the finished laminate. Again the MVP for the unsupported film must be obtained under the same conditions as the MVTR data for the laminate.

The apparent thicknesses of the barrier layer shown in Table C-4 seem entirely reasonable. Although the equivalent of 3 mils of adhesive material was employed, some of the adhesive solution undoubtedly wicked into the fabrics and reduced the effective thickness of the final barrier. The slight increase in thickness with increasing Ioplex content is probably a reflection of the increased viscosity of the filled system which reduced the above tendency for wicking.

Similar conclusions concerning the barrier laminate thickness are obtained from analysis of the vacuum permeameter results in Table C-3. In this case, however, the resistance of the fabric and foam in the laminate can be neglected, since most of this portion of the structure was in contact with a high vacuum during measurement. Under these conditions the pores are no longer filled with stagnant air. The limiting case would occur when moisture transport takes place through the fabric and foam by so-called Knudsen diffusion (C-1). The ratio of the permeability of a porous fabric in which Knudsen diffusion of water vapor is taking place to the permeability of the same fabric in which diffusion of water vapor is taking place through stagnant air is given approximately by:

$$\bar{P}_k/P_D = 1.5 \times 10^4 d_e \sqrt{T/M}/D_{12} \quad C-4$$

where d_e is the pore size in the fabric (cm), T is the absolute temperature ($^{\circ}K$), M is the molecular weight of the permeating gas and D_{12} is the diffusion constant of water vapor in stagnant air (ca. $0.2 \text{ cm}^2/\text{sec}$ at atmospheric conditions). Even if the pores in the fabric are only 1μ in diameter, this ratio is approximately 10, indicating a negligible resistance offered by the fabric compared to the barrier-adhesive layer.

From the data in Table C-3 the estimated barrier thickness is, therefore, about 0.6 mils for the unfilled adhesive and about 1 mil for the sample containing 20% Ioplex, which agree with the values presented in Table C-4.

The importance of the resistance to moisture transport offered by macroscopically porous materials when the measurements are made at atmospheric pressure and the reduction or elimination of this resistance when measurements are made under vacuum conditions as indicated by Equation C-4 cannot be overemphasized. This indicates that even if a moisture driving force of 100 to 0% R.H. were used in the ASTM cup test, a discouragingly low MVTR could be obtained for a laminate which under

TABLE C-4

COMPARISON OF LAMINATE AND UNSUPPORTED FILM RESULTS

A. Adhesive System: 75/25 Estane 5703/5740

<u>Ioplex Content</u> <u>(Wt. %)</u>	<u>(MVTR)* Barrier, Cal'd.</u> <u>(gm/100 in²/24 hrs)</u>	<u>l_{app}**</u> <u>(mil)</u>
0	87	0.5
20	145	0.8
30	227	1.0
40	238	1.7

B. Adhesive System: 65/35 Estane 5703/5740

<u>Ioplex Content</u> <u>(Wt. %)</u>	<u>(MVTR) Barrier, Calc.</u> <u>(gm/100 in²/24 hrs)</u>	<u>l_{app}</u> <u>(mil)</u>
0	90	0.6
20	167	1.0
30	310	0.9
40	460	1.1

*MVTR for adhesive barrier layer calculated from data in Table C-2 and Equation C-4

**Apparent thickness of barrier adhesive layer obtained by dividing the MVP of an unsupported film of the same composition by (MVTR) barrier, calculated. See Equation C-2

simulated space conditions would be entirely satisfactory for pervaporative cooling. In fact, it is to be expected that vacuum permeameter measurement of the MVTR of the laminates containing 30 and 40% Ioplex in the adhesive layer would be comparable to the encouraging values shown in Table C-1.

This consideration is also important in designing a laminate structure, since it shows that as little porous supporting and insulating material as possible should be located on the high pressure side of the laminate and the bulk of it should, if possible, appear on the vacuum side. In addition, the pores in these materials should be as large as is commensurate with other requirements.

Taking all of the above factors into consideration it would appear as if the laminates studied in this work are suitable first generation products which encourage further consideration of the idea to use barrier-moderated pervaporative cooling in space suits. Further, it would appear that the desired level of MVTR is within reach if a reformulation of the polyurethane adhesive and utilization of improved techniques currently under development to disperse Ioplex powder in the adhesive are employed.

V CONCLUSIONS

1. The moisture vapor permeance (MVP) of the polyurethane adhesive employed as the barrier layer in the laminates under investigation is about 40 gm-mils/100 in²-24 hrs. at 35°C and a driving force of 100 to 0% R.H. This places it among the most water permeable organic polymers. However, for the proposed barrier moderated pervaporative cooling of a space suit the MVP must be about 1000 gm-mils/100 in²-24 hrs.

2. The oxygen permeability constant of this same material is about 10⁻⁸ cc(STP)-cm/cm²-sec-atm at 23°C which is a very low value for an amorphous, elastomeric material. This would lead to about 0.3 lb/hr of oxygen being lost from a space suit by permeation through a 1-mil barrier of this polyurethane having an area of 20 ft².

3. The permselectivity of this polyurethane for water vapor versus oxygen is about 10,000 when separate measurements for each gas are made. This very high value is generally observed only in polymers which undergo considerable swelling in water.

4. Polyurethanes do not swell appreciably in water and the high permselectivity noted in 3 above is probably due to "alignment-type" diffusion of moisture through the polymer. Therefore, the high permselectivity should also be observed when moisture and oxygen are

simultaneously transported through the polymer. In the majority of highly water-permeable polymers this selectivity is lost when simultaneous transport of moisture and oxygen is taking place.

5. Incorporation of Ioplex powder into the polyurethane dramatically increases its moisture permeability without increasing its oxygen permeability. A two to threefold increase in MVP results from a 20% loading of Ioplex. MVP's within a factor of two of that required for pervaporative cooling of a space suit can be obtained at a 40% loading of Ioplex.

6. Satisfactory, gas tight, adhesive barriers approximately 1-mil thick can be placed between the foam and fabric layers of the proposed laminate.

7. After taking into consideration the water vapor flow resistance offered by the fabric and foam in the laminate when moisture vapor transmission rates (MVTR) are determined at atmospheric pressure, the permeability of the adhesive-barrier layer is comparable to the value determined for an unsupported film of the same composition and thickness.

8. At atmospheric pressure the foam and fabric portions of the laminate contribute about 25% of the moisture transport resistance if the barrier layer contains no Ioplex. The fractional resistance increases with increasing Ioplex loading. The resistance becomes negligible when vacuum transport measurements are made and, therefore, under simulated space conditions the resistance can be neglected if these materials are placed on the low pressure (vacuum) side of the laminate.

9. Reformulation of the polyurethane adhesive with a suitable polyether to increase its moisture permeability and use of new Ioplex dispersion techniques now under development by industry would make it possible to prepare laminates meeting the gas and moisture permeability requirements for barrier-moderated pervaporative cooling of a space suit.

VI REFERENCES

- C-1. Carmen, P.C., "Flow of Gases Through Porous Media", Butterworths Scientific Publication, London (1956).
- C-2. Fricke, H., "Phys. Rev." 24, 575 (1924).
- C-3. Keilen, B., "The Mechanism of Desalination by Reverse Osmosis". Final Report to Office of Saline Water, Contract No. 14-01-0001-272. (Aerojet Report No. 2661). Aerojet-General Corp., Azusa, California, August, 1963.
- C-4. Michaels, A.S., H.J. Bixler and R.M. Hodges, Jr., "Kinetics of Water and Salt Transport in Cellulose Acetate Reverse Osmosis Desalination Membranes," to be published.
- C-5. Reid, C.E. and E.J. Breton, J. Appl. Polymer Sci. 1, 133 (1959).
- C-6. Rogers, C.E., "Permeability and Chemical Resistance", Chapter 9, Engineering Design for Plastics, E. Baer, Ed., Reinhold Publishing Corp., New York (1964).
- C-7. Saunder, J.H. and K.C. Frisch, "Polyurethane Chemistry and Technology", Part II, Technology, Interscience Publishers, New York (1964).

"IOPLEX" RESINS

The "Ioplex" resins are a class of polymeric materials which offer the following unique combination of chemical, physical, and electrical properties:

1. Electrical conductivity
(resistivity as low as 10^3 ohm-centimeters)
2. Extremely high dielectric constant
(up to 500,000)
3. Electrical characteristics sensitive to applied voltage, frequency, and water and micro-ion content
4. Permeability to water, salt, and other electrolytes
5. Low gas permeability
6. Ion absorption and ion exchange capability
7. Resistance to corrosive chemicals, elevated temperatures
8. Transparency
9. Adaptable to standard plastic fabrication techniques, such as molding, casting, coating, spinning.

Physical Properties

These materials, which are known generically as "Polyelectrolyte complexes," are synthesized by reacting, under carefully controlled conditions, linear water-soluble ionic polymers of opposite electrical charge. The resulting "Ioplex" resins are transparent, virtually colorless and odorless solids whose physical properties are intermediate between those of conventional organic polymers and inorganic glasses. Because of the extremely high degree of ionic cross-linking which exists in these structures, they are infusible, insoluble in all common solvents, and tend to be hard and brittle unless properly plasticized.

By the use of special processing techniques, these resins can be converted into viscous solutions with which it is possible to deposit films as thin as one micron on a variety of surfaces (e.g., metal, glass, ceramic, other plastics), to cast unsupported films, and to spin monofilament and staple fibers.

Electrical Properties

Of the many unusual properties exhibited by the "Ioplex" resins, their electrical behavior is perhaps the most striking. Because of their peculiar micro-ionic structure, they behave as anomalous, complex dielectrics; furthermore, these characteristics are profoundly sensitive to minor variations in the concentration of water and other plasticizers, and to the type and concentration of micro-ion present in the complex.

The AC resistivities of the "Ioplex" resins are normally 10^3 to 10^8 ohm-centimeters, while dielectric constants range up to 500,000 at low frequencies (60-1000 cycles). Dissipation factors are naturally quite high, ranging from 0.03 to 1.0 or higher for formulations exhibiting high dielectric constants.

A wide range of electrical characteristics can be obtained by small modifications in the polymer or additive concentrations within the "Ioplex" resins. The following typical properties have been obtained with plasticized "Ioplex" films:

<u>"Ioplex"</u> <u>Film Type</u>	<u>Volume Resistivity</u> <u>(ohm-cm)</u>		<u>Dielectric Constant</u>	
	<u>100 cps</u>	<u>10,000 cps.</u>	<u>100 cps</u>	<u>10,000 cps.</u>
3-Z	60,000	1,000	650,000	85,000
3-X	80,000	1,600	500,000	30,000
2-Z	100,000	2,400	140,000	15,000
2-X	140,000	4,000	180,000	6,000
1-Y	6,800,000	--	300	--

"IOPLEX" RESINS
FOR HIGH MVT PLASTICS

The Ioplex resins, when incorporated as fine powders or fibers into urethane, acrylic, or vinyl polymers, provide a new technique for obtaining high moisture-vapor-transmissive (MVT) plastics for wearing apparel, footwear, and upholstery. Composite materials containing "Ioplex" will provide:

1. High Moisture Vapor Transmission
(10 to 50 times higher than unfilled polymer)
2. Low gas and liquid permeabilities
(no pores or holes required)
3. Excellent physical properties
(in comparison to unfilled polymer)
4. No unique incorporation or fabrication methods required.

Description

The "Ioplex" resins, which are known generically as "Poly-electrolyte complexes," are transparent, virtually colorless and odorless solids which can be prepared in the form of fine powders, fibers, films and coatings. Because of the extremely high degree of ionic crosslinking which exists in these structures, they are infusible, insoluble in all common solvents, and stable under normal plastics processing conditions.

"Ioplex" resins -- ionically crosslinked polyelectrolyte structures -- appear to be highly attractive materials for use on the development of the modulating barrier-layer. They represent at present the only ion-exchange and ionically conductive polymer systems which can be applied from solution as coatings or saturants, and whose electrical characteristics are capable of precise control during resin-formulation. In addition, these resins are extremely and specifically sorptive for water, and show higher water-transmissivity than any other known polymer. The further important facts that (a) the resins are tough, elastomeric, and adhesive to other materials, and (b) they retain their flexibility (when properly formulated) even at low relative humidities, provide additional support to the belief that they may be choice for this demanding application. It is, therefore, recommended that initial feasibility-evaluation of the electroendosmotic principle be conducted with these resin systems.

Moisture Vapor Transmission

The "Comfort Factor" of a material for wearing apparel and footwear is closely related to the "breathability" of the material, i.e., its ability to transmit moisture vapor produced by the human body in the form of perspiration. The success of natural leather as a shoe material, for example, is primarily due to the close correlation of its MVT to that required to evaporate the moisture produced by the human foot:

	<u>Moisture Production and Transmission Rates gm/100 sq in/24 hrs</u>
"Insensible" Sweat Production by the Human Foot (with minimum physical exertion)	84 - 195
Typical values for men's-weight shoe upper materials, finished	50-100
MVT of Top Grain Cowhide, unfinished	300

The most common method of providing "breathability" in a synthetic material is to utilize a porous structure, in which there is a mass flow of gas or vapor through pores or holes extending through the material. The principal drawback of this technique, however, is that the same pores which allow gas flow will also permit the flow of liquid water through the material, thereby rendering it non-waterproof. The application of a surface coating to prevent liquid water transmission will at the same time block the pores to moisture vapor, thereby greatly reducing the MVT of the finished material.

The incorporation of "Ioplex" powders into a polymer matrix, however, provides high MVT without the necessity for pores through the material. Typical MVT data for "Ioplex" -polymer composites of this type are shown below and on the attached graph:

<u>MVT(g/100 in²/24 hr/mil)*</u>			
<u>"Ioplex-Y" Content</u> <u>% by Weight</u>	<u>Vinyl Plastisol</u>	<u>Vinyl-Acrylic Latex</u>	<u>Thermoplastic Urethane</u>
0	35	200	80
20	100	500	400
40	300	900	1150

*Divide by desired film thickness to yield units of g/100 in²/24 hrs.

The unique character of the "Ioplex" resins for this application is illustrated by comparison with casein, a typical natural hydrated polymer, which provided no increase in MVT when incorporated up to 40% into the thermoplastic urethane system.

While these data indicate the effectiveness of "Ioplex" powders in increasing the MVT of a variety of synthetic polymers, they do not represent the optimum which can be obtained. Improved "Ioplex" formulations are being developed which show a tenfold increase in the MVT of a thermoplastic urethane at the 20% level, compared with the fivefold increase shown above.

Ease of Fabrication

"Ioplex" powders may be readily blended with a wide variety of thermoplastic and thermosetting polymers and fabricated into films or coatings by conventional means.

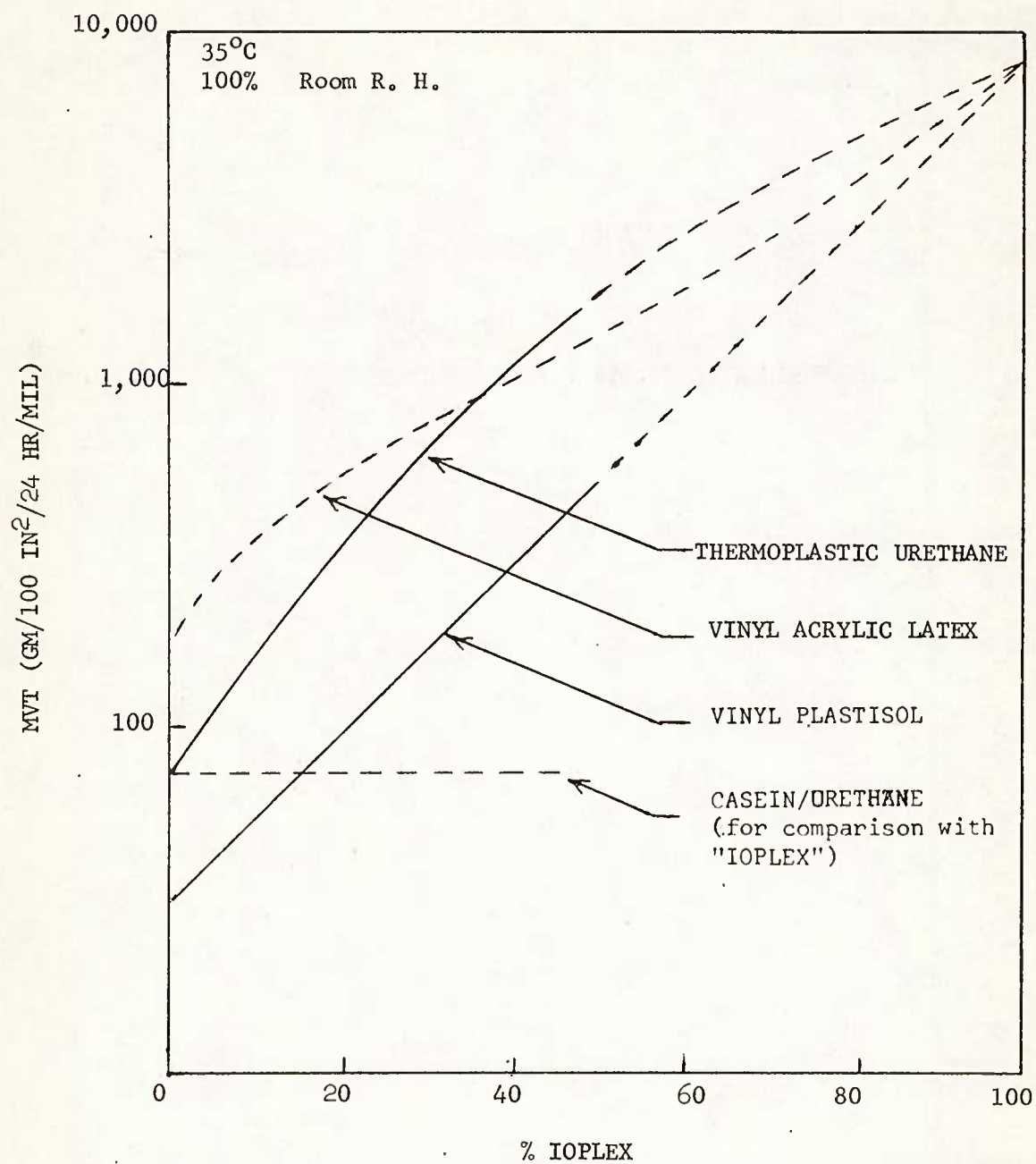


FIGURE C-5. MVT OF "IOPLEX" / PLASTIC COMPOSITES

APPENDIX D

EXPERIMENTAL STUDY OF POLYURETHANES

CONTENTS	PAGE
PART I AN INVESTIGATION OF WATER PERMEATION THROUGH ULTRA-THIN POLYURETHANE MEMBRANES	82
EXPERIMENTAL TECHNIQUE	82
a. Dissolving the Elastomer	82
b. Film Preparation on Glass	82
c. Film Preparation on Water	82
d. Determination of Thickness	83
e. Measurement of Permeation Rates	83
POSSIBLE SOURCES OF ERROR	86
DISCUSSION OF RESULTS	89
CONCLUSIONS	95
DERIVATIONS AND SAMPLE CALCULATIONS	96
NOMENCLATURE	99
PART II STUDIES ON THE STRUCTURE OF RUBBERY POLYURETHANES	150
INTRODUCTION	100
A. TRANSITION TEMPERATURE MEASUREMENTS	100
1. Samples	102
2. TMA Measurements	102
3. DSC Results	105
B. OPTICAL ANALYSIS OF STRUCTURE	105
1. Visual Appearance	105
2. Optical Microscopy	109
3. Light Scattering Measurements	109
4. Strain-Optical Coefficient	110
5. X-Ray Diffraction	110
DISCUSSION	110
PART III PERMEATION OF WATER VAPOR THROUGH A POLYURETHANE MEMBRANE	110
THEORY AND REVIEW OF LITERATURE	114
A. Definition of Terms	114
B. Development of Equations	115
C. Effect of Variables	115
D. Theoretical Models of Sorption	117

	Page
EXPERIMENTAL WORK	121
A. Equipment	121
B. Procedure	123
CALCULATIONS	126
A. Data Collected	126
B. Data Preparation	126
C. Calculations	127
D. Sources of Experimental Error	128
EXPERIMENTAL RESULTS	129
A. Tabulated Results	129
B. Graphical Presentation of Results	129
DISCUSSION OF RESULTS	144
CONCLUSION AND RECOMMENDATIONS	152
PART IV SORPTION AND DIFFUSION OF ETHANOL IN A POLYURETHANE	154
INTRODUCTION	154
EXPERIMENTAL PROCEDURE	155
TREATMENT OF THE DATA	157
RESULTS AND DISCUSSION	158
1. Equilibrium Results	158
2. Transient Results	161
REFERENCES	167

LIST OF FIGURES

<u>FIGURE</u>		<u>PAGE</u>
D-1	Flux vs. Thickness; 99.5°F-D.B., 86.5°F-W.B., 45% R.H.	87
D-2	Flux vs. Thickness; 99.5°F-D.B., 76.5°F-W.B., 35% R.H.	88
D-3	Flux (Normalized for Thickness) vs. Thickness; 99.5°F-D.B., 81.5°F-W.B., 45% R.H.	90
D-4	Flux (Normalized for Thickness) vs. Thickness; 99.5°F-D.B., 76.5°F-W.B., 35% R.H.	91
D-5	Reciprocal Flux vs. Thickness; 99.5°F-D.B., 81.5°F-W.B., 45% R.H.	92
D-6	Reciprocal Flux vs. Thickness; 99.5°F-D.B., 76.5°F-W.B., 35% R.H.	93
D-7	Reciprocal Flux vs. Thickness of Thicker Films at 45% R.H.	94
D-8	Flux (Normalized for Thickness) vs. Thickness, 45% R.H.	98
D-9	Modulus-Temperature Curves for Two Estane Polyester Type Polyurethanes	101
D-10	Sample Displacement Temperature Curve for Polyester Polyurethane with Thermomechanical Analyzer	103
D-11	Differential Scanning Colorimeter Traces for a Polyester and a Polyether Type Polyurethane	106
D-12	Types of Sorption Isotherms	118
D-13	High Vacuum Sorption Apparatus	122
D-14	High Vacuum Pumping System	122
D-15	Sorption Isotherm at 30°C	136
D-16	Sorption Isotherm at 35°C	137
D-17	Sorption Isotherm at 40°C	138
D-18	Sorption Isotherm at 50°C	139
D-19	Effect of Concentration on the Diffusion Coefficient at 30°C.	140

LIST OF FIGURES

<u>FIGURE</u>		<u>PAGE</u>
D-20	Effect of Concentration on the Diffusion Coefficient at 35°C.	141
D-21	Effect of Concentration on the Diffusion Coefficient at 40°C.	142
D-22	Effect of Concentration on the Diffusion Coefficient at 50°C.	143
D-23	Variation of the Solubility Coefficient with Activity at 30°C.	145
D-24	Variation of the Solubility Coefficient with Activity at 35°C.	146
D-25	Variation of the Solubility Coefficient with Activity at 40°C.	147
D-26	Variation of the Solubility Coefficient with Activity at 50°C.	148
D-27	Effect of Temperature on the Diffusivity and the Solubility Coefficient	149
D-28	Langmuir Analysis of 40°C Isotherm	151
D-29	Volume Fraction Activity Coefficient and Clustering Function Versus Volume Fraction	153
D-30	Diagram of Quartz Balance Sorption System	156
D-31	Temperature Dependence of Ethanol Solubility in the Polyester Polyurethane; Samples Immersed in the Liquid	159
D-32	Sorption Isotherms Representing Concentration of Ethanol (glcc) as a Function of Partial Pressure (p/p_0)	160
D-33	Sorption-Time Curve for Ethanol	163
D-34	Concentration Dependence of the Diffusion Constant of Ethanol	164
D-35	Comparison of Sorption-Time Curve for Ethanol at 19.5°C, 0 ---6 MM HG with Theoretical Curves Calculated for Diffusion with Concurrent Reaction	165

LIST OF TABLES

<u>TABLE</u>		<u>PAGE</u>
D-1	Solvents and Effect on Polymer	83
D-2	Concentration and Thickness Settings for Cast Films	84
D-3	Transition Temperatures of Various Polyurethanes (Pentrometer Determination)	104.
D-4	Transition Temperatures for Several Polyurethanes (DSC Determinations)	107.
D-5	Summary of Optical-Mechanical Data	111
D-6	Results of Runs 1 and 2 at 30°C	130
D-7	Results of Runs 3 and 4 at 35°C	131
D-8	Results of Runs 5 and 6 at 40°C	132
D-9	Results of Runs 7 and 8 at 50°C	134

PART I

AN INVESTIGATION OF WATER PERMEATION THROUGH
ULTRA-THIN POLYURETHANE MEMBRANES

EXPERIMENTAL TECHNIQUE

a. Dissolving the Elastomer

The first step in the preparation of the membranes was dissolving the elastomer in a suitable solvent. From all the solvents tried, only tetrahydrofuran and cyclohexanone exhibited acceptable qualities. Table D-1 lists all the solvents used and describes the resulting solutions and films.

b. Film Preparation on Glass

The first films were cast on Teflon with little success, because the film had a tendency to stick to the Teflon. Glass proved to be a more suitable substrate for casting than Teflon. In making the film, the solution containing the elastomer was poured on a clean glass plate, and then a stainless steel blade, which had thickness settings from 0 to 10 mils, was drawn over the solution to form a fairly even film on the glass. In using a volatile solvent such as THF, the casting had to be done quickly so that the film did not begin to form until it had been drawn on the glass plate.

The concentration of the polyurethane solution and the thickness setting on the blade were changed to produce films of different thicknesses. Table D-2 shows the concentration of the solution used and the thickness setting for each film that was made on glass. It might be noted here that the thickness also had a small dependence upon the speed in which the film was cast, i.e., if the film were drawn slowly with the blade, the resulting film would be thicker.

Films of two microns and greater could be pulled up from the glass without destroying the film, but films less than 2 microns had to be removed with the help of water. The glass plate, on which the film was cast, was lowered into the water; the water permeated through the film and released it from the glass underneath. Since these extremely thin films were difficult to handle, only a few films below 2 microns were made.

c. Film Preparation on Water

Film castings were also done on water. Films formed on water with a tetrahydrofuran solution were extremely rough and uneven in thickness due to the miscibility of THF and water. The solution of cyclohexanone and the polymer worked very well for film casting on water,

TABLE D-1

Estane 5740X140

<u>SOLVENT</u>	<u>REMARKS</u>
Toluene	Diluent - swells polymer
Methylene Chloride	Diluent - small amount dissolved
Methyl Isobutyl Ketone	Small amount of swelling
"Cellosolve" Acetate	Diluent
Methyl Ethyl Ketone	Diluent
Cyclohexanone	Solvent - makes a continuous film
1, 4 Dioxane	Solvent - possible deterioration of solution with age
Acetone	Diluent
THF	Solvent - makes a continuous film
Pyridine	Solvent - makes a cloudy discontinuous film
Dimethyl Formamide	Solvent - makes a cloudy discontinuous film
Dimethyl Sulfoxide	Solvent - makes a cloudy discontinuous film

TABLE D-2

Estane 5740X140

<u>THICKNESS</u>		<u>SURFACE</u>	<u>% SOLUTION</u>	<u>PREPARATION</u>
<u>MILS</u>	<u>MICRONS</u>			<u>THICKNESS SETTING</u>
0.028	0.7	Glass	5% THF	#2
0.04	1.0	Glass	5% THF	#2
0.052	1.3	Glass	5% THF	#2
0.092	2.3	Glass	5% THF	#4
0.10	2.5	Glass	5% THF	#4
0.12	3.0	Glass	5% THF	#4
0.14	3.5	Glass	5% Cyclohexanone	#4
0.14	3.5	Glass	5% THF	#4
0.152	3.8	Glass	5% THF	#4
0.16	4.0	Glass	5% THF	#6
0.204	5.1	Glass	10% THF	#4
0.398	9.95	Glass	10% THF	#6
0.608	15.2	Glass	10% THF	#10
0.696	17.4	Glass	15% THF	#8
0.90	22.5	Glass	15% THF	#9
0.95	23.5	Glass	15% THF	#10
3.1	77.5	Glass	20% Cyclohexanone	30 mils
3.9	97.5	Glass	20% Cyclohexanone	50 mils
11	275	Glass	25% Cyclohexanone	100 mils
	3.35	Water	10% Cyclohexanone	
	3.8	Water	10% Cyclohexanone	
	4.1	Water	5% Cyclohexanone	

since cyclohexanone is not very soluble in water. The method involved dropping a small amount of solution on the water and letting it spread under the influence of the surface tension of water.

Many variables affected the thickness of the film formed on water. Some of these variables could not be controlled. The thickness was affected mostly by the concentration of the solution, surface tension of the water, amount of solution used, and the solubility of the solvent in water. These variables could all be controlled, whereas the amount of spreading of the solution on the water could not. Although the spreading should be controlled by the above factors, it was found that the amount of spreading was not reproducible. Since the spread of the solvent was a contributing factor to the thickness of the film, control of the thickness was difficult. After the film had been formed on water, a rectangular piece of mylar film, from which a circle was cut, was placed on the polyurethane film. After the polyurethane film had adhered to the mylar, it was picked up and allowed to dry.

d. Determination of Thickness

A weighing technique was used in determining the thickness of the ultra-thin films.

The elastomer film was placed on a 15-inch square circle pretared of mylar film and weighed on a semi-micro balance. By knowing the area of the film and the specific gravity (D-16) (1.11) of the elastomer, a reproducible method for determining the film thickness was developed. The film was readily removed from the mylar.

e. Measurement of Permeation Rates

To measure the steady state permeation rate, the films were placed in stainless steel cells which were then filled with demineralized water. One side of the unsupported film was in contact with the permeant water while the other side was exposed to an atmosphere of constant humidity and temperature. This method of determining the permeation rate is discussed by C.E. Rogers (D-49) and H.B. Hopfenberg (D-38). For the very thin films, less than 2 mils, only enough water was placed in the cell to cover the film. This was done to keep the resulting deformation to a minimum since the "bulge" would not only cause the film to stretch and become thinner, but also increase the surface area of the film. Both of these factors would increase the permeation rate.

An Aminco air bath was used to maintain the constant humidity and temperature. A Mettler balance was set up on top of the air bath with its weighing pan suspended inside the Aminco bath so that weighings of the cells could be done without removing them from the constant humidity and temperature. The cells were weighed periodically to determine the weight loss due to permeation.

From the weighings of the samples, the permeation rate was calculated for each film thickness. From these data, three graphs were drawn: one of flux vs. thickness, normalized flux vs. thickness and thirdly, reciprocal flux vs. thickness.

POSSIBLE SOURCES OF ERROR

The presence of microscopic pores in the thin films would affect the calculated moisture vapor transmission rate. To check for this possibility, two thin films, 1.35 microns and 1.95 microns thick were placed one on top of another to see if the two-layered film of 3.3 microns would have the same flux as a single film of the same thickness. Theoretically, if pores did exist, they would be covered up by the second layer. Thus the combined two-layered film would essentially be free from any microscopic pores. It can be seen in Figure D-1 that the flux values for this double-layered film coincides with those of single-layered films of the same thickness. Therefore, it was assumed that no pores existed in the single-layered films.

Since the films were made using two different substrates, water and glass, and two different solvents, THF and cyclohexanone, it was thought that these different methods of making the film might alter the film's physical characteristics and subsequently affect the MVTR.

First, films cast on glass using tetrahydrofuran and cyclohexanone as solvents were compared with each other to see if any difference occurred in the MVTR. Since it was easier to cast films from a THF (more volatile) than a cyclohexanone solution, only four films were cast on glass from a cyclohexanone solution. Figure D-2 shows that the choice of solvent, either THF or cyclohexanone, had little or no effect upon the MVTR qualities of the film.

In the same manner, films cast on water from a cyclohexanone solution were compared to films cast on glass. The results on Figure D-1 showed that there was little or no difference in the MVTR.

If a stagnant layer of the permeant, water, were allowed to build up on the downstream side of the film during its immersion in the Aminco air bath, then the calculated MVTR would be lower than it should be. It is the author's belief that enough air was circulating in the bath so that this build up of a stagnant layer did not occur.

As mentioned earlier, the thickness of each sample film was determined by weighing each film. An error in determining the thickness might be introduced, for it was noted that occasionally a small static charge was present on the mylar film. The charge was probably induced on

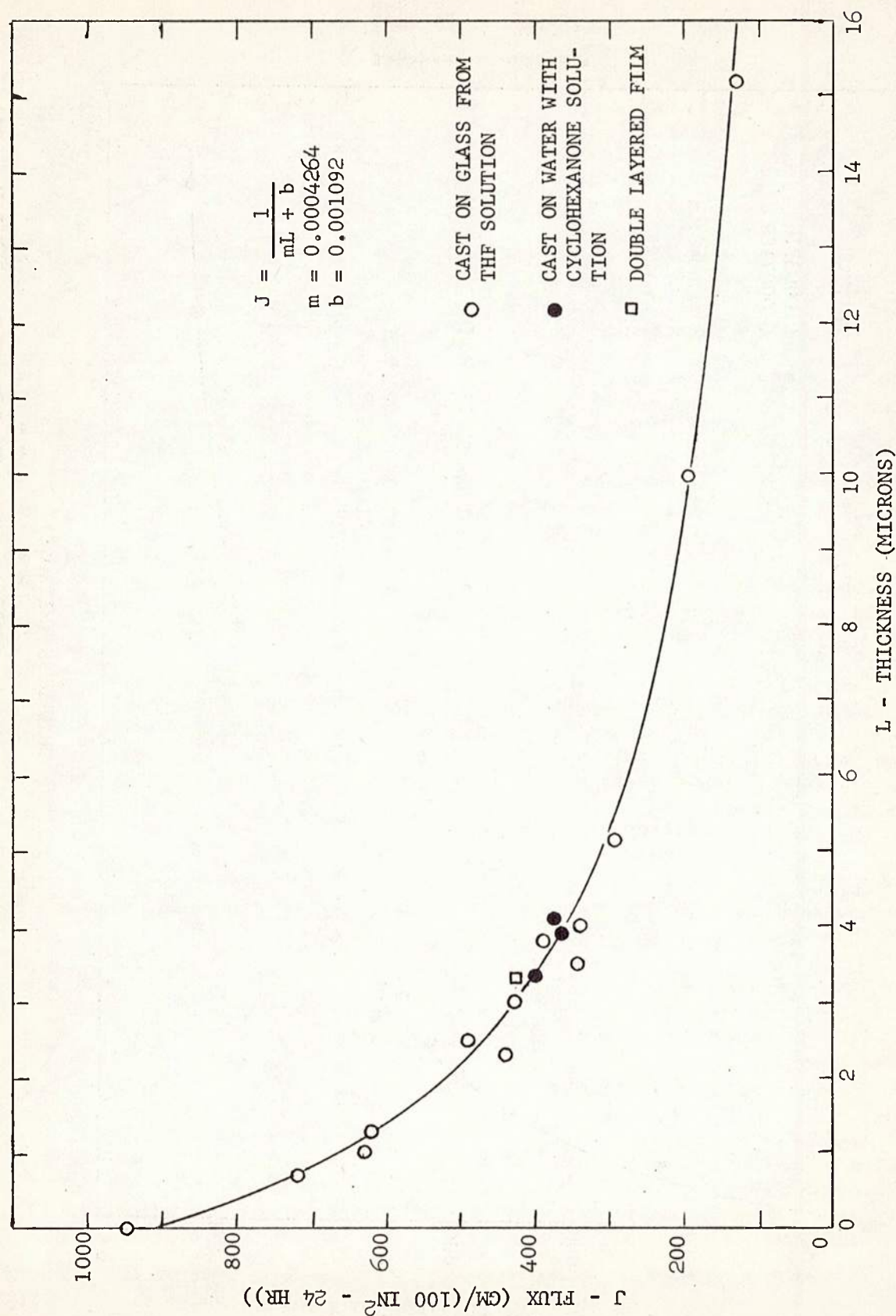


FIGURE D-1. FLUX VS. THICKNESS; 99.5°F - D.B., 86.5°F - W.B., 45% R.H.

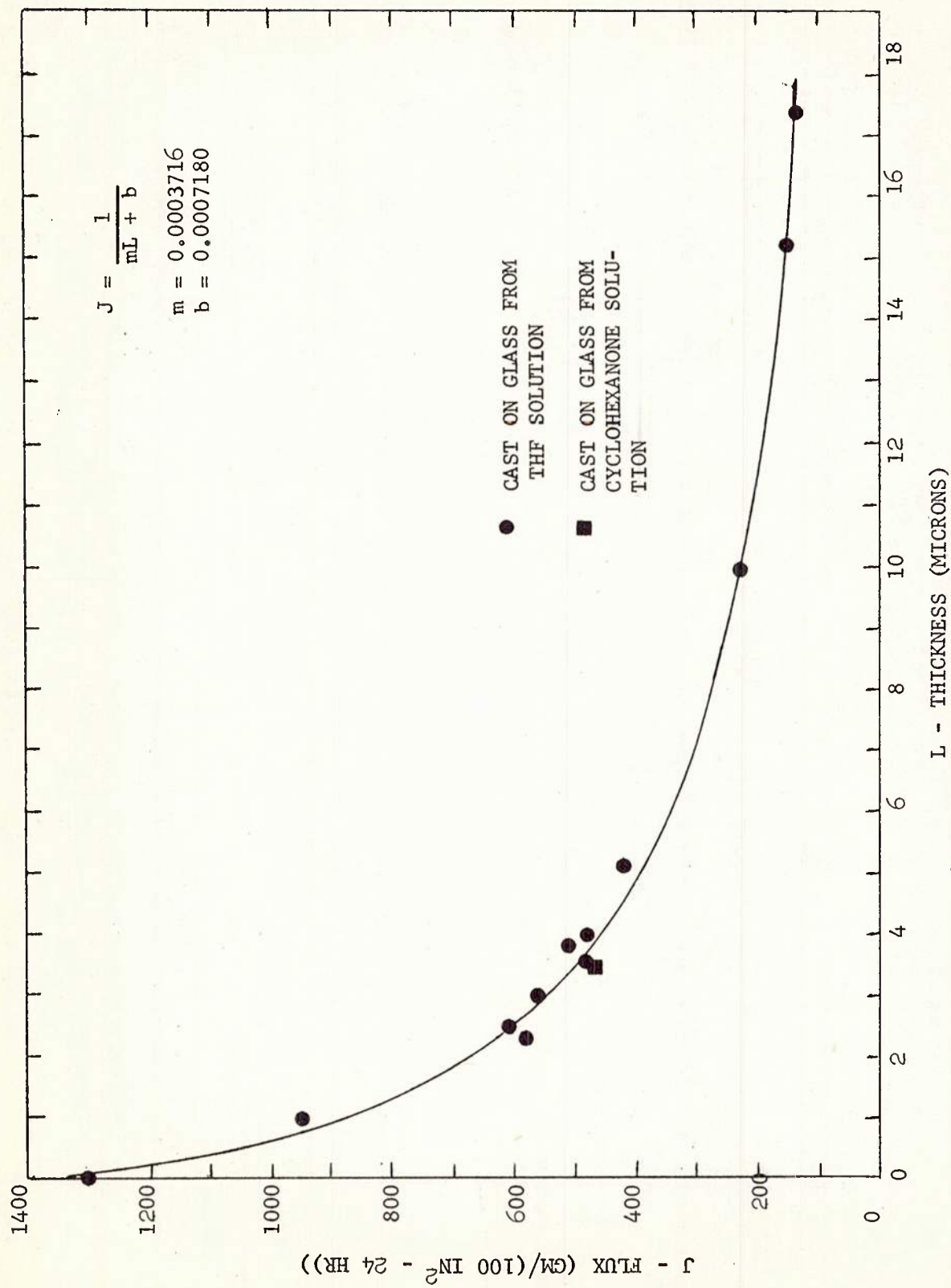


FIGURE D-2. FLUX VS. THICKNESS; 99.5°F - D.B., 76.5°F - W.B., 35% R.H.

the film when it was being cleaned. The static charge was sometimes great enough to increase the thickness determinations for thinner films by as much as 10%, presumably by an attraction with the base of the balance case. This problem was resolved through the use of an anti-static cleansing fluid which was used on the mylar film preceding its weighing. The method involved pouring the fluid on the mylar film and rubbing until it was dry.

DISCUSSION OF RESULTS

The cells were run at two different relative humidities (45% and 35%), keeping the dry bulb temperature constant at 99.5°F. For each of the two conditions, three graphs were drawn.

The first graph shows the relationship between the flux and thickness of the membrane. These results can be seen on Figures D-1 and D-2. The MVTR value for zero thickness was determined from a cell which had no membrane.

The second graph plots the normalized flux vs. the thickness. Theoretically, the value for the normalized flux should be constant; Figures D-3 and D-4 definitely show that they are not constant but decrease to zero as the thickness approaches zero.

The film thickness and the evaporation of water, if thought of as impedances in series, both control the MVTR value for each film. The total impedance, obtained by adding the impedances of the thickness and the evaporation of water, is the value for the reciprocal flux. The impedance offered by the water (b) will be taken as the reciprocal of the evaporation of water with dimensions of $(\text{GM}/100 \text{ in}^2\text{-24 HR})^{-1}$. The impedance donated by the thickness is proportional to the thickness (L) and is symbolized by mL where m is the proportionality constant. For the impedances to be dimensionally consistent, m has the units of $(\text{GM-Micron})/(\text{100 in}^2\text{-24HR})^{-1}$ and L is in microns. If the above assumptions are correct, the relationship between flux (J) and thickness (L) can be expressed by the following equation: $1/J + ML + b$.

If reciprocal flux $1/J$ is plotted against thickness (L) the graph should be a straight line. Figures D-5, D-6 and D-7 show that it is a straight line. The method of least squares (D-5) was then used in determining the best straight line through the points.

From the slope and the intercept of the straight line, an equation for flux vs. thickness and normalized flux vs. thickness was derived. Equation for the straight line of reciprocal flux vs. thickness:

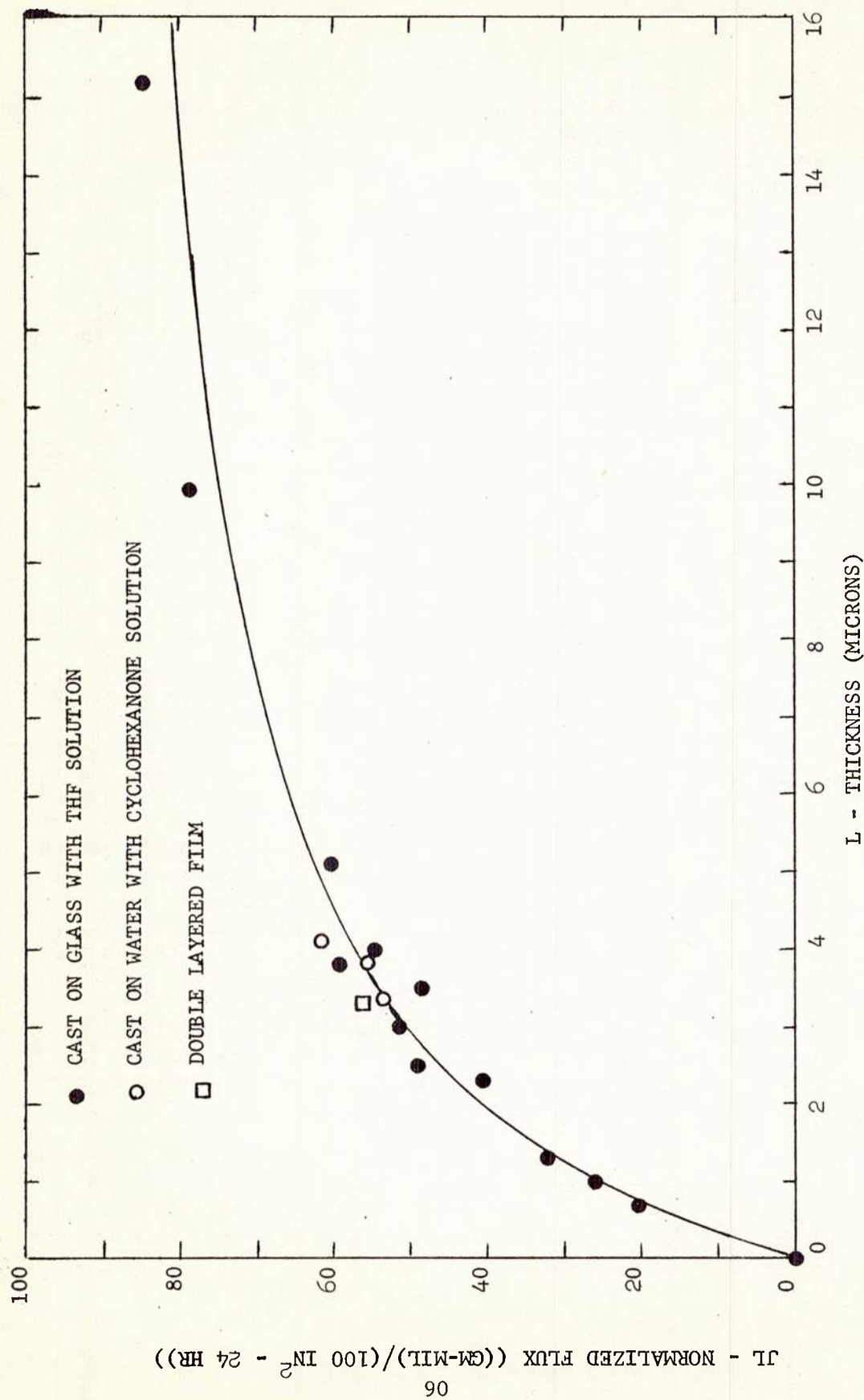


FIGURE D-3. FLUX (NORMALIZED FOR THICKNESS) VS. THICKNESS; 99.5°F - D.B., 81.5°F - W.B., 45% R.H.

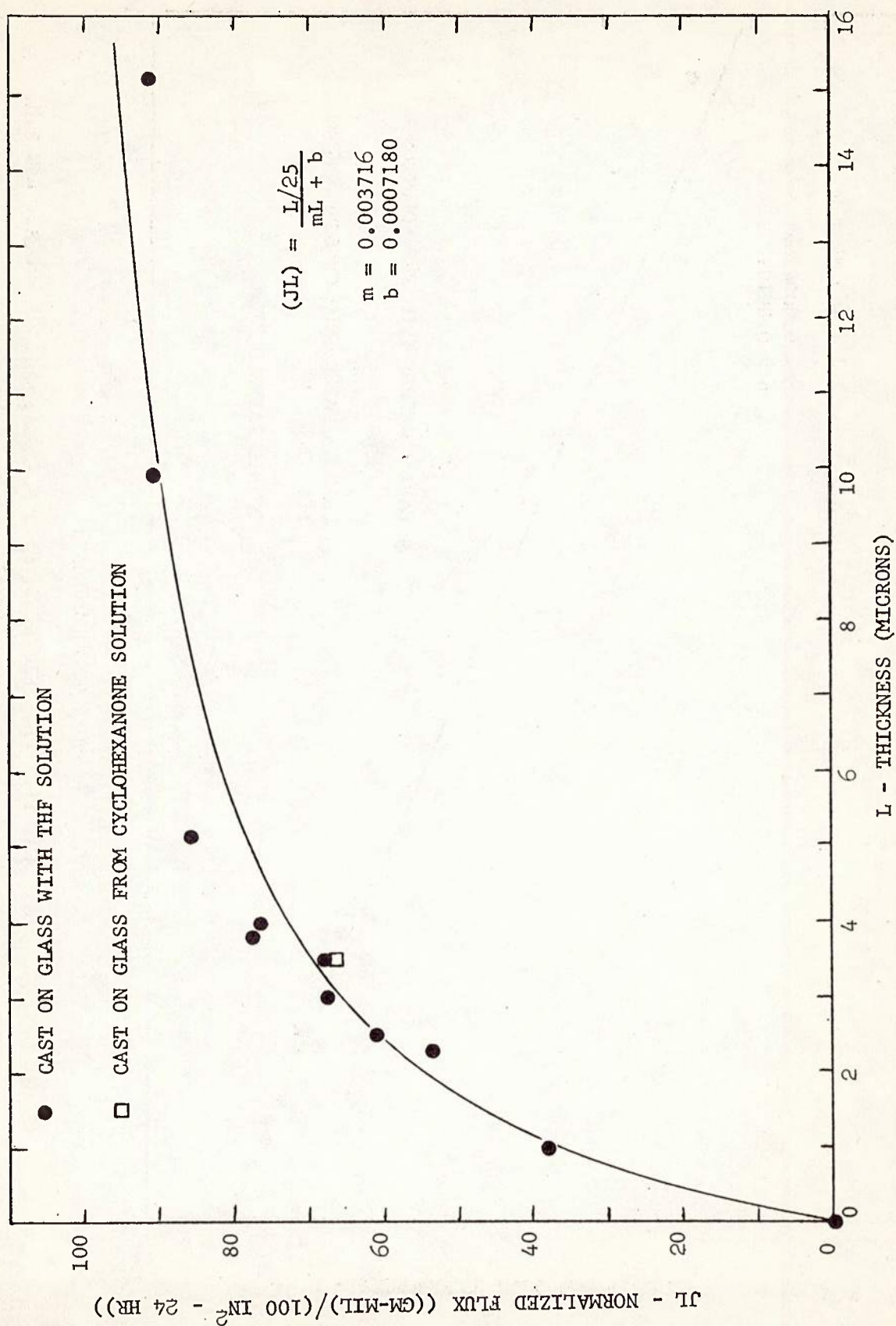


FIGURE D-4. FLUX (NORMALIZED FOR THICKNESS) VS. THICKNESS; 99.5°F - D.B., 76.5°F - W.B., 35% R.H.

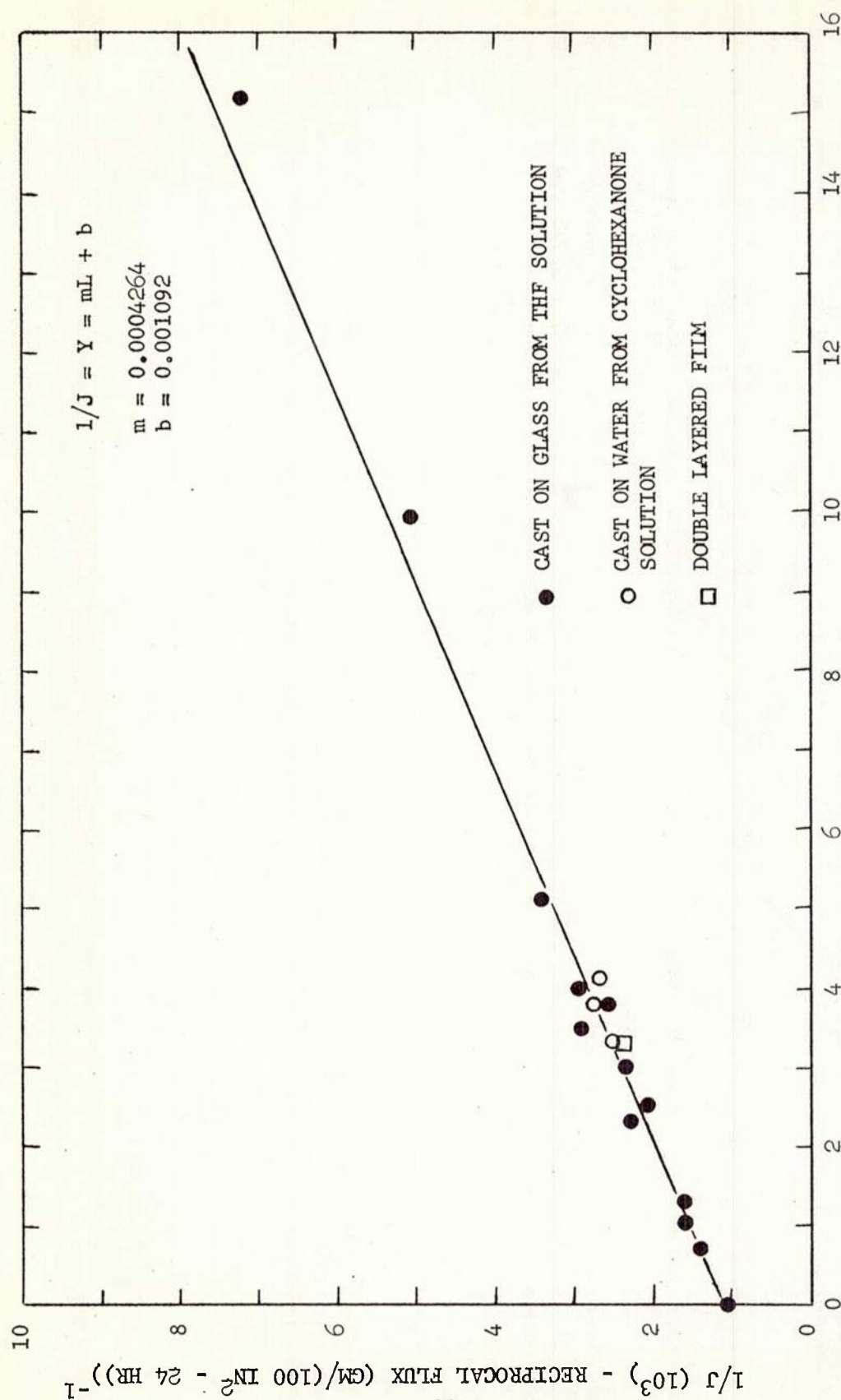


FIGURE D-5. RECIPROCAL FLUX VS. THICKNESS; 99.5°F - D.B., 81.5°F - W.B., 45% R.H.

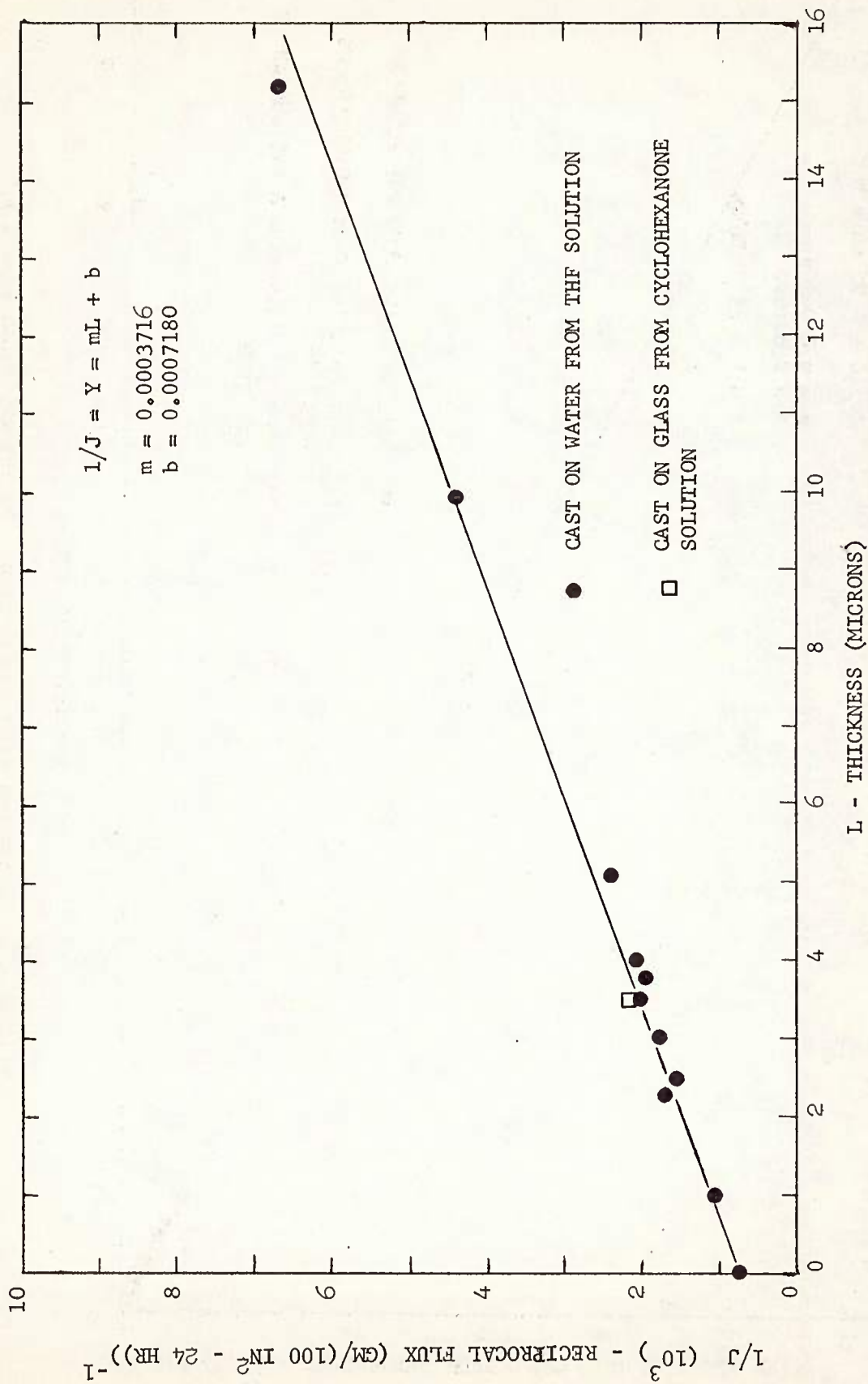


FIGURE D-6. RECIPROCAL FLUX VS. THICKNESS; 99.5°F - D.B., 76.5°F - W.B., 35% R.H.

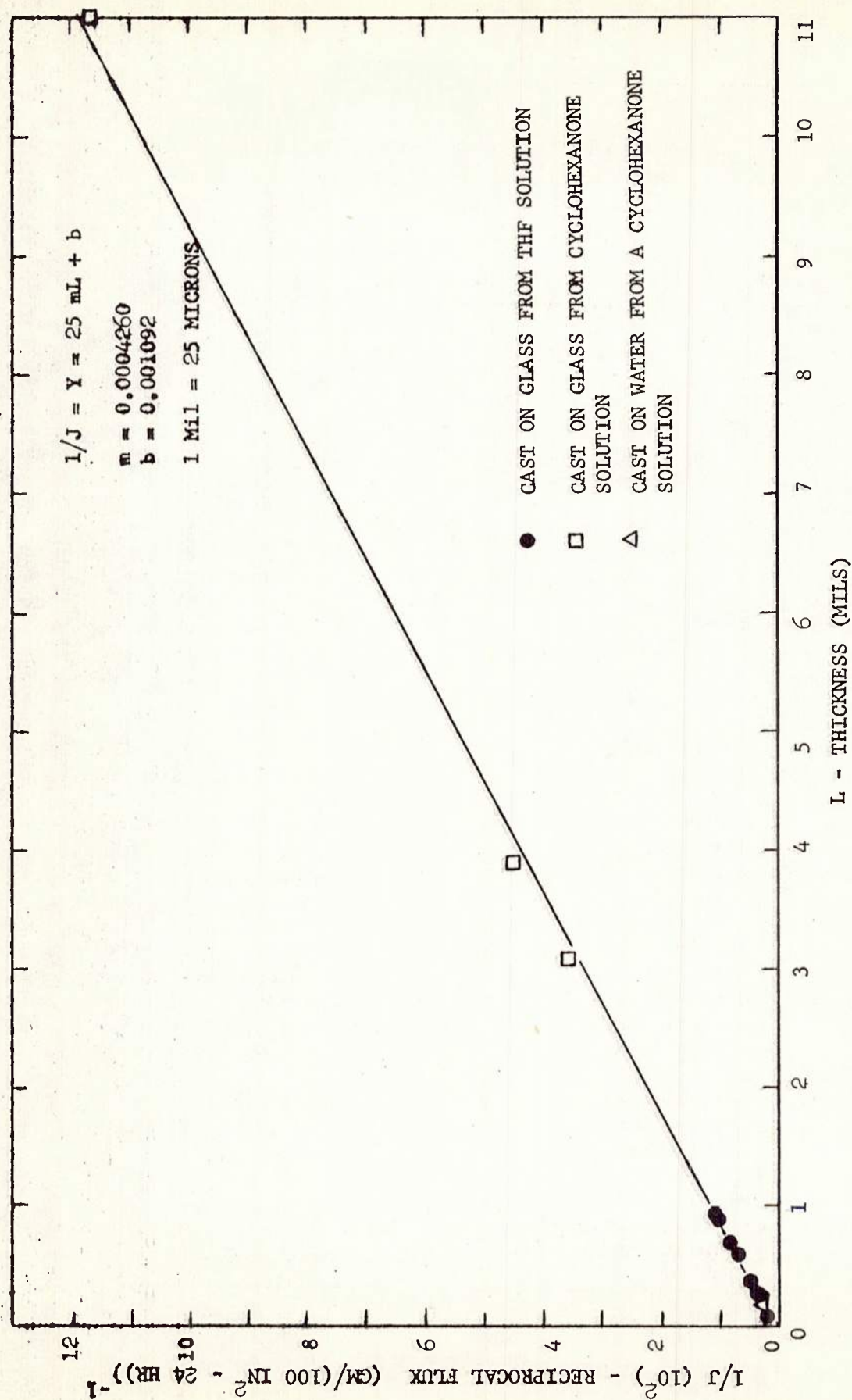


FIGURE D-7. RECIPROCAL FLUX VS. THICKNESS OF THICKER FILMS AT 45% R.H.

$$Y = \frac{1}{J} = mL + b.$$

Equation for flux vs. thickness:

$$J = 1/(mL + b)$$

Equation for normalized flux vs. thickness:

$$JL = L/(mL + b)$$

where JL = normalized flux.

It was found, however, that when the curve of flux vs. thickness was drawn, using the value for the slope and intercept obtained from the best straight line of reciprocal flux vs. thickness, the curve did not coincide very well with the experimentally determined points for very small thicknesses. The reason for the poor fit of the curve to the original data points was the fact that the reciprocal flux for small thicknesses was not weighted heavily enough when the best straight line was drawn, simply because the reciprocals of numbers of increasing magnitude (flux rate) decrease in magnitude. In other words, as the flux increases, instead of having greater influence on the straight line determination, it has less influence.

This problem was overcome by fitting the best curve to the plot of flux vs. thickness according to the method of least squares. The derivation for the least squares method is found following this discussion.

The parameters, m and b , were determined not from the best straight line of reciprocal flux vs. thickness, but rather from the graph of flux vs. thickness, where the flux values are weighted as they should be, i.e., the greater the flux, the greater the weight of that point.

CONCLUSIONS

With a proper choice of solvents, it was relatively easy to cast films on both glass and water. THF was found to be the best solvent for casting on glass and cyclohexanone the best for casting on water.

When the glass-cast films were first compared to those cast on water, it was thought that there would be a considerable difference in the MVTR values, because of the internal stresses which developed in the glass-cast films but not found in the films cast on water.

The films cast on glass adhered to the substrate and did not allow the film to shrink as the solvent evaporated. The water-cast films, however, were completely mobile and were allowed to shrink during the forming process. Apparently the internal stresses had very little effect on the MVTR values. The comparison of the two films can be seen on Figure D-1.

In theory, the value for normalized flux should remain constant for any thickness. As it can be seen in Figures D-3, D-4 and D-8, this is not so. For thinner films (below 4 mils), the rate evaporation of water controls the flux value rather than the film thickness. Hypothetically, if the rate of evaporation of water were infinitely high, then the value for normalized flux would remain constant, for the flux value would be solely dependent upon thickness. For thicker films, above 4 mils (100 microns), Figure D-8 shows that the controlling factor is predominately the thickness as the line is almost straight and horizontal.

Since it was found that a simple relationship existed between the flux and the film thickness, it can be concluded that the permeability is not affected by the surfaces of the film. That is, the permeability at the surface is the same as at the interior of the film and the overall permeability of the film is controlled solely by bulk film properties.

DERIVATION AND SAMPLE CALCULATIONS

Derivation of the least squares method for the equation,

$$J = 1/(mL + b)$$

The equation $J = 1/(mL + b)$ describes the relationship between the flux, J , and the thickness L . Rearranging the equation we have:

$$1 = JmL + Jb$$

The residual is defined as $(1 - JmL - Jb)^2$. The best values of m and b are those that make the sum of the squares of the residuals a minimum i.e., $\sum(1 - JmL - Jb)^2 = \text{a minimum}$.

This occurs when

$$\frac{\partial \sum(1 - JmL - Jb)^2}{\partial m} = \frac{\partial \sum(1 - JmL - Jb)^2}{\partial b} = 0$$

$$\begin{aligned} \text{D-1} \quad \frac{\partial \sum(1 - JmL - Jb)^2}{\partial m} &= 2 \sum(1 - JmL - Jb)(JL) = 0 \\ &= 2 \sum(JL - J^2 L^2 m - J^2 L b) = 0 \\ &= \sum JL - m \sum J^2 L^2 - b \sum J^2 L = 0 \end{aligned}$$

D-2

$$\begin{aligned}
 \frac{\partial \Sigma (1 - JmL - Jb)^2}{\partial b} &= 2 \Sigma (1 - JmL - Jb)(J) = 0 \\
 &= 2 \Sigma (J - J^2mL - J^2b) = 0 \\
 &= \Sigma J - m \Sigma J^2L - b \Sigma J^2 = 0
 \end{aligned}$$

We now have two equations with two unknowns (m and b)

From Equation D-2

$$m = \frac{\Sigma J - b \Sigma J^2}{\Sigma J^2L}$$

Substituting into Equation D-1 the value for m:

$$\Sigma JL - \left(\frac{\Sigma J - b \Sigma J^2}{\Sigma J^2L} \right) \Sigma J^2L^2 - b \Sigma J^2L = 0$$

$$\Sigma JL - \frac{\Sigma J \Sigma J^2L^2}{\Sigma J^2L} + \frac{b \Sigma J^2 \Sigma J^2L^2}{\Sigma J^2L} - b \Sigma J^2L = 0$$

$$b \left(\frac{\Sigma J^2 \Sigma J^2L^2}{\Sigma J^2L} - \Sigma J^2L \right) = \frac{\Sigma J \Sigma J^2L^2}{\Sigma J^2L} - \Sigma JL$$

$$b = \frac{\Sigma J \Sigma J^2L^2 - \Sigma JL \Sigma J^2L}{\Sigma J^2 \Sigma J^2L^2 - (\Sigma J^2L)^2}$$

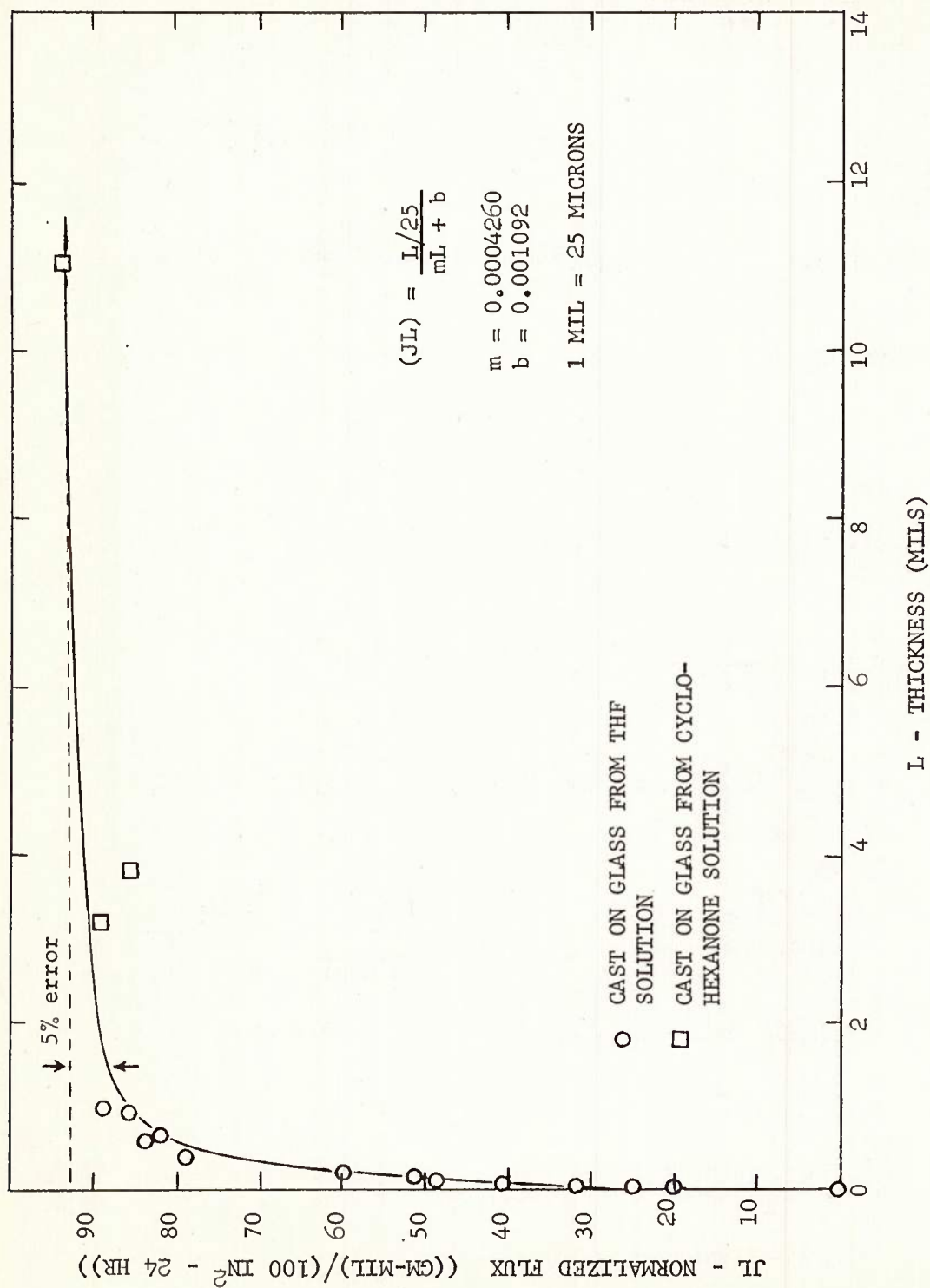


FIGURE D-8. FLUX (NORMALIZED FOR THICKNESS) VS. THICKNESS; 45% R.H.

Calculation of flux, normalized flux and reciprocal flux from the moisture vapor transmission data:

Weight loss for cell #1 at 45% relative humidity for 24 hours was 6.7097 grams.

$$\text{Flux: } J = \frac{\text{wt. loss}}{100 \text{ in}^2 \times 24 \text{ hrs.}}$$

$$\text{Area of cell: } 1.768 \text{ in}^2$$

$$\text{Therefore, } J = \frac{6.7097 \times 100 \text{ in}^2}{1.768 \text{ in}^2 (100 \text{ in}^2 \times 24 \text{ hrs})} = \frac{389 \text{ grams}}{100 \text{ in}^2 \times 24 \text{ hrs.}}$$

The film of cell of #1 had a thickness of 3.8 microns

$$\text{Normalized flux: } JL = \frac{\text{gm} \times \text{mil}}{100 \text{ in}^2 \times 24 \text{ hrs.}}$$

$$\text{Therefore, } JL = 59.28 \frac{\text{gm} \times \text{mil}}{100 \text{ in}^2 \times 24 \text{ hrs.}}$$

$$\text{Reciprocal flux: } 1/J = \frac{0.002564}{\text{gm}/100 \text{ in}^2/24 \text{ hrs.}}$$

NOMENCLATURE

- b A parameter whose reciprocal is equal to the evaporation of water in gm/100 in²/24 hrs.
- J Flux in gm/100 in²/24 hrs.
- L Thickness in microns.
- m A parameter whose reciprocal is equal to the asymptote of normalized flux vs. thickness.
- MVT Moisture vapor transmission.
- THF Tetrahydrofuran.
- Y Reciprocal flux in (gm/100 in²/24 hrs)⁻¹.

PART II

STUDIES ON THE STRUCTURE OF RUBBERY POLYURETHANES

INTRODUCTION

This section summarizes some of the results obtained during the initial stages of work on the structure and properties of rubbery polyurethanes. This work was undertaken, at first, as a limited effort to supply data necessary for interpreting the results being obtained on the permeability behavior of structurally controlled samples. However, it was realized subsequently that there were certain unresolved questions concerning the structural organization of the polyurethanes which were important to an understanding of the mechanical as well as the permeability behavior and the scope of the effort was expanded accordingly. This section has been organized both to summarize data on characteristic parameters that are of general interest and to present some preliminary interpretation of the results in terms of polyurethane structure.

A. Transition Temperature Measurements

The determination of transition temperatures in polyurethanes has been carried out primarily in terms of the mechanical test methods (D-52). Such measurements have identified the presence of two transitions in rubbery polyurethanes; a transition occurring below room temperature associated with vitrification of the sample and a second transition occurring above 100° C where the elevated rubbery plateau modulus undergoes a sharp drop. This behavior is illustrated by modulus temperature curves for two polyester based samples, taken from work by Cooper and Tobolsky (D-20) (Figure D-9), which will be discussed more fully later.

Volume-temperature measurements have also been used for determining the low temperature glass transition (D-57). However, the calorimetric methods have not been used to examine the thermal transitions except in the highest temperature region where a study of decomposition behavior has been carried out by combined differential thermal analysis (DTA) and thermogravimetric analysis (TGA) (D-56). Perhaps the use of the calorimetric methods to explore a wider temperature range of behavior in the polyurethanes has been discouraged by the reported absence of any discernible low temperature glass transition using DTA (D-32).

The limitation of DTA was also noted in some early runs on a polyester based polyurethane in the current work. Therefore, the penetrometer or thermomechanical analyzer (TMA) has been used to explore transitional behavior at low temperatures and the differential scanning calorimeter has been used at room temperature and above. The combined results have proven to be especially useful in defining the various mechanical and associated thermal transitions that can be found in the polyurethanes.

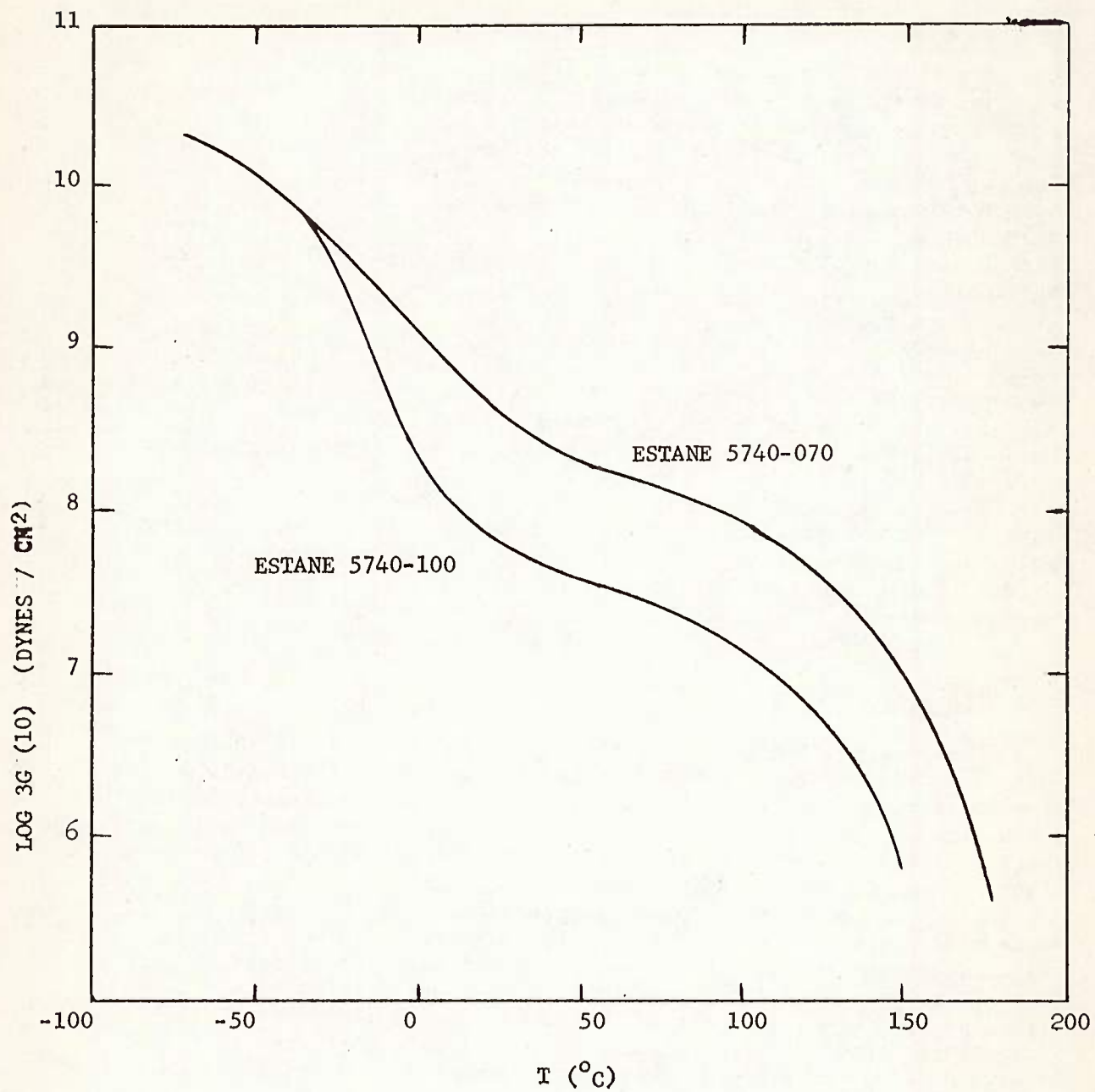


FIGURE D-9. MODULUS - TEMPERATURE CURVES FOR TWO ESTANE POLYESTER TYPE POLYURETHANES. (D-20)

(1) Samples

A series of structurally controlled laboratory grade samples was supplied by the Mobay Chemical Company. The composition of these samples was 3.2 moles MDI, 2 moles of 1,4 butanediol and 1 mole of prepolymer of molecular weight 2000, whether polyester or polyether. The polybutylene adipate (PBA), polytetramethylene oxide (PTMO), polypropylene oxide (PPO) and polyethylene oxide (PEO) based polyurethanes were all supplied as cured 50 to 70 mil sheet. In addition, a semicured 30 mil and a "green" completely uncured PTMO sample were available.

In support of the work on water vapor permeability, thermal transitions were also measured on several commercial samples of incompletely specified composition. The Estane samples 5470-070 and 5740-100 are polyester based elastomers reported to contain 1,4 butanediol, MDI and a low molecular weight polybutylene adipate, with about 39% MDI in 070 and 32% in 100 (D-20). These two samples are of particular interest since modulus temperature data have been published (D-20). The Estane sample 5740-140 and duPont sample LD-550 are both polyether based elastomers probably containing polytetramethylene oxide. The Estane samples 5740-070 and 5740-140 were provided as chopped material in approximately one eighth-inch cubes and the Estane 5740-100 and the duPont LD-550 were 6 to 10 mil films.

(2) TMA Measurements

The penetrometer module obtainable as an accessory to the duPont DTA instrument provides a rapid mechanical test method for determining the location of thermal transitions, including the low temperature transition. Since the displacement of the weighted probe with increasing temperature depends on the opposing effects of volume expansion and the drop in modulus which occurs in a transition region, the location of the transition depends on the sample dimensions, choice of heating rate and on the load of the probe. These several factors were investigated and standard conditions involving sample thickness of 1/16 inch or greater, a heating rate of 5°C/min., and 5 to 20 gm. probe loadings were used. In general, the runs were repeated from three to five times since there was considerable variability in the location of the transition temperature, even though a marked transition was observed in each run.

A representative temperature displacement curve for the Mobay PTMO sample is shown in Figure D-10, and the results obtained on the various polyurethane samples are tabulated in Table D-3. It should be mentioned that these samples were not dried prior to the determinations. There is some evidence that in samples saturated with water, T_1 is displaced by about 2°C to lower temperatures but T_2 is unaffected.

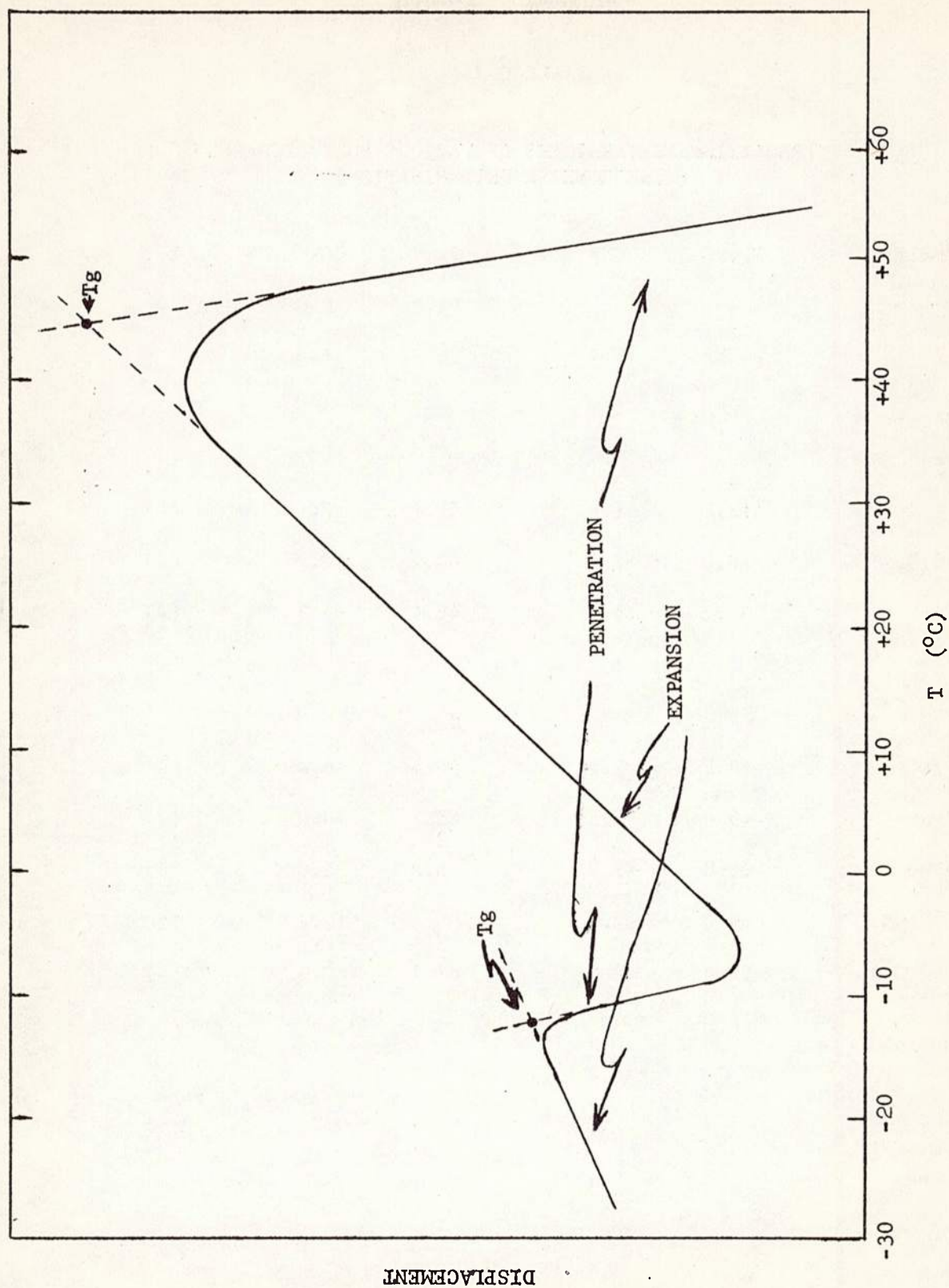


FIGURE D-10. SAMPLE DISPLACEMENT TEMPERATURE CURVE FOR POLYESTER POLYURETHANE OBTAINED WITH THERMOMECHANICAL ANALYZER

TABLE D-3

TRANSITION TEMPERATURES OF VARIOUS POLYURETHANES
(PENETROMETER DETERMINATION)

SAMPLE	T ₁ , °C	90% CONF., °C	T ₂ , °C	90% CONF., °F	T ₃ , °F	T, °C
Polystyrene	—	—	91.8	<u>+2.0</u>	—	—
Neoprene	-46.2	<u>+3.4</u>	28	<u>+1.6</u>	—	—
Polyester Based PU:						
Estane 5740-070	-12.8	<u>+1.6</u>	59.7	<u>+2.1</u>	(-)	—
Estane 5740-100	-18.0	<u>+2.4</u>	60.2	<u>+2.7</u>	(-)	—
Mobay PBA	-45.2	<u>+3.3</u>	46.4	<u>+3.3</u>	(-)	—
Polyether Based PU:						
Mobay PEO	-48.5	<u>+2.1</u>	55.4	<u>+6.4</u>	(-)	—
Mobay PPO	-49.7	<u>+3.5</u>	65.3	<u>+4.0</u>	(-)	—
Mobay PTMO	-85.0	<u>+2.9</u>	56.0	<u>+5.0</u>	153	7.5
du Pont LB-550	-60.0	<u>+2.0</u>	—	<u>+3.8</u>	120	8
Estane 5740-140	-51.4	<u>+2.0</u>	67.7	<u>+2.1</u>	(-)	—

All of the polyurethanes display at least two transitions, one occurring well below 0°C (T_1) and a second (T_2) in the 50 to 70°C range with the single exception of LD-550. This series of measurements was not extended above 100°C except for two of the samples, LD-550 and Mobay PTMO both of which display a high temperature transition (T_3). Since a transition in this temperature range is commonly observed in the DSC results reported in the section which follows, very likely a transition temperature occurring well above 100° would be found in the other samples as well if the TMA measurements were extended to higher temperatures.

(3) DSC Results

A number of the samples were also run on the Perkin Elmer DSC instrument over the range 40°C to 300°C commonly using scanning rates of 10 deg./min. These samples were first dried 16 hours or longer in a vacuum oven at 50°C and single discs which closely fit the sample cup were cut from the films. Typical scans for the Mobay PTMO and Estane PBA (5740-100) samples appear in Figure D-11. The observed transition temperatures are summarized in Table D-4. An indication of the appearance of the transition is given by numbers next to the transition temperature which correspond to examples sketched below the table. In general, the higher the number the more marked the transition.

There appears to be three characteristic transitions which occur above room temperature. The 30 mil Mobay PTMO sample displays a pronounced transition at 152-153°C which corresponds precisely with the transition temperature observed by TMA. All of the other samples display a transition (by DSC) in broadly the same temperature range, 140 to 170°C. In addition, all of the samples display a transition at 80 to 90°C, and it is tempting to identify these with the T_2 transition revealed at 20°C lower temperatures by the TMA. There are also transitions in almost all samples near or above 200°C. In the Mobay PTMO this appears as a fusion peak rather than a displacement in heat capacity.

In addition there are variable and sometimes highly irregular peaks occurring at still higher temperature, manifestations of sample degradation, most of which are not reported.

B. Optical Analysis of Structure

1. Visual Appearance

All of the 50 to 70 mil Mobay polyether based polyurethanes showed turbidity. The PEO was the least turbid, the PPO showed

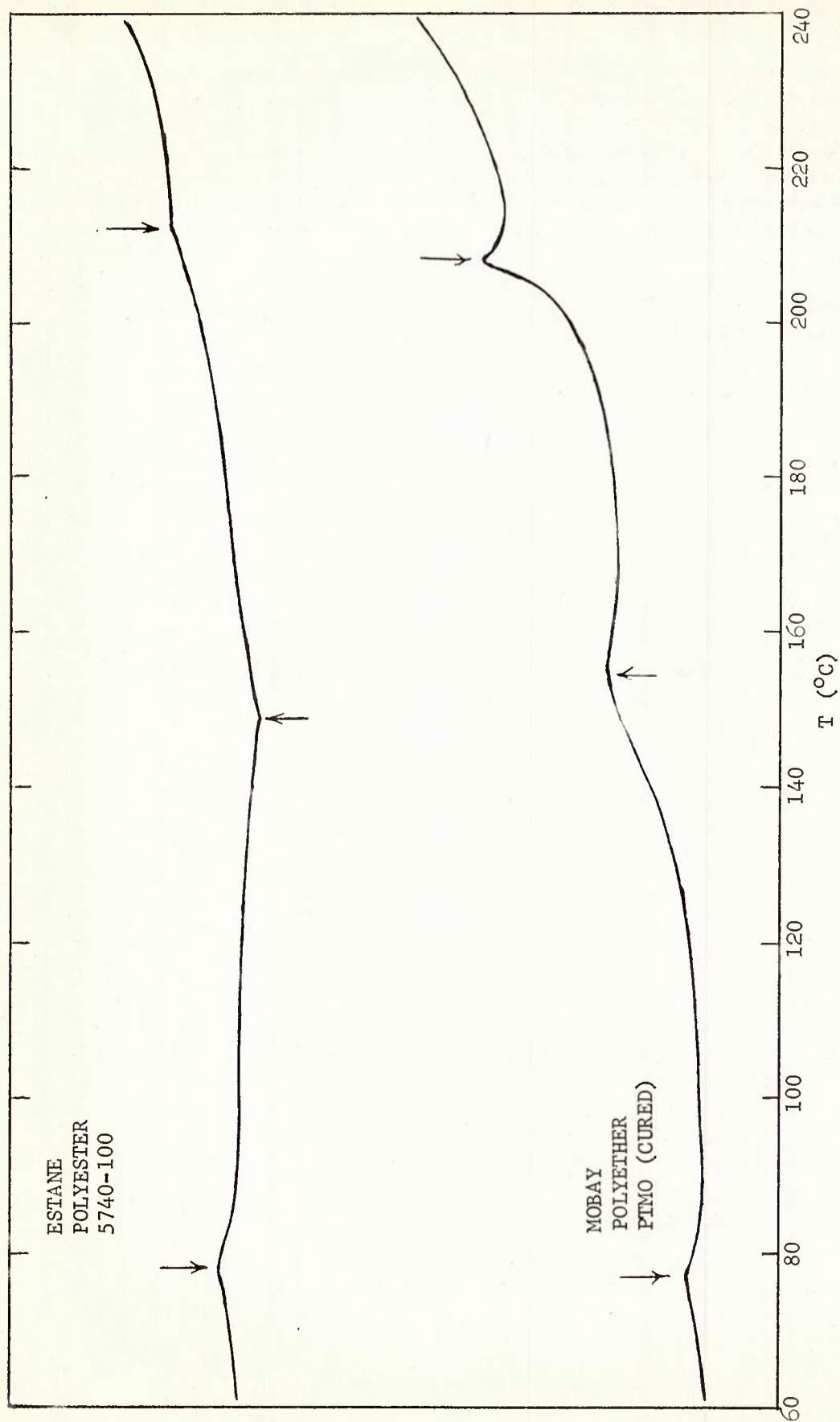


FIGURE D-11. DIFFERENTIAL SCANNING CALORIMETER TRACES FOR A POLYESTER AND A POLYETHER TYPE POLYURETHANE.







TABLE D-4

TRANSITION TEMPERATURES FOR SEVERAL POLYURETHANES
(DSC DETERMINATIONS)

SAMPLE	T ₂ , °F	T ₃ , °C	T ₄ , °F	T, °C
Polyether PU:				
(1) Mobay PTMO 30 Mil Cured Film	82 (3)	152-153 (3)	207-209 (6)	(-)
(2) Mobay PTMO 7-10 Mil Compression Molded, Green Stock	81-83 (3)	162-163 (1)	203-209 (5)	(-)
(3) Mobay PTMO Green Stock	80-83 (1-2)	163-4 (1)	195-200 (5)	(-)
(4) Estane 5740x140 Sections From Cubes	90-92 (4)	152-4 (1) (170 2)	203-205 (3-4)	
Polyester PU:				
(1) Mobay PBA 12-15 Mil Film	82 (3)	167 (1-2)	210 (3-4)	
(2) Estane 5740-100 10-12 Mil Film	79 (1)	155-156 (1)		250-260 (1)
(3) Estane 5710 Sections From Cubes	83-86 (1-2)	150-160 (1)		
(4) Estane 5707 Sections From Cubes	86 (2)	(Smeared out Transition Range 125-140°)		200°C (2)

TABLE D-4 (CONTINUED)

KEY FOR APPEARANCE OF TRANSITION

- | | | |
|-----|---|-----------------------------------|
| (1) |  | WEAK BUT DEFINITE CHANGE IN SLOPE |
| (2) |  | SHARPER CHANGE IN SLOPE |
| (3) |  | WEAK BASE LINE DISPLACEMENT |
| (4) |  | STRONG BASE LINE DISPLACEMENT |
| (5) |  | WEAK DISTRIBUTED ENDOTHERMIC |
| (6) |  | MARKED ENDOTHERMIC PEAK |

appreciably more turbidity but the 30 mil film and green stock were milky. In contrast, the 10-12 mil Mobay PBA sample is clear and even 100 mil thick samples of the Estane 5740-070 and -100 samples were essentially clear. Part of the scattering in the thick sheets was due to surface scattering, but even under conditions where this is minimized there is a high level of bulk scattering especially evident in all the Mobay PTMO samples. The turbidity indicates that variations in internal structure are present which give rise to fluctuations in refractive index on the scale of the wavelength of visible light. This turbidity could result from microscopic voids formed perhaps from moisture present during synthesis. The scrupulous attention given to the exclusion of moisture during the synthesis and casting and the clarity of the Mobay PBA film suggest that the turbidity in the polyether sample is not in fact due to microvoids but to inherent structural entities.

2. Optical Microscopy

Polyether samples were compression molded to obtain films of 7-10 mil thickness for examination by polarization optical microscopy. At high magnification (600 x), well-separated birefringent spherulitic structure up to 8μ in diameter were observed. The use of a Kofler-slot stage showed that extinction (between crossed polarizers) of these structures occurred at about 205°C.

3. Light Scattering Measurements

Light scattering measurements were performed on films coated with immersion oil and sandwiched between cover slips to minimize surface scattering. Patterns were photographed using a low intensity gas laser source (6328Å) and photometric determinations were made using a Brice Phoenix photometer with suitably narrowed collimating and receiver slits.

Measurements were at first performed on the 30 mil Mobay film and on the 7-10 mil compression molded films, but owing to the extremely high level of turbidity in these samples, the scattering behavior was dominated by the depolarization arising from secondary scattering. In no case was there any evidence of the typical spherulitic scattering pattern that might have been expected from the microscopically observed birefringent regions.

Reliable measurements were finally carried out on a very thin (1 mil) solution cast film. This film was free of any evidence of the surface irregularity observed under the microscope in other thin solution cast films. The H_V scattering (measured with polarizer vertical and analyzer horizontal) amounted to about 15% of the V_V

scattering (analyzer and polarizer vertical) over the range of scattering angles from 5° to 40° . This indicates that about 20% of the scattering is due to orientation fluctuations and 80% to fluctuations in density. A Fourier inversion of the scattering data revealed that appreciable correlations in density and orientation persist to distances of well over 1 micron. Since the relative orientation and density correlation functions are completely superimposable, both types of scattering arise from the same structure. It can also be concluded that the contribution of secondary scattering is negligible. There is evidence that the correlation function can be resolved into two distinct regions and the results will be submitted to further analysis to determine whether such an interpretation is warranted.

4. Strain - Optical Coefficient

The birefringence (Δ) was determined at 25°C as a function of strain (α) at low elongations for the Mobay PTMO and PBA samples. The results are summarized in Table D-5 and compared with reported values for natural rubber and polyethylene.

It is evident that the strain optical coefficient (Δ/ϵ) is closer to the value of polyethylene than to that of natural rubber and even higher in the clear polyester than in the turbid polyether sample. This could be interpreted as indicating that the birefringence in these polyurethane samples arises from the orientation of anisotropic structural entities, as in polyethylene, rather than from molecular chain orientation as in natural rubber.

However, the stress optical coefficients (Δ/σ) for both polyurethane samples are in the same range as that of natural rubber. The correspondence in Δ/σ , in contrast to Δ/ϵ values, is due to the higher modulus values of the polyurethane samples.

5. X-ray Diffraction

The X-ray diffraction pattern of the unoriented Mobay PBA as well as the PTMO sample showed only an amorphous halo. The polyether at an extension ratio of 4.5 showed a crystalline pattern consisting of three prominent but diffuse equatorial maxima. The weaker layer line spacings present in oriented crystalline polytetramethylene oxide (D-19) were absent in the oriented polyurethane sample. The polyester sample at an extension ratio of 3 showed two diffuse equatorial maxima and, again, no evidence of layer line spacings. No patterns were taken of samples at any other extensions.

DISCUSSION

The multiple thermal transitions observed in the polyurethanes are evidence of discrete changes in the structural organization and perhaps

TABLE D-5

SUMMARY OF OPTICAL - MECHANICAL DATA

SAMPLE	E (kg/cm ²)	$\Delta/\epsilon \times 10^2$	$\Delta/\sigma \times 10^4$ (cm ² /kg)
Mobay PTMO*	95	1.29	1.36
Mobay PBA*	157	2.4	1.53
Natural Rubber**	10***	.2***	1.95
Polyethylene**	150x10 ²	3	0.02

* Measured values

** Literature values

*** Depends on degree of cross-linking

in molecular structure that occur with increasing temperature. Evidently T_1 is the vitrification temperature or low temperature glass transition that has also been observed by mechanical and volume expansion measurements (D-57, D-52). Since T_1 increases with concentration of the aromatic diisocyanate (D-57), it is difficult to make comparisons of these results with others reported in the literature. However, the values for the two polyester based Estane samples compare favorably with values of -10°C for 5740-70 and -23°C for 5740-100 estimated from the modulus temperature curves obtained by Cooper and Tobolsky (D-20). Furthermore, the trend of T_1 values for the polyethers is consistent with Dickinson's observation that PTMO based samples have the lowest T_g while the T_g values for the other two polyether based samples are similar but substantially higher (D-25). The relative values of T_g for the three Mobay polyether samples, however, differ from the temperature of the mechanical loss peak at 1 C/S reported as -55°C for PEO, -60°C for PPO and -74°C for PTMO, all determined on high molecular weight polyether samples (D-60). The differences are not unidirectional. They might be due to several factors including: (1) the influence of crystallinity on the T_g of the polyethers; (2) the effect of low prepolymer molecular weight on the T_g of PTMO-measured by TMA, and PPO - determined by extrapolation to zero urethane content (D-57); (3) the influence of the aromatic urethane regions.

The transitions identified by TMA at $50-60^\circ\text{C}$ (T_2) and by DSC at $80-90^\circ\text{C}$ (T_2) and at $140-160^\circ\text{C}$ (T_3) are more difficult to assign. Since there is no transition observable by DSC from 40 to 80°C and, correspondingly, no transition found by TMA from 60 to 100°C , it seems logical to conclude that, in fact, the T_2 transition observed by DSC is the counterpart of the T_2 transition revealed by TMA but shifted -20°C , perhaps as a result of the decline in modulus with temperature which occurs even over the plateau region of the mechanical data. However, even with this simplification the problem remains that there is no evidence in the mechanical data for any transition occurring over the temperature range $50-90^\circ\text{C}$ which, in fact, corresponds to almost the middle of the rubbery plateau region (D-20). Further evidence on the nature of this transition will be discussed after considering the transition T_3 .

On first consideration the assignment of T_3 appears uncomplicated. The sharp decline in the elevated rubbery modulus of the polyurethanes usually occurs in the range of T_3 . As an example, Cooper and Tobolsky's data on the Estane samples are consistent with a transition temperature above 120°C while the transition temperatures of the Mobay polyester samples which he studied occur somewhat above 150°C . The nature of this transition remains controversial. The transition has been discussed in terms of a dissociation of the strong secondary bonding forces between aromatic urethane regions of the chain. These interactions are responsible for many of the properties which distinguish polyurethane elastomers from

covalently crosslinked rubbers, including reversible elasticity in linear and, therefore, thermoplastic polymers and advantageous mechanical and ultimate properties. The bonding has commonly been ascribed to pairwise intermolecular hydrogen bonding (D-36, D-57). More recently, Cooper and Tobolsky have suggested that an association of the soft and hard segments of the polyurethane chains occur in analogy with the behavior of styrene/isoprene block copolymers. In this latter system, specific interaction forces are clearly of less importance than the organization of the styrene and isoprene segments into regions large enough to give rise to two distinct glass transitions. It is clear from their model that Cooper and Tobolsky regard T_3 as the glass transition concerned with the aromatic urethane segments.

However, there is evidence that an alternative assignment for T_3 is more appropriate. It has been suggested that T_3 corresponds to the temperature at which allophonate bond dissociation occurs (D-64). In keeping with this explanation, it has been noted that below 150°C the polymer acts as though it were lightly crosslinked since an irregular extrudate is produced, but above 150°C a smooth uniform extrudate is obtained (D-64). It has also been noted in the current work that this transition is somewhat weaker in the green PTMO stock (see Table D-4).

If the assignment of T_3 as the temperature of allophonate bond dissociation is correct, then T_2 can be identified as the transition which represents the dissociation of a secondary bonded network. This is consistent with the dissociation temperature of low molecular weight urethanes (D-64). There is still the need to account for the absence of an equally distinct mechanical transition at T_2 . Perhaps this is a result of a gradual softening below the transition, as evidenced by the decline of the modulus and, additionally, the persistence of polar interactions which restrain segmental motion above the transition. Evidently, the relation between the mechanical behavior and thermal transition needs further consideration.

Finally, at 200-210°C there is a transition (T_4) especially prominent in the PTMO sample. Although this is approaching the temperature of urethane bond dissociation, (D-55, D-56) the transition in PTMO is definitely connected with the spherulitic regions which melt out at this temperature. These high melting regions are probably composed of aromatic urethane segments which have crystallized as the results of association either in the intact polymer or following some chain scission under molding conditions. The high temperature appears consistent with the 230°C melting point reported for the urethane formed from *m*-toluenediisocyanate and hexanethylene glycol (D-51). It is not expected that there would be any contribution to the X-ray pattern from these regions since the concentration, estimated from the heat of fusion per gram reported for polymers, is only about 1-5%.

The high value of the strain optical coefficient reported in Table D-5 coincides with the high modulus for these elastomers and it appears that this cannot in itself be taken as evidence for domain structure any more than the modulus values. However, if proof of such domain structure can be obtained, then the strain optical coefficient in conjunction with bond polarizabilities for the constituent groups might yield some further information about internal organization.

The onset of crystallinity with sample extension indicates that this process must be taken into account in understanding the stress-strain curve and the ultimate tensile properties for these polyurethanes. Although references have been made to the occurrence of crystallinity in polyurethanes with high molecular weight polyether or polyester segments (D-52), there does not appear to be any published work dealing with the effect of orientation-induced crystallinity on the mechanical properties.

PART III

PERMEATION OF WATER VAPOR THROUGH A POLYURETHANE MEMBRANE

THEORY AND REVIEW OF LITERATURE

A. Definition of Terms

Diffusion has been defined as the process in which components are transported from one portion of a system to another as a result of a concentration gradient (D-9,-50). The coefficient of the rate equation describing the permeation or flux is called the diffusion coefficient and is usually represented by the symbol D . One of the main interests in the study of diffusion is the evaluation of the diffusion coefficient for a given system as a function of such parameters as penetrant concentration and temperature. Two experimental methods which are typical for this purpose are the "sorption" method and the "permeation" method.

McClaren (D-43) defines adsorption as the process by which molecules are attached to sites on the surface of a solid; the surfaces include not only the external surface, but also the internal surfaces about molecular groups. Absorption is the process whereby the penetrant and solid form mixtures similar to actual solutions (D-43). The total uptake of penetrant by a solid has been termed sorption by McBain (D-40) and may include both absorption and adsorption. The process of sorption of a vapor is considered to involve two stages: condensation of the vapor onto the solid followed by solution of the

condensed vapor (D-3,-12). In the usual "sorption" experiment, a film of a solid is exposed to vapor of a given penetrant substance at a given pressure, and the gain or loss in weight of the film is measured as a function of time (D-30,-39). In a permeation experiment, the amount of penetrant vapor flowing through a film is measured as a function of time under the condition that one surface of the film is allowed to come in contact with penetrant vapor at a constant pressure, and the other surface is exposed to a vacuum or lower pressure (D-30).

The equilibrium concentration is defined as the amount of penetrant held in the film per unit weight of dry film at equilibrium. The solubility or solubility coefficient can be defined as a ratio of the equilibrium concentration to the partial pressure of the vapor in the gas phase. This solubility coefficient is similar to Henry's Law coefficient.

B. Development of Equations

Fick's diffusion equation or Fick's second law of diffusion applied to one dimensional flow is generally taken as the basis for analyzing data of diffusion (D-34). Fick's equation is analogous to the Fourier heat flow equation:

$$\partial C_i / \partial t = \partial (D \partial C_i / \partial x) / \partial x \quad D-3$$

where C_i is the concentration of the penetrant, t is time, and D is the diffusion coefficient.

The methods of evaluating D from kinetic behavior during sorption, i.e., unsteady state, have been examined in great detail by Crank (D-21,-22) and co-workers (D-23,-24). When D is a function only of C , the behavior is said to be "Fickian", (D-45) and the diffusion equation can then be solved so as to relate the diffusion coefficient with the amount of vapor taken up by or remaining in the sample at any time.

It is the practice to regard a given sorption curve as "Fickian" when it has the following features (D-30):

1. Both sorption and desorption curves (fraction uptake or loss versus the square root of time) are linear in the region of small value of the time.
2. Above the linear portions both sorption and desorption curves are always concave to the time axis.

The solution of Fick's diffusion equation for sorption of a gas or vapor in a thin sheet of solid for the case where the sheet is initially at a uniform concentration C_0 , and the surfaces are kept at a constant concentration C_1 is:

$$M_t/M_\infty = 1 - (8/\pi^2) \sum_{n=0}^{\infty} 1/(2n+1)^2 \exp(-(2n+1)\pi/l)^2 Dt) \quad D-4$$

M_t is the amount of sorbent taken up at time t , for a film of thickness l , and M_∞ is the amount taken up at equilibrium.

For the case where D is independent of C , the following approximations can be made: for small values of time where M_t/M_∞ is much less than 0.5,

$$M_t/M_\infty = (4/\pi^{1/2}) (Dt/l^2)^{1/2} \quad D-5$$

For Fickian behavior, a plot of M_t/M_∞ versus $t^{1/2}$ is initially linear with a slope of $(16D/\pi)^{1/2}$. If $t_{1/2}$ is the time at which $M_t/M_\infty = 0.5$ then, (D-22)

$$D = 0.04939/(t/l^2)_{1/2} \quad D-6$$

and for large values of time (t) (D-45,-49) where M_t/M_∞ is greater than 0.4

$$M_t/M_\infty = 1 - (8/\pi^2) \exp(-\pi^2 Dt/l^2) \quad D-7$$

which can be rewritten as,

$$\ln(M_\infty - M_t) = K - \pi^2 Dt/l^2 \quad D-8$$

A plot of $\ln(M_\infty - M_t)$ versus t approaches a straight line at values of M_t/M_∞ greater than 0.4. The slope of this straight line equals $D\pi^2/l^2$.

The concentration, C , is related to the vapor pressure by, (D-49)

$$C = Sp \quad D-9$$

where S is the solubility.

C. Effect of Variables

Diffusion and the diffusion coefficient are affected by many factors, which can be classified into four categories: (1) solid related factors, (2) penetrant factors, (3) conditions of the environment surrounding the penetrant-solid system, and (4) penetrant-solid interactions.

Chemical changes in a polymer may have a pronounced effect on the diffusivity. Any factor which tends to change the polymer chain segment mobility or density, such as the addition of side groups or chains in double-bond formation, will affect diffusion rates (D-3,-6). The molecular weight and structure of the penetrant molecule will also affect the diffusivity, i.e., the smaller and simpler molecules will diffuse through a polymer system much easier and, therefore, faster. (D-2,-11, -30,-46,-48) The diffusivity generally increases with increasing similarity between the components. (D-49) The diffusion coefficient of a polymer penetrant is generally dependent on the concentration of the penetrant in the polymer (D-2,-22,-24,-35,-44,-48) and sometimes exhibits a time dependency. (D-22,-44) The temperature dependence of the diffusion coefficient has been found to follow an Arrhenius-type equation (D-3,-6,-8,-12,-35,-49) of the form,

$$D = D_0 \exp(-E_D/RT) \quad D-10$$

where E_D is the apparent activation energy for diffusion, R is the universal gas constant and T is the absolute temperature.

The magnitude of the solubility is also affected by several factors. It has been found to also follow an Arrhenius-type equation, (D-8,-13)

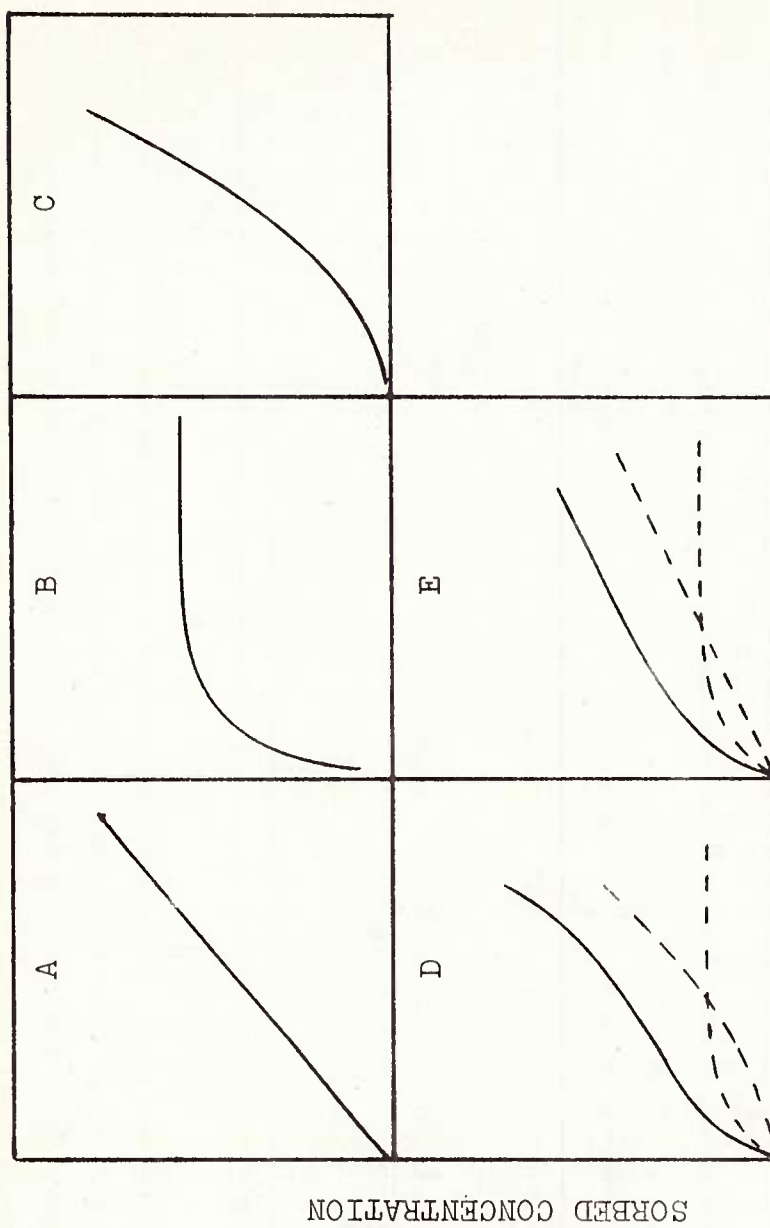
$$S = S_0 \exp(-\Delta H_s/RT) \quad D-11$$

where ΔH_s is the apparent heat of solution. Affinity of the penetrant for the polymer, molecular weight, size and structure affects the solubility. The swelling of the polymer by the penetrant changes the internal structure and also the solubility coefficient. (D-2,-13,-18,-29)

D. Theoretical Models of Sorption

A sorption isotherm is a curve which relates the equilibrium concentration of penetrant in the solid to the concentration of the penetrant in the surrounding environment at any constant temperature. One of the first demands of a theory of sorption is that it gives an experimentally correct sorption isotherm. Once the sorption is described, the diffusion behavior of a system can be partially, if not fully explained.

There are three basic types of isotherm commonly discussed. They are represented as types A, B, and C of Figure D-12. These three, and their combinations, form the bulk of the theories developed to date. Type A is the Henry's Law isotherm where the concentration of penetrant in the solid is linearly dependent upon the pressure. A type B isotherm is characteristic of a system where only a monolayer



PRESSURE OR ACTIVITY

FIGURE 12 TYPES OF SORPTION ISOTHERMS

of sorbed substance is formed on the polymer surfaces. The Langmuir equation (D-11,-40) is a simple relation leading to a type B isotherm, and it is probably the best known of all isotherm equations. This is largely due to its simplicity, of the physical picture behind it, and partly because a great many experimental isotherms fit the theory reasonably well. (D-1) The solubility coefficient from the more common form of the Langmuir equation can be written:

$$S = C/P = bC_m/(1 + bP) \quad \text{D-12}$$

The maximum possible sorption of the completed monolayer corresponds to a concentration of C_m adsorbed on localized sites and b is a parameter characteristic of the system. At low pressures, Langmuir's equation reduces to a form of Henry's Law isotherm.

The principal assumptions contained in the Langmuir equation (D-1) are:

1. The energy of adsorption is constant, which implies uniform sites and no interactions between adsorbate molecules.
2. The adsorption is on localized sites, which implies no translational motion of adsorbate molecules in the plane of the surface.
3. The maximum adsorption possible corresponds to a complete monolayer.

The type C isotherm is observed when the forces between the penetrant and the polymer are relatively small. A semiempirical equation that describes a type C isotherm as found by Rogers (D-49) is that one usually attributed to Freundlich. (D-1,-28)

$$S = S_0 \exp(\sigma C) \quad \text{D-13}$$

σ is a parameter characteristic of the polymer-penetrant pair at a given temperature.

The Brunauer, Emmet, and Teller equation was developed (D-17) mainly to account for multilayer adsorption which results in type D isotherms. The equation was derived on the assumption that the Langmuir equation could be applied to each layer. In its usual form the heat of adsorption of the first layer, Q_1 , is assumed different from that of subsequent layers. The heat of adsorption of the second and subsequent layers is assumed to be equal to the heat of vaporization of the pure liquid penetrant, Q_L . The expression for the solubility coefficient

is:

$$S = c/p = \beta C_m / (p_o - p) [1 + (\beta - 1)p/p_o] \quad D-14$$

where p_o is the saturated vapor pressure and is approximately $\exp(Q_1 - Q_L)/RT$. (Dole (D-25) has stated that a statistical analysis shows that this is not valid although it does work in some cases.) The BET equation can also predict the isotherms of types B and C depending on the relative magnitude of Q_1 and Q_L . There are also many variations and adaptations of the BET isotherm equation. (D-1, -49)

Several other isotherm equations have been proposed to account for the type D and E curves observed for sorption in polar systems. These relations are based on the concept that there are at least two different modes by which the entering penetrant is sorbed. For example, a relation which is essentially a combination of a Langmuir or BET-type adsorption isotherm and a lattice theory isotherm has been proposed by Hill and Rowen. (D-37) Another interpretation of the type D isotherm considers that it is the result of two simultaneous sorption processes. (D-49) One process, dominant at low penetrant concentration, corresponds to a type B isotherm due to preferential sorption of penetrant onto a limited number of active sites in the solid, and the other process is a type C sorption.

The data of Michaels, Vieth, and Barrie (D-47) for the sorption of gases on crystalline polyethylene terephthalate corresponded to a type E isotherm. A combination of a type A, Henry's Law isotherm, and a type B, Langmuir isotherm, was found to qualitatively explain the resultant curves.

The interpretation given to an experimental sorption isotherm can help greatly in the analysis of concentration dependent diffusion coefficients. The diffusion coefficients of organic vapors in polymers usually increase as the penetrant concentration is raised. With water vapor as the penetrant, the normal concentration dependence has been found to be less marked and quite often shows no concentration dependence. Even more striking is the inverse dependence found in polymethylmethacrylate, (D-14, -31) silicone rubber (D-14) and ethyl cellulose. (D-11, -59) This inverse concentration dependence is interpreted in terms of clustering of the water molecules which renders an ever-increasing proportion of the overall concentration relatively immobile. A model has been developed by Gordon and his colleagues (D-33) to evaluate the fractions of polymeric water present in the polymer. Barrie and Platt (D-14) have derived relationships from Gordon's model and combined them with the diffusion equation to describe the magnitude and form of the concentration dependence of the diffusion coefficient.

Zimm and Lundberg (D-63) have presented a clustering function that does not predict sorption isotherm but interprets them in molecular terms. It was derived mainly to describe the gross changes in the limiting value of the activity coefficient from system to system. A relation between the cluster integral and the activity coefficient has been derived by Zimm (D-62) which allows a simple calculation of the mean number of penetrant molecules in excess of the mean concentration of penetrant molecules in the neighborhood of a given penetrant molecule, in other words, the clustering tendency of the sorbant.

EXPERIMENTAL WORK

A. Equipment

A gravimetric, sorption-desorption technique was used to study the diffusion and solubility behavior of water vapor in a polyester-based polyurethane. A sorption balance of simple design developed by McBain and Bakr, (D-42) which consists of a sensitive helical quartz spring suspended in an all-glass thermostated jacket, is the most widely used system for this purpose. The accuracy of this system is limited by the time required to measure the extension of the spring with a cathetometer. This could be a significant factor in systems with a high diffusion coefficient. Therefore, a Cahn Electrobalance was used in this study since the output can drive a recorder to provide a continuous record of the weight changes. This system not only provides greater versatility and accuracy, but is easily adapted to vacuum work since a glass vacuum bottle accessory allowed the balance to be operated in a vacuum system. The model RG 2000 Electrobalance has a rated sensitivity of 0.1 micrograms and a capacity of 2.5 grams with full-scale recording ranges of 0-20 micrograms to 0-1 gram. The recording range may be changed while weighing, thus making the balance adaptable for various ranges of sample size and solubility.

The Cahn balance was designed for a one millivolt recorder, and this sensitivity is required for rated balance sensitivity, but higher voltage spans can be used with lowered sensitivities. For this reason, the Moseley model 7100B, two-pen, strip-chart recorder was used. It had a variable calibration of one millivolt up to ten volts full scale for both pens. Also, the chart speed may be varied from one inch per hour to two inches per second. High-speed response and a wide strip chart made this recorder very versatile as it was able to accurately record both the very slow and very quick impulses from the balance with readable results.

The sorption system, as shown in Figure D-13, was contained in a Thelco Model 6 oven which was large enough to contain that portion

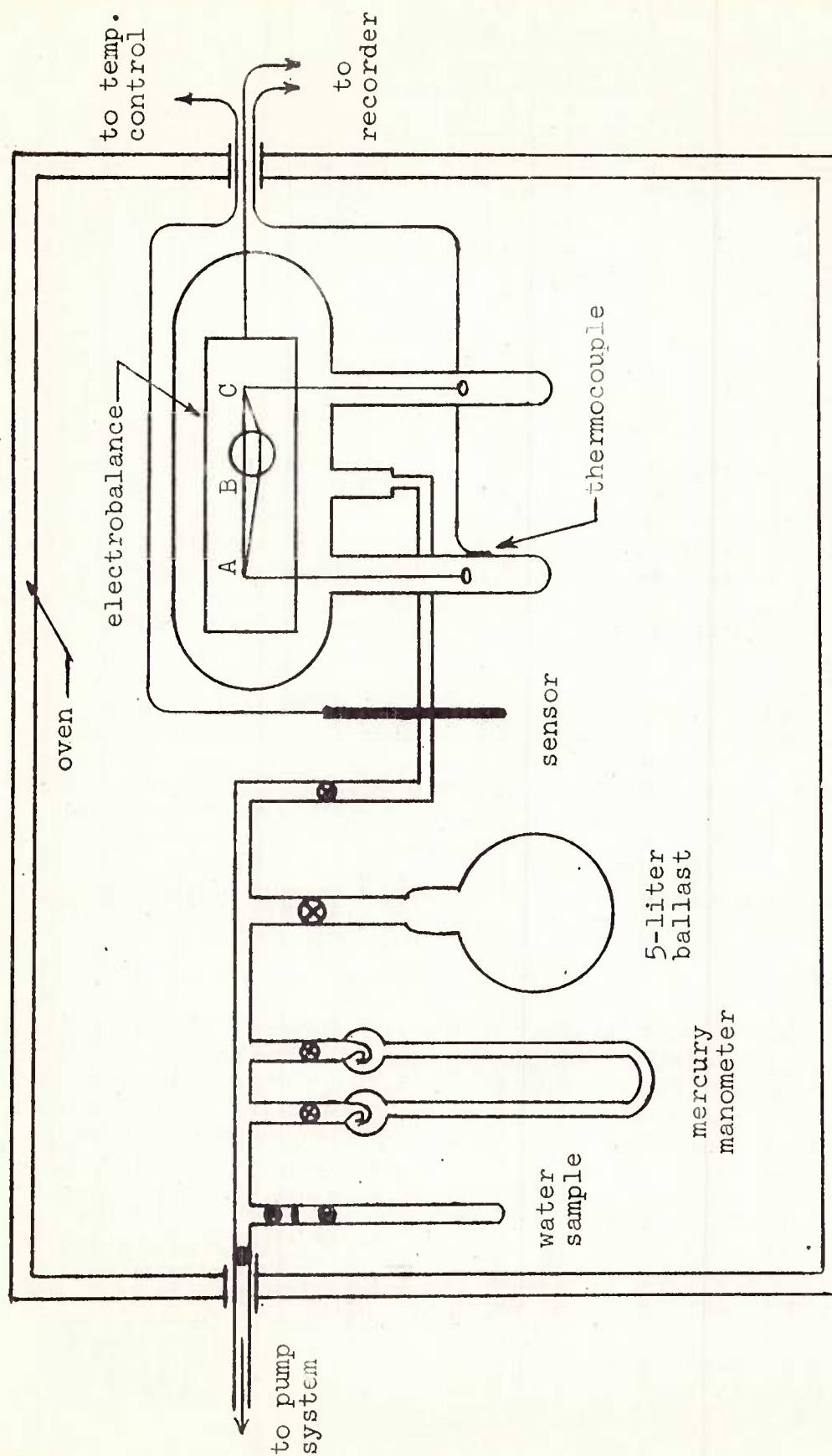


FIGURE D-3 HIGH VACUUM SORPTION APPARATUS

of the system which required isothermal conditions. Glass doors enabled observation of the system without excessive heat loss. The heat was distributed by natural convection because the vibration of blowers or fans of forced convection ovens would interfere with the sensitive operation of the balance. The temperature was monitored by a copper-constantan thermocouple placed on the sample tube of the balance. Its output was recorded on the second channel of the recorder. Thus, a simultaneous time record was obtained of both the temperature of the sample, and the weight changes of the sample. After a few trial runs, the temperature control of the oven was found to be unsatisfactory and a Fisher Proportional Temperature Controller was installed. The sensing element was a thermistor encased in a stainless steel tube suitable for use in a temperature range of 0-150°C. A time constant of less than one second gave the controller a sensitivity of 0.01°C because the added resistance to heat flow of the glass would tend to further dampen temperature fluctuations allowed by the controller.

A five-liter ballast flask was incorporated to minimize the effect of the sorption or desorption of vapor by the sample on the total pressure. The pressure of the vapor was measured with a U-tube mercury manometer which was read with a cathetometer accurate to a tenth of a millimeter.

The vacuum pumping system was used to eliminate the air in the system and thus obtain an accurate dry weight. All measurable quantities of gases within the system had to be removed so that only one component, water, was involved. Figure D-14 is a schematic diagram of the pumping system. The roughing and fore pumps were two-stage mechanical pumps.

The film thickness was measured with a dial-type thickness gauge which had divisions of 0.5 mils up to its capacity of 22.9 mils.

B. Procedure

1. Preliminary

Preparation of the water and polymer sample was an important part of the procedure and careful attention to details was necessary to insure reliable and reproducible results. Degassed, demineralized water was used as a penetrant. The water was degassed by first freezing it, and then by evacuating the air space above. This process was repeated until no increase in pressure was noticed when the sample tube was opened prior to evacuation. The size and weight of the polyurethane sample was limited by the restrictions placed by the balance and the diffusion process itself. The more sensitive position of the balance beam required the sample to weigh less than one gram and restricted its weight variation to less than 200 milligrams.

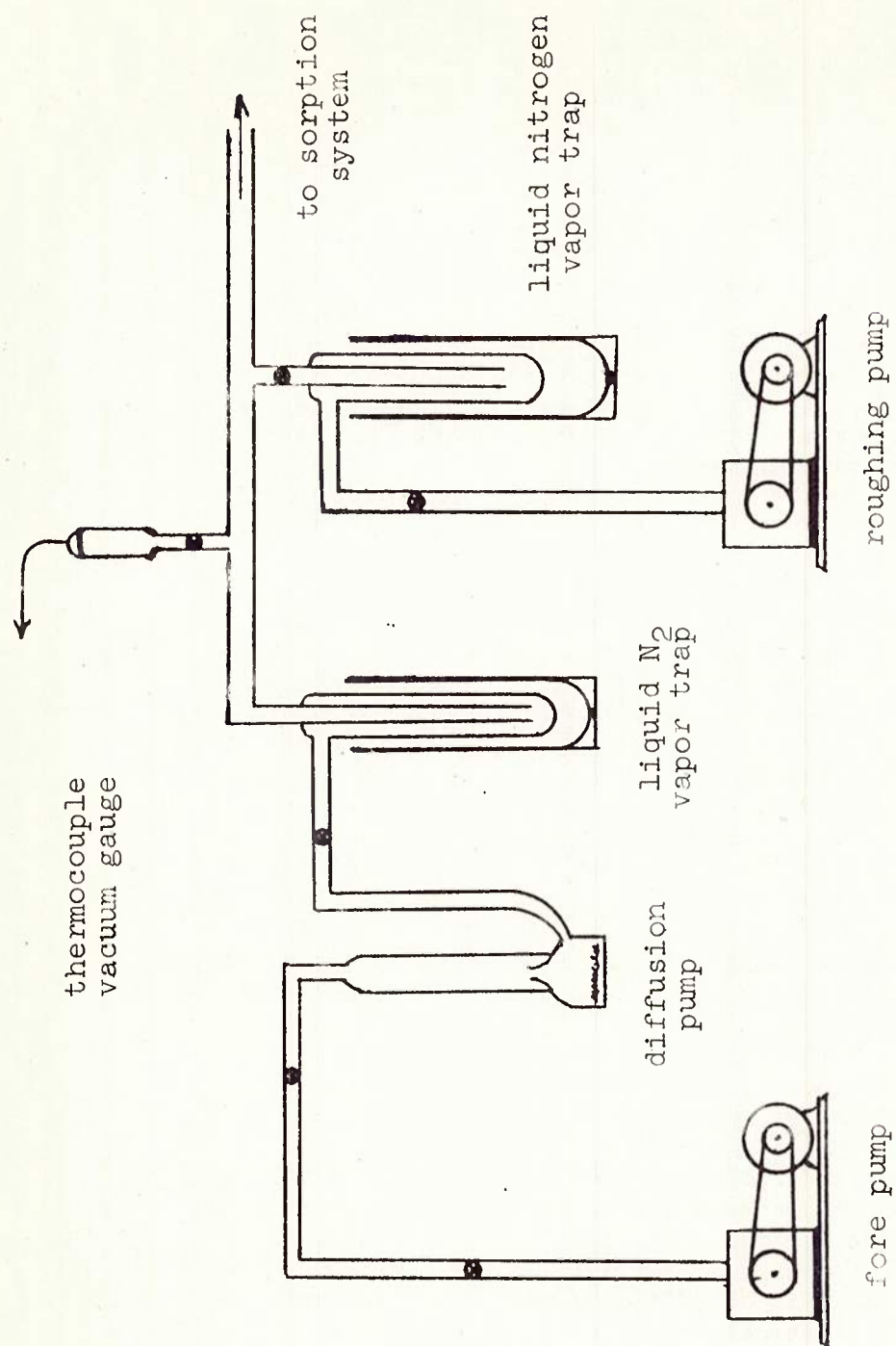


FIGURE D-4: HIGH VACUUM PUMPING SYSTEM

The kinetics of the diffusion process itself placed some limits on the thickness of the film sample. From an examination of the diffusion equations used (Equations D-5,D-6,D-8), it is apparent that the amount of time necessary to complete a sorption or desorption cycle is governed by the film thickness; the thinner the film, the faster the sorption to equilibrium. If the system reacted very quickly, i.e., half-time of less than 20 seconds, great attention must be paid to accurate time records. On the other hand, very long half-times would limit the number of runs which could be made. Also, it must be remembered that the diffusion was assumed to take place in one dimension only, and thus edge diffusion must be insignificant.

From initial tests on the sample material, it was decided that a 10-15 mil thickness would be appropriate for the test equipment. The test sample was cut into a 1 x .5 inch piece, and the surface cleaned with carbon tetrachloride to remove impurities resulting from its preparation and handling. Ten thickness measurements were taken across the surface of the film and the average of 12.35 mils was used in the calculations. The sample weighed approximately 135 milligrams. The calibration of the balance required a prior knowledge of order of magnitude solubilities and the weight of the sample in order to get the most accurate results. Detailed instructions in the manual provided with the balance made the calibration procedure straightforward. The balance was calibrated open to the atmosphere.

After the calibration was completed, the sample was suspended from a 0.1 millimeter nichrome wire in hangdown tube A (Figure D-13). The system was sealed and the sample was outgassed. The outgassing was continued until no weight change was noticed on the most sensitive scale. The weight of the outgassed sample was then used as the dry weight for all calculations.

2. Measurement Procedures

There are two methods used by experimenters in the study of the kinetics of sorption (D-24,-30). In the integral method, a sorption is always followed by its complementing desorption, and the concentration of the penetrant in the sample at the start of the sorption and at the end of a desorption is always zero. In a study of concentration dependence using the integral method, the concentration change gets very large as the average concentration studied increases. The second method, and the one used here, is called the interval method. The interval method is a progression technique, where each new sorption or desorption begins where the previous one finished. This means that the concentration interval can remain as small as desired and will not be a factor influencing the solution of the equations. Also, the smaller the increment, the more closely the calculated diffusion coefficient approaches the point value.

The procedure followed for taking data was a fairly simple one. Because of the known volume distribution between the ballast and balance, the pressure of the vapor required in the ballast could be calculated and preset. Water vapor was added to the ballast tank from the reservoir to the previously determined pressure and the reservoir then closed off from the system. Any opening and closing of valves involved opening the oven door with a resulting temperature drop, but if it were done quickly and with a quick response from the temperature controller, temperature variations were minor. During the run, they were insignificant. When the temperature of the system had returned to the preset condition, the valves connecting the ballast and the balance were opened, and the sample was exposed to the new pressure of water. Periodically, the pressure of the system was read and recorded on the chart. The chart speed was varied for easiest reading of results and varied from two inches per minute to two-tenths of an inch per minute. The variation of speed as the experiment progressed also prevented an accumulation of paper with little information on it.

When the sample reached a steady state with no additional sorption of vapor, the balance was closed off from the ballast and preparation was made for the next sorption test. Rogers (D-49) suggests that steady state is attained in the practical sense when there is no sensible change in weight over a time interval comparable to the interval required to attain that value. The desorption procedure was essentially the same except that the water vapor was removed from the ballast by means of the liquid nitrogen trap and vacuum pump to a previously determined pressure.

During the sorption cycles, a drop in pressure of approximately 0.5 millimeters of mercury was noticed during the early portions of the run. This was attributed to the sorption of water by the glass. At the lower pressures, this drop was sometime significant, but the sorption data in this range could be neglected because the corresponding desorptions did not display this drop in pressure and gave the required information. In addition, a further check was provided in that each series of sorptions and desorptions at one temperature was duplicated.

CALCULATIONS

A. Data Collected

The actual data collected for each interval of sorption or desorption consisted of the weight change versus time with the corresponding temperature and pressure as recorded on the strip chart. Other data necessary for the calculations included the vapor pressure of water at the operating temperature, the dry weight, and the thickness of the sample.

B. Data Preparation

A Gerber Analog Data Reduction System 4, is capable of reducing a strip chart of graphical information to digital sets of numbers with a 0.01% accurate analog to digital electrical conversion. By means of a scanning head, with potentiometric output through a digital voltmeter, the data are transposed to a typewriter and/or keypunch. For the analysis of the Cahn sorption data, the Gerber instrument at NLABS was

calibrated to distinguish 100 units per inch for both the x (time) and y (weight) coordinates. With this sensitivity setting and by the manual setting of the cross hairs on the strip chart trace, the output of the Gerber System was reproducible to 1 unit.

The strip chart was reduced to computer cards which were used as the input to a General Electric 225 digital computer for the first analysis of the data.

C. Calculations

A computer program was written to facilitate the analysis of the mass of experimental data taken with the sorption system. It processed the raw data and calculated the diffusion coefficient of the sample by three alternate methods. The program also calculated the equilibrium concentration and the solubility of the sorbed component in the film.

The diffusion coefficient was calculated from the solution of the diffusion equations (see Equations D-5, D-6, D-8) assuming concentration independence and no swelling. It was believed that the small concentration intervals used would nullify the effect of any concentration dependence shown by the sample.

Different values of \bar{D} (the mean diffusion coefficient) were determined for each of the three stages of sorption; less than 50% complete, 50% complete, and more than 40% complete. The equation

$$M_t/M_\infty = (4/\pi)^{1/2} (\bar{D}t/l^2)^{1/2} \quad \text{D-5}$$

is applicable for the solution of a relative weight gain or loss of less than 50%. From the input data, the computer calculated M_t/M_∞ versus $t^{1/2}$, and by the method of least squares calculated the equation of the best straight line through the points. The slope of this line is $(16\bar{D}/\pi)^{1/2}$. A listing of the residuals provided an indication of the accuracy of the fit. The data of some preliminary runs were plotted and the lines calculated by hand. It was found that this line did not go through the origin. After some consideration, the non-zero origin was attributed to an experimental condition that shifted it by a small amount. This was a result of not having an instantaneous pressure increment and also possibly due to the effect of having the vapor stream entering directly below the balance beam, thereby causing a temporary movement of the beam. The computer program was rewritten to accommodate a shift in the origin. The calculation of \bar{D} at 50% sorption was a straightforward solution of Equation D-6 with t at $M_t/M_\infty = 0.5$. For \bar{D} at more than 40% sorption, a least square straight line was calculated for the data of $\ln(M_\infty - M_t)$ versus t . The slope of this line is equal to $D\pi^2/l^2$.

The equilibrium concentration at each pressure was calculated on a dry weight basis; i.e., the sum total of water sorbed at the end of each pressure increment divided by the dry weight of the film sample.

$$C = \sum M_{\infty} / M_0 \quad D-15$$

where M_{∞} is the weight of water sorbed and M_0 is the dry weight of the film. The solubility was calculated using the relation

$$S = C/P \quad D-9$$

where C is the equilibrium concentration and p is the partial pressure.

D. Sources of Experimental Error

There were several possible sources of error in the experimental procedures. Some were due to inaccurate measurements and others due to the inherent error of the solution of a concentration dependent D by an equation derived for a concentration independent D . The error introduced by the latter source was reduced to a negligible value by the use of small concentration increments.

Errors introduced by the balance and/or the recorder were deemed negligible for the following reason. The balance could give inaccurate readings due to a failing in the electronic circuit, but this would cause erratic behavior not possibly accountable to the sample. Therefore, that data would not be used. A zero shift in the recorder is a most frequent source of error. By using the weight changes of the sample and not the absolute weight in the calculations, this error was eliminated.

Temperature control was such that no change in the thermocouple trace could be observed after a run was started. Pressure changes were noticed and caused some error at the low concentrations in the sorption cycle. Water vapor is introduced or added to the balance bottle for the sorption cycles. During the first one or two minutes, the pressure dropped five or six tenths of a millimeter of mercury. It was shown that the equipment was sorbing some of the vapor as the pressure dropped when water was introduced in the system, even in the absence of a film sample. As this drop always was of the same magnitude, it had a much greater effect on the analysis at low partial pressures, since it was a larger percentage change. For this reason the data for sorption in the low pressure range were neglected and only that of the corresponding desorption test was used.

Due to a fault in the design of the equipment, a temporary shift in the recorder trace was observed at much less than one minute. The

water vapor inlet or outlet to the balance bottle was located directly below the beam (see Figure D-13). The introduction or removal of vapor caused a draft against the beam. The tracing on the recorder could be partially corrected by extrapolating to the later portion of the curve to zero time. Additional correction was provided by the computer with the zero shift correction.

A larger amount of scatter was noticed in the calculation of D using Equation D-8. An error analysis (D-56) showed that the effect of errors in the readings of time and weight had twice the effect in Equation D-8 as in the other methods of solution. Consequently, these results were not used in the analysis.

EXPERIMENTAL RESULTS

A. Tabulated Results

The results of the experimental work on the butylene adipate based polyurethane are presented in the following tables. The data are presented in the order in which they were taken. That is, the pressure and concentration indicated in a line above one set of data represent the equilibrium pressure and concentration existing within the film sample at the beginning of that cycle.

The nomenclature and units of the tables are defined below:

- p = partial pressure, mm. Hg.
- p/P_0 = relative pressure (activity).
- C = concentration of water in the film, gms. H_2O /gm. film.
- S = solubility coefficient, gm. H_2O /gm. film/mm Hg.
- \bar{D}_1 = diffusion coefficient based on the initial slope of M_t/M_∞ versus $t^{1/2}$, $cm.^2/sec.$
- \bar{D}_2 = diffusion coefficient based on the half-time, where $M_t/M_\infty = 0.5$, $cm.^2/sec.$
- \bar{D}_3 = diffusion coefficient based on the limiting slope of $\ln(M_\infty - M_t)$ versus t , $cm.^2/sec.$

B. Graphical Presentation of the Results

The experimental results are presented graphically below. Figures D-15, D-16, D-17 and D-18 show the sorption isotherms at the four operating temperatures. That is, the equilibrium-concentration at the end of each cycle is plotted against the activity. In figures D-19 through D-22 inclusively, the diffusion coefficients are plotted as a

TABLE D-6

RESULTS OF RUNS 1 AND 2 AT 30°C

RUN #1

SORPTION CYCLE

<u>P</u>	<u>P/P_O</u>	<u>C(10²)</u>	<u>S(10⁴)</u>	<u>$\bar{D}_1(10^7)$</u>	<u>$\bar{D}_2(10^7)$</u>	<u>$\bar{D}_3(10^7)$</u>
4.9	0.1541	0.1600	3.266	3.021	3.040	3.112
10.3	0.3239	0.3521	3.419	2.723	2.740	2.556
14.7	0.4623	0.5204	3.540	2.679	2.696	2.668
20.4	0.6415	0.7737	3.792	2.264	2.278	2.320
25.1	0.7893	1.031	3.107	2.374	2.389	2.547

DESORPTION CYCLE

<u>P</u>	<u>P/P_O</u>	<u>C(10²)</u>	<u>S(10⁴)</u>	<u>$\bar{D}_1(10^7)$</u>	<u>$\bar{D}_2(10^7)$</u>	<u>$\bar{D}_3(10^7)$</u>
19.8	0.6226	0.7535	3.806	2.281	2.295	2.319
14.9	0.4686	0.5376	3.608	2.075	2.088	2.263
10.0	0.3145	0.3491	3.491	2.170	2.183	2.306
4.9	0.1541	0.1865	3.807	2.688	2.705	2.723
0.0	0.0	0.0	-----	2.383	2.398	2.138

RUN #2

SORPTION CYCLE

<u>P</u>	<u>P/P_O</u>	<u>C(10²)</u>	<u>S(10⁴)</u>	<u>$\bar{D}_1(10^7)$</u>	<u>$\bar{D}_2(10^7)$</u>	<u>$\bar{D}_3(10^7)$</u>
5.6	0.1761	0.2263	4.041	2.488	2.503	2.323
10.2	0.3208	0.3786	3.712	2.584	2.600	2.657
15.4	0.4843	0.5704	3.704	2.516	2.532	2.501
20.2	0.6352	0.7791	3.857	2.440	2.455	2.516
25.4	0.7987	1.052	4.140	2.218	2.232	2.507

DESORPTION CYCLE

<u>P</u>	<u>P/P_O</u>	<u>C(10²)</u>	<u>S(10⁴)</u>	<u>$\bar{D}_1(10^7)$</u>	<u>$\bar{D}_2(10^7)$</u>	<u>$\bar{D}_3(10^7)$</u>
19.9	0.6258	0.7779	3.909	2.017	2.029	2.279
14.8	0.4654	0.5674	3.834	2.189	2.202	2.514
10.7	0.3365	0.4084	3.817	2.550	2.566	2.651
5.6	0.1761	0.2416	4.315	2.623	2.609	2.773
0.0	0.0	0.0	-----	2.387	2.401	2.240

TABLE D-7

RESULTS OF RUNS 3 and 4 AT 35°C

RUN #3

SORPTION CYCLE

<u>P</u>	<u>P/P₀</u>	<u>C(10²)</u>	<u>S(10⁴)</u>	<u>$\bar{D}_1(10^7)$</u>	<u>$\bar{D}_2(10^7)$</u>	<u>$\bar{D}_3(10^7)$</u>
6.4	0.1517	0.2242	3.503	3.393	3.414	3.534
10.1	0.2393	0.3139	3.108	3.369	3.389	3.398
15.1	0.3578	0.4464	2.956	3.455	3.476	3.617
19.8	0.4692	0.5870	2.965	2.934	2.952	3.001
25.5	0.6043	0.7857	3.081	3.061	3.080	3.056
30.1	0.7133	1.006	3.343	2.302	2.316	1.869
35.5	0.8412	1.233	3.472	2.913	2.931	3.082

DESORPTION CYCLE

<u>P</u>	<u>P/P₀</u>	<u>C(10²)</u>	<u>S(10⁴)</u>	<u>$\bar{D}_1(10^7)$</u>	<u>$\bar{D}_2(10^7)$</u>	<u>$\bar{D}_3(10^7)$</u>
29.5	0.6991	0.9579	3.247	2.358	2.372	2.862
24.8	0.5877	0.7704	3.106	2.414	2.429	2.468
20.2	0.4787	0.6174	3.056	2.967	2.986	3.133
15.2	0.3602	0.4626	3.044	3.111	3.130	3.187
9.8	0.2322	0.3187	3.252	3.059	3.078	3.334
5.3	0.1256	0.2058	3.883	3.420	3.441	3.462
0.0	0.0	0.0	-----	3.016	3.034	2.754

RUN #4

SORPTION CYCLE

<u>P</u>	<u>P/P₀</u>	<u>C(10²)</u>	<u>S(10⁴)</u>	<u>$\bar{D}_1(10^7)$</u>	<u>$\bar{D}_2(10^7)$</u>	<u>$\bar{D}_3(10^7)$</u>
5.9	0.1398	0.2084	3.531	3.594	3.616	3.455
10.0	0.2370	0.3158	3.158	3.365	3.386	3.207
15.0	0.3555	0.4449	2.966	3.289	3.310	3.456
19.0	0.4716	0.5936	2.983	3.058	3.077	3.193
24.8	0.5877	0.7556	3.047	2.903	2.921	2.956
30.5	0.7227	0.9914	3.250	2.848	2.866	2.844
35.0	0.8294	1.231	3.518	2.690	2.706	3.158

DESORPTION CYCLE

<u>P</u>	<u>P/P₀</u>	<u>C(10²)</u>	<u>S(10⁴)</u>	<u>$\bar{D}_1(10^7)$</u>	<u>$\bar{D}_2(10^7)$</u>	<u>$\bar{D}_3(10^7)$</u>
29.7	0.7038	0.9914	3.338	2.259	2.273	2.601
24.6	0.5829	0.7929	3.223	2.488	2.503	2.696
19.7	0.4668	0.6090	3.091	2.823	2.840	3.039
14.5	0.3436	0.4518	3.116	2.993	3.011	3.171
10.3	0.2441	0.3377	3.278	3.230	3.250	3.300
5.4	0.1280	0.2124	3.934	3.225	3.245	3.404
0.0	0.0	0.0		2.937	2.255	2.792

TABLE D-8

RESULTS OF RUNS 5 AND 6 AT 40°C

RUN #5

SORPTION CYCLE

<u>P</u>	<u>P/P₀</u>	<u>C(10²)</u>	<u>S(10⁴)</u>	<u>D₁(10⁷)</u>	<u>D₂(10⁷)</u>	<u>D₃(10⁷)</u>
7.3	0.1320	0.2099	2.875	3.710	3.732	3.287
11.2	0.2025	0.2797	2.497	4.407	4.434	4.661
15.0	0.2712	0.3512	2.342	4.671	4.700	4.689
20.5	0.3707	0.4724	2.304	3.870	3.894	3.882
25.3	0.4575	0.5837	2.307	4.513	4.541	4.063
30.4	0.5497	0.7159	2.355	3.746	3.769	4.064
35.5	0.6420	0.8703	2.452	3.318	3.339	3.970
40.5	0.7324	1.043	2.574	3.669	3.692	3.959
44.5	0.8047	1.184	2.660	3.012	3.031	3.079
51.2	0.9259	1.475	2.881	2.753	2.770	3.933

DESORPTION CYCLE

<u>P</u>	<u>P/P₀</u>	<u>C(10²)</u>	<u>S(10⁴)</u>	<u>D₁(10⁷)</u>	<u>D₂(10⁷)</u>	<u>D₃(10⁷)</u>
44.7	0.8083	1.331	2.978	6.596	6.636	9.495
39.3	0.7107	0.9980	2.539	3.373	3.394	3.652
34.9	0.6311	0.8565	2.454	3.067	3.085	3.393
30.2	0.5461	0.7303	2.418	3.435	3.456	4.114
24.9	0.4503	0.5956	2.392	3.357	3.377	3.309
19.7	0.3562	0.4819	2.446	4.006	4.031	4.237
14.8	0.2676	0.3746	2.531	4.203	4.229	4.494
10.0	0.1808	0.2708	2.708	4.130	4.155	4.505
5.0	0.0904	0.1754	3.508	4.462	4.490	4.546
0.0	0.0	0.0	-----	3.515	3.537	2.544

TABLE D-8 (cont.)

RUN #6

SORPTION CYCLE

<u>P</u>	<u>P/P₀</u>	<u>C(10²)</u>	<u>S(10⁴)</u>	<u>$\bar{D}_1(10^7)$</u>	<u>$\bar{D}_2(10^7)$</u>	<u>$\bar{D}_3(10^7)$</u>
2.6	0.0470	0.1203	4.626	6.656	6.697	5.504
4.5	0.0814	0.1596	3.546	4.595	4.623	4.721
10.0	0.1808	0.2623	2.623	4.687	4.716	4.775
15.5	0.2803	0.3729	2.406	4.519	4.547	4.777
20.6	0.3725	0.4831	2.345	4.292	4.318	4.509
25.1	0.4539	0.5871	2.339	4.560	4.588	5.222
29.7	0.5371	0.7014	2.362	4.310	4.337	4.565
34.9	0.6311	0.8538	2.446	3.690	3.713	4.316
40.1	0.7251	1.025	2.557	3.504	3.525	4.046
45.2	0.8174	1.231	2.724	3.133	3.153	3.410
50.4	0.9114	1.446	2.870	3.313	3.333	4.019

DESORPTION CYCLE

<u>P</u>	<u>P/P₀</u>	<u>C(10²)</u>	<u>S(10⁴)</u>	<u>$\bar{D}_1(10^7)$</u>	<u>$\bar{D}_2(10^7)$</u>	<u>$\bar{D}_3(10^7)$</u>
44.4	0.8029	1.207	2.718	2.641	2.658	3.036
39.5	0.7143	1.035	2.620	2.758	2.775	3.044
35.4	0.6401	0.8631	2.438	3.255	3.275	3.574
29.1	0.5262	0.7041	2.420	3.178	3.198	3.413
24.6	0.4448	0.5810	2.362	3.804	3.828	3.932
20.1	0.3635	0.4690	2.333	4.108	4.133	4.347
15.3	0.2767	0.3682	2.407	4.353	4.380	4.943
10.9	0.1953	0.2794	2.587	4.612	4.641	4.619
5.5	0.0995	0.1802	3.276	4.556	4.585	4.614
2.9	0.0524	0.1350	4.657	5.132	5.214	4.929
0.0	0.0	0.0	----	3.410	3.431	2.399

TABLE D-9

RESULTS OF RUNS 7 AND 8 at 50°C

RUN #7

SORPTION CYCLE

<u>P</u>	<u>P/P₀</u>	<u>C(10²)</u>	<u>S(10⁴)</u>	<u>$\bar{D}_1(10^7)$</u>	<u>$\bar{D}_2(10^7)$</u>	<u>$\bar{D}_3(10^7)$</u>
2.6	0.0281	0.0337	1.297	11.47	11.54	13.10
5.8	0.0627	0.0807	1.391	9.139	9.196	8.301
10.0	0.1081	0.1331	1.331	7.518	7.565	8.038
15.1	0.1632	0.1959	1.297	7.350	7.395	8.609
20.2	0.2183	0.2601	1.288	7.474	7.521	9.068
30.2	0.3264	0.4069	1.347	6.884	6.927	8.323
40.7	0.4399	0.5653	1.389	6.941	6.984	8.859
50.8	0.5491	0.7414	1.460	6.363	6.402	7.571
60.4	0.6528	0.9269	1.535	6.052	6.089	6.822
68.4	0.7393	1.118	1.634	5.418	5.451	6.478
74.8	0.8085	1.270	1.698	5.540	5.570	7.308
79.9	0.8636	1.422	1.779	4.844	4.874	5.061
82.6	0.8928	1.511	1.829	4.079	4.104	3.731

DESORPTION CYCLE

<u>P</u>	<u>P/P₀</u>	<u>C(10²)</u>	<u>S(10⁴)</u>	<u>$\bar{D}_1(10^7)$</u>	<u>$\bar{D}_2(10^7)$</u>	<u>$\bar{D}_3(10^7)$</u>
70.0	0.7566	1.139	1.627	4.599	4.628	4.512
60.2	0.6507	0.9188	1.526	4.990	5.021	5.626
50.4	0.5447	0.7261	1.441	5.662	5.697	5.358
40.1	0.4334	0.5533	1.380	6.132	6.170	5.669
29.8	0.3221	0.3979	1.335	6.245	6.284	6.375
19.7	0.2129	0.2633	1.337	6.906	6.949	6.687
14.7	0.1589	0.1972	1.342	6.838	6.880	7.328
10.2	0.1102	0.1415	1.387	7.322	7.367	7.215
7.3	0.0789	0.1078	1.477	6.795	6.837	7.959
4.4	0.0476	0.0693	1.574	7.377	7.423	7.177
0.0	0.0	0.0	----	5.365	5.398	1.513

TABLE D-9 (cont.)

RUN #8

SORPTION CYCLE

<u>P</u>	<u>P/P₀</u>	<u>C(10²)</u>	<u>S(10⁴)</u>	<u>$\bar{D}_1(10^7)$</u>	<u>$\bar{D}_2(10^7)$</u>	<u>$\bar{D}_3(10^7)$</u>
2.0	0.0216	0.0131	0.655	11.43	11.50	9.577
5.1	0.0551	0.0554	1.086	7.693	7.740	7.627
10.2	0.1102	0.1170	1.147	8.018	8.068	8.020
15.3	0.1654	0.1805	1.180	7.436	7.482	7.526
20.6	0.2227	0.2451	1.190	7.205	7.249	7.724
31.0	0.3351	0.3952	1.275	7.223	7.268	7.441
41.1	0.4442	0.5593	1.361	6.390	6.430	6.868
50.8	0.5491	0.7204	1.418	6.177	6.215	7.602
59.9	0.6474	0.9028	1.507	5.548	5.582	6.232
69.4	0.7501	1.118	1.611	5.482	5.516	4.960
74.5	0.8052	1.265	1.698	4.516	4.544	5.007
78.9	0.8528	1.389	1.760	4.998	5.029	5.765

DESORPTION CYCLE

<u>P</u>	<u>P/P₀</u>	<u>C(10²)</u>	<u>S(10⁴)</u>	<u>$\bar{D}_1(10^7)$</u>	<u>$\bar{D}_2(10^7)$</u>	<u>$\bar{D}_3(10^7)$</u>
71.9	0.7771	1.206	1.677	5.122	5.153	4.937
64.4	0.6961	1.046	1.624	5.444	5.477	5.806
58.7	0.6345	0.8921	1.520	5.462	5.495	7.192
50.3	0.5437	0.7258	1.443	6.065	6.103	6.432
29.4	0.4259	0.5509	1.398	6.146	6.184	6.915
29.4	0.3178	0.3883	1.321	6.578	6.618	7.089
20.4	0.2205	0.3618	1.283	6.719	6.760	7.089
16.1	0.1740	0.2029	1.260	7.330	7.375	7.396
10.4	0.1124	0.1331	1.280	7.451	7.497	6.827
8.4	0.0908	0.1079	1.285	8.358	8.410	7.338
4.7	0.0508	0.0635	1.352	7.623	7.610	7.386
0.0	0.0	0.0	----	8.190	8.240	5.325

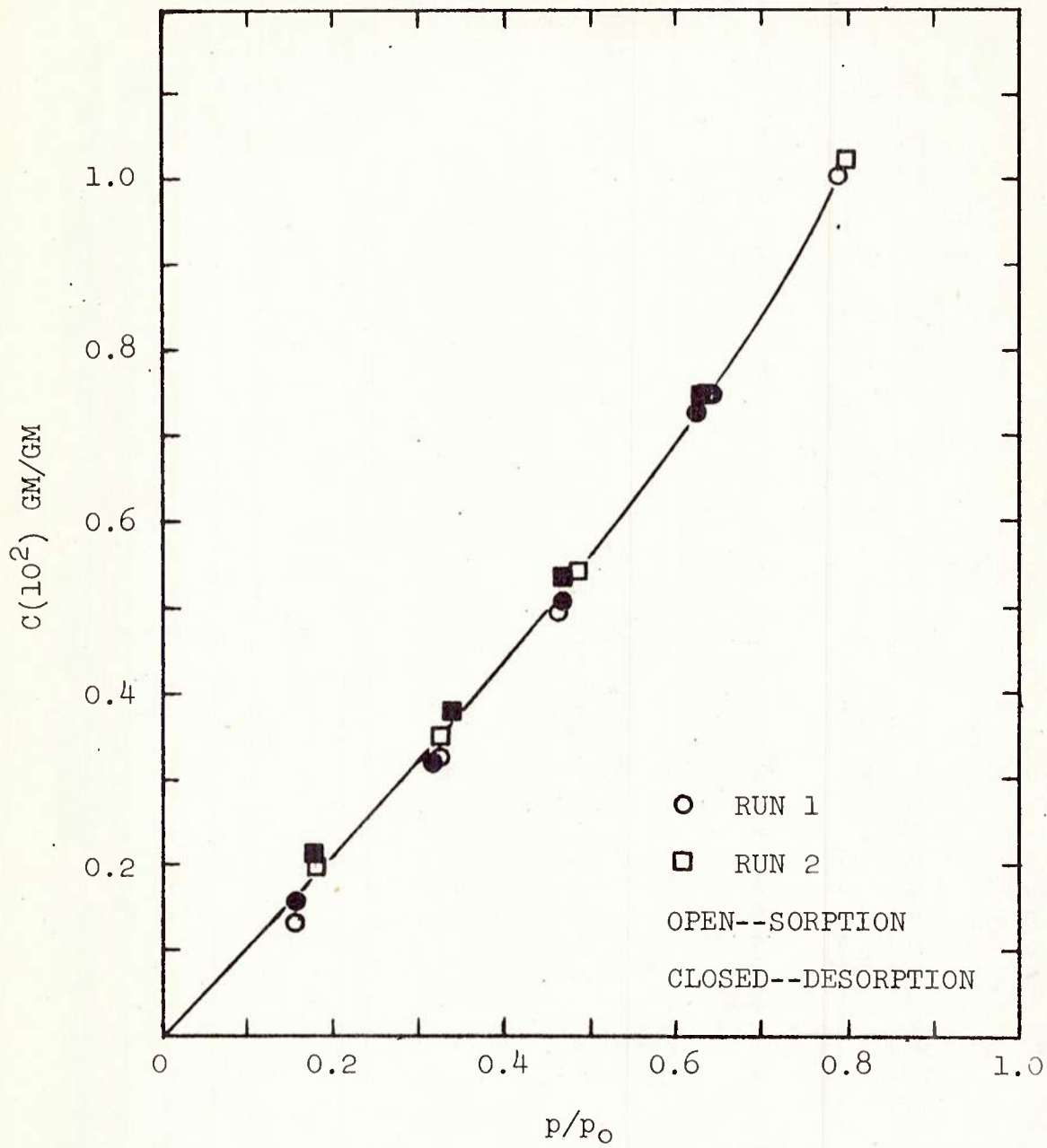


FIGURE D-15 SORPTION ISOTHERM AT 30°C

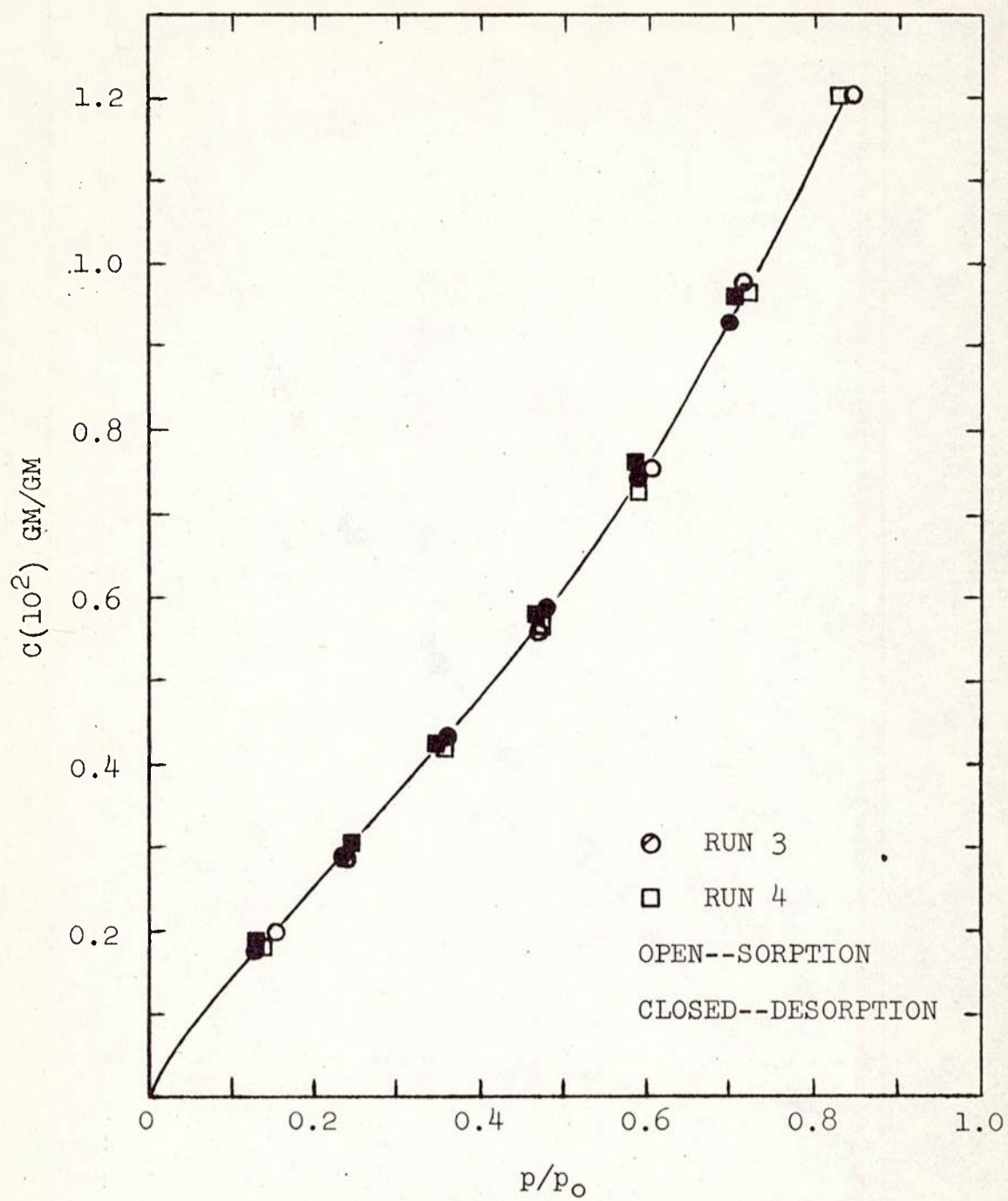


FIGURE D-16 SORPTION ISOTHERM AT 35°C

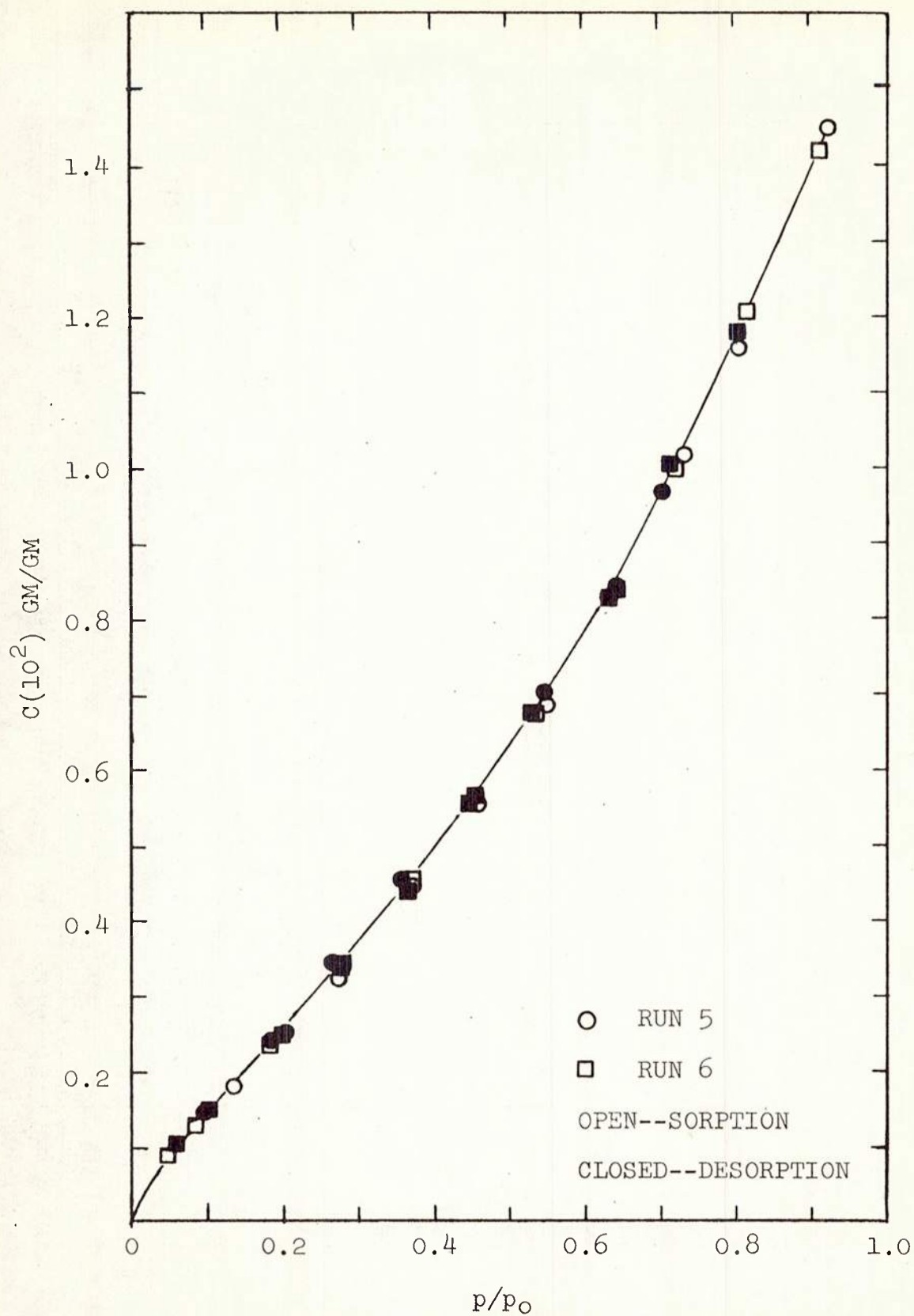


FIGURE D-17 SORPTION ISOTHERM AT 40°C

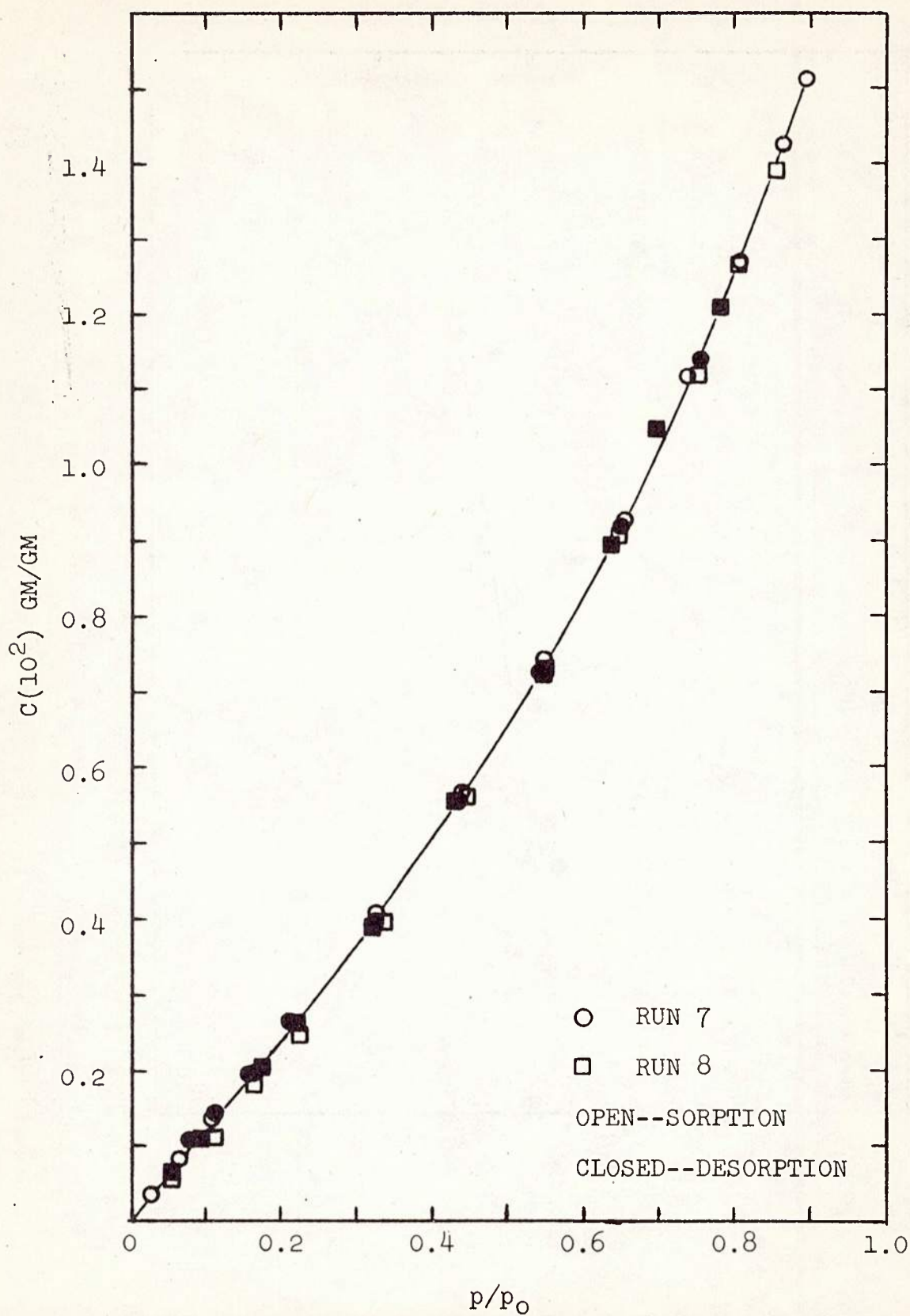


FIGURE D-18 SORPTION ISOTHERM AT 50°C

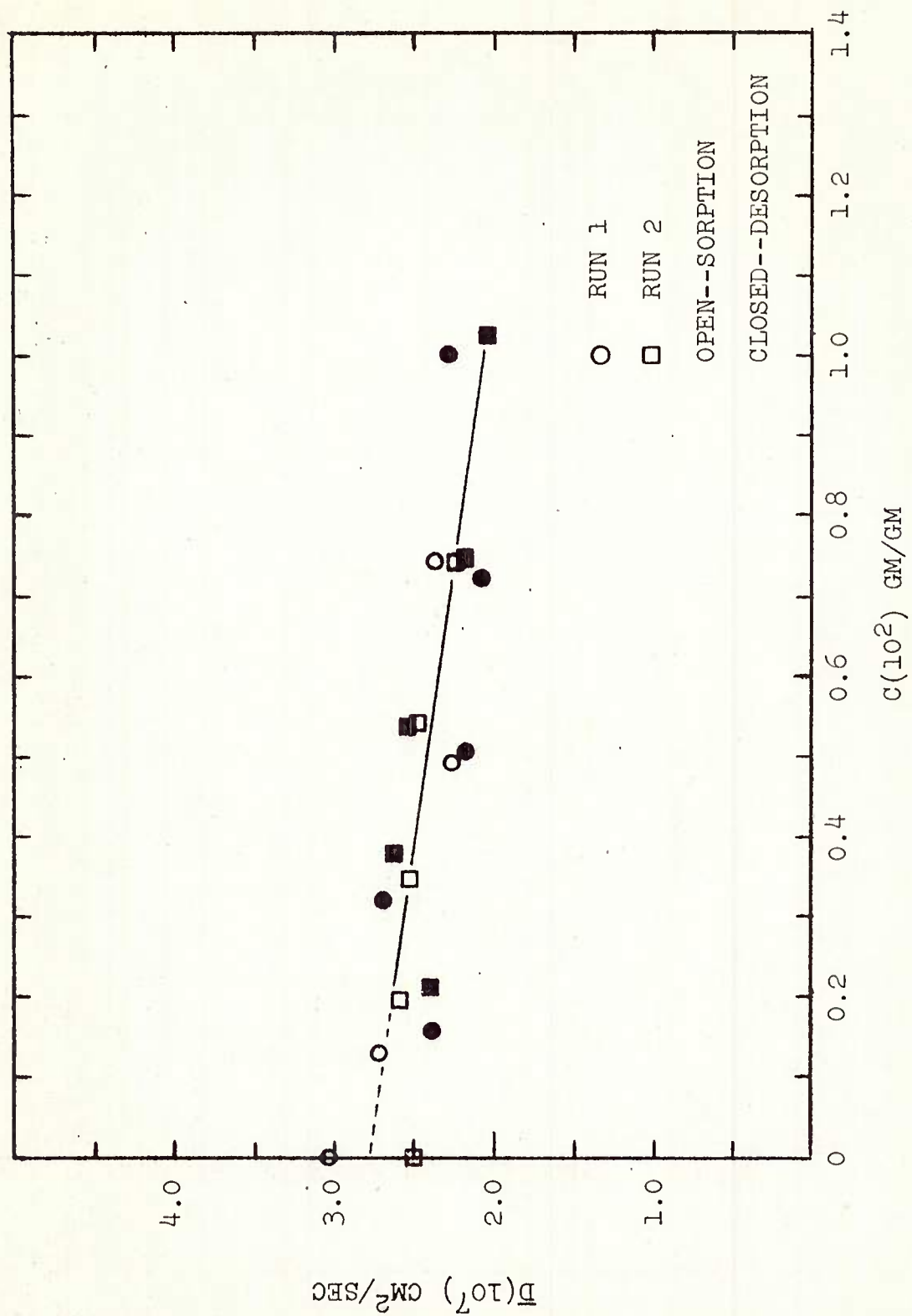


FIGURE D-19 EFFECT OF CONCENTRATION ON THE DIFFUSION COEFFICIENT AT 30°C

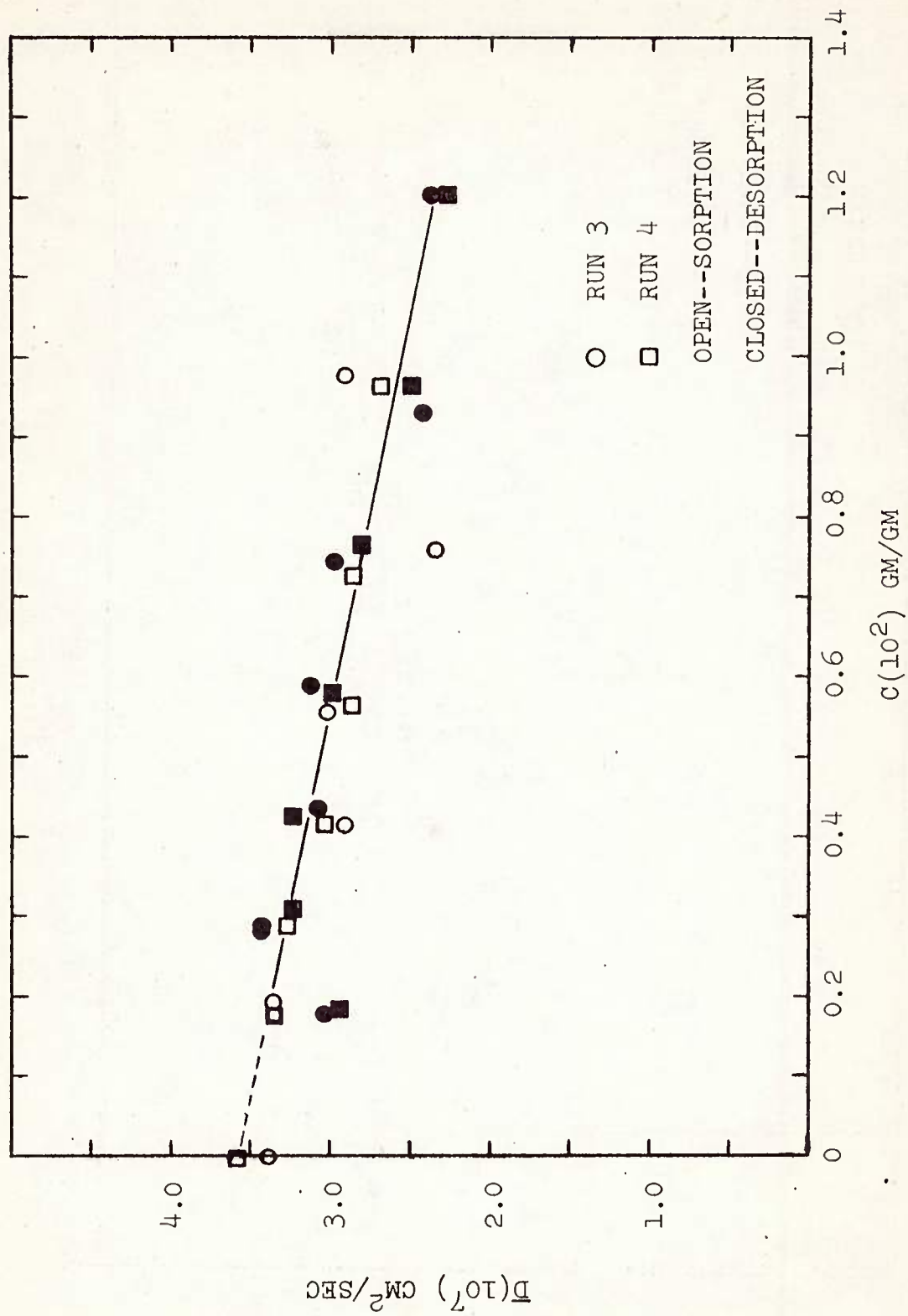


FIGURE D-20 EFFECT OF CONCENTRATION ON THE DIFFUSION COEFFICIENT AT 35°C

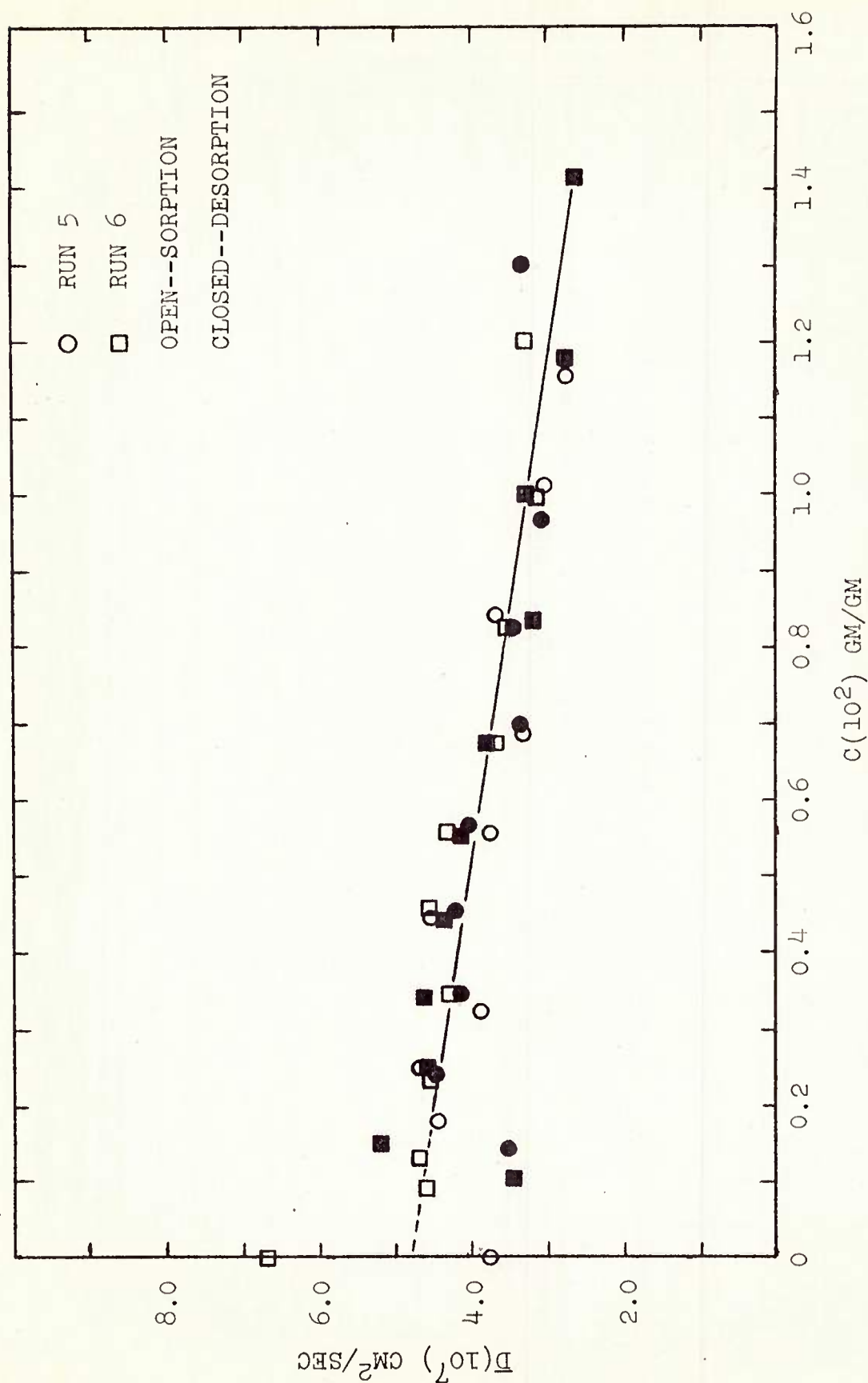


FIGURE D-21 EFFECT OF CONCENTRATION ON THE DIFFUSION COEFFICIENT AT 40°C

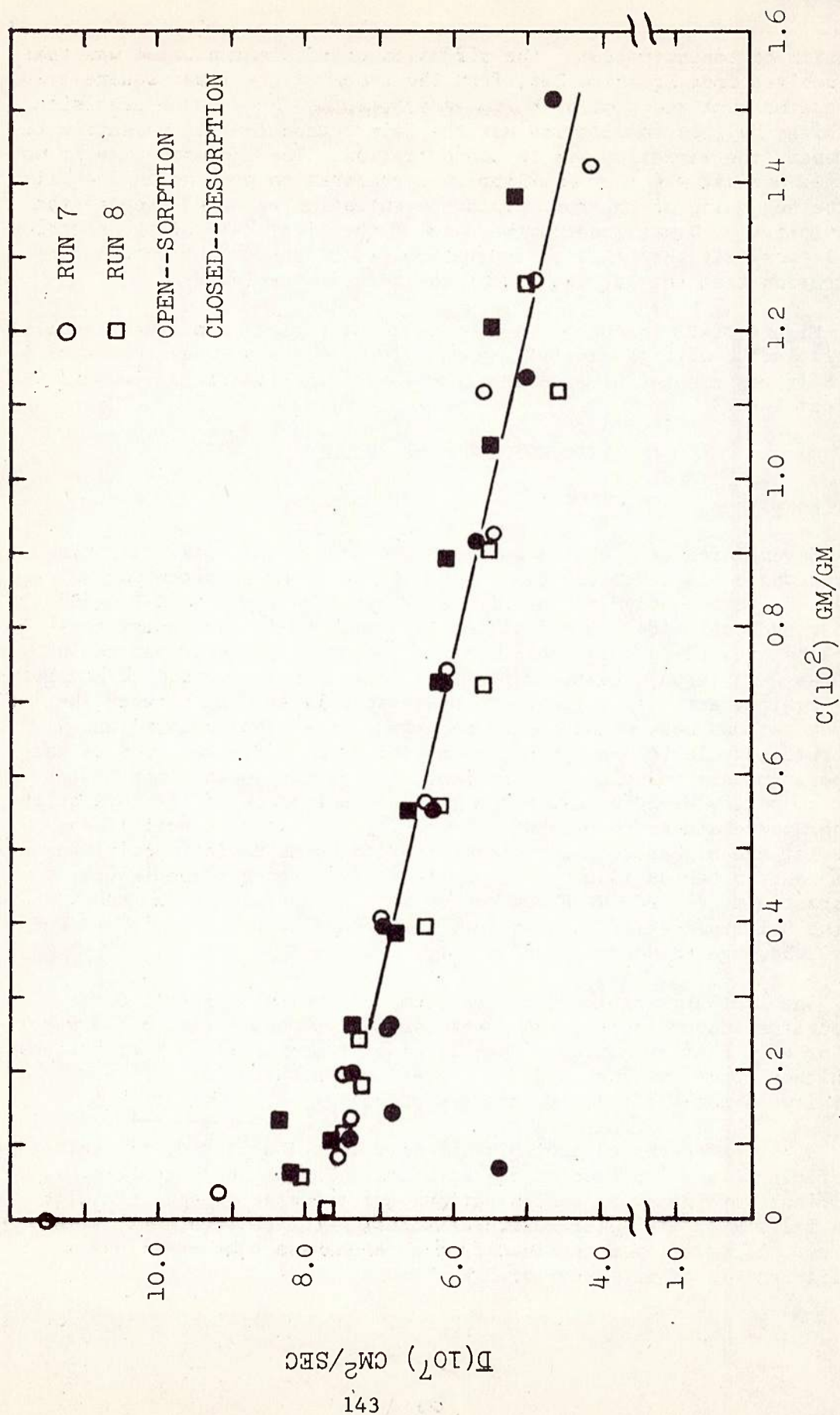


FIGURE D-22 EFFECT OF CONCENTRATION ON THE DIFFUSION COEFFICIENT AT 50°C

function of concentration. The diffusion coefficient plotted was that one derived from Equation D-6, from the slope of the least square line calculated from the plot of M_t/M_∞ versus $t^{1/2}$. The greater precision exhibited by this calculation was the main reason for its selection to represent the variation due to concentration. The concentration it was plotted against was that equilibrium concentration present in the film at the beginning of the run. This concentration was used because the calculation of D was made on the data of the first half of the sorption and it was felt that this concentration was closer to the actual concentration than that at the end of the sorption cycle.

Figures D-23 through D-26 represent the variation of the solubility coefficient S with the activity p/p_0 . The temperature dependence of D and S is represented by an Arrhenius plot of the logarithm of D and S against $1/T$ K.

DISCUSSION OF THE RESULTS

A. Results

Several features of the sorption and diffusion process in this polyurethane elastomer are similar to the behavior reported for water in several other polymers, particularly ethyl cellulose, (D-11,-59) rubber hydrochloride, (D-61) silicone rubber, (D-14) and polymethylmethacrylate. (D-14,-31) The sorption isotherms are represented in Figures D-15 through D-18, as plots of concentration (gms. H_2O /gm. polymer) against activity (p/p_0). No hysteresis is evident between the concentrations determined on the sorption cycle (open points) and desorption cycle (closed points), and the data of the two runs at each temperature are coincident. The isotherms at the lower temperatures seem to follow Henry's Law, but a closer examination of the data of the higher temperatures reveals a nonlinearity at the lower activities. Also, at the higher concentrations, the isotherms deviate positively from Henry's Law as is common to systems with strong sorbent-sorbent interactions. (D-49) When the concentrations are plotted as Henry's Law solubility coefficient, as in Figures D-23 to D-26, it is evident that adherence to Henry's Law is more apparent than real.

The isotherms of the different temperatures show little or no temperature dependence at the lower concentrations, indicating a very low or zero heat of mixing. The effect of temperature is more noticeable at higher concentrations where a higher concentration at the same activity is noted as the temperature rises.

A horseshoe-shaped curve is obtained from the plot of the solubility coefficient as a function of the activity. The higher solubility coefficients at the lower concentrations are evidence of specific site hole filling by the water molecules entering the polyurethane matrix. The heat of solution determined from an Arrhenius plot of solubility coefficient is of the order of 9 kcal/mole.

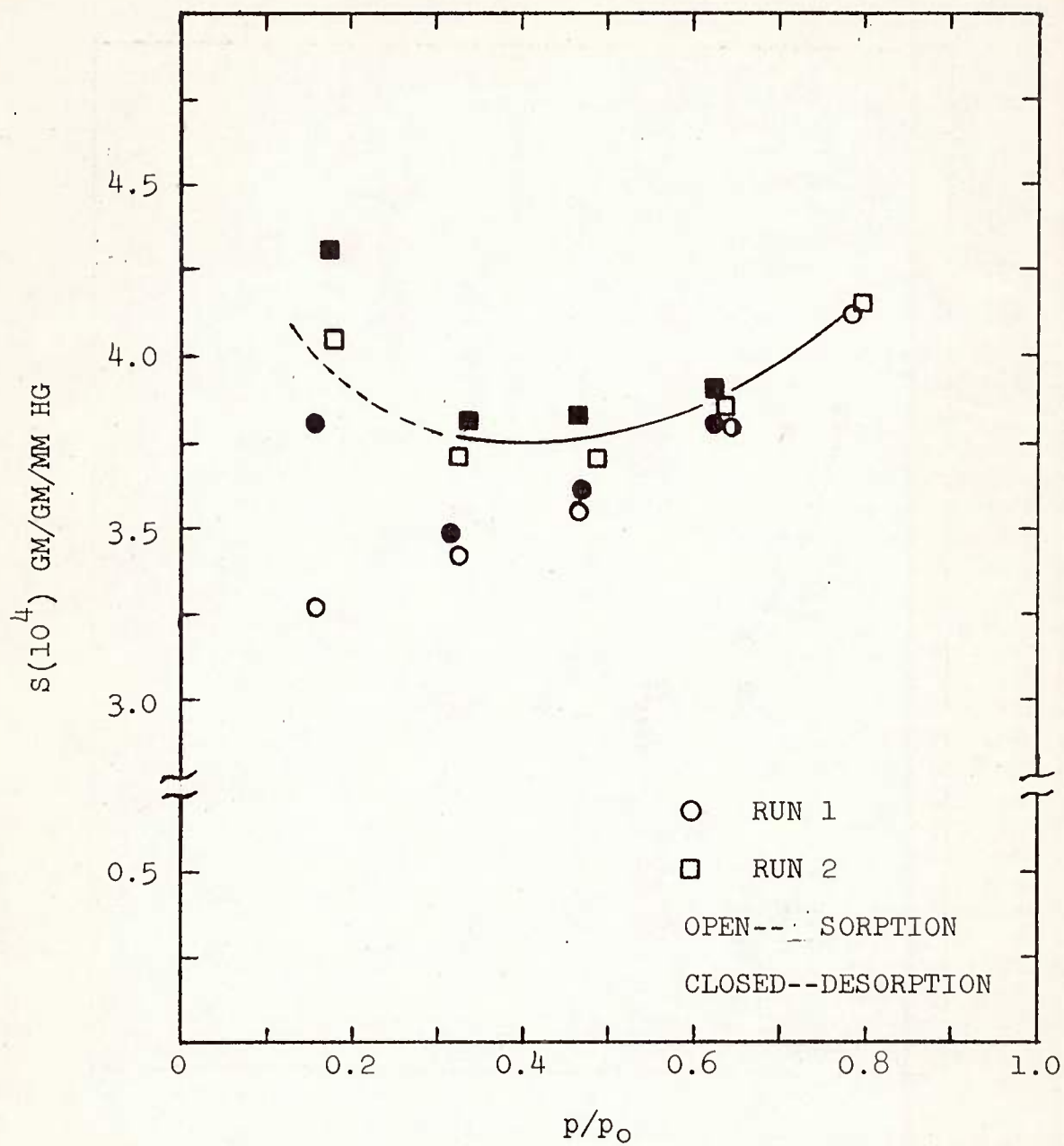


FIGURE F-23 VARIATION OF THE SOLUBILITY COEFFICIENT
WITH ACTIVITY AT 30°C

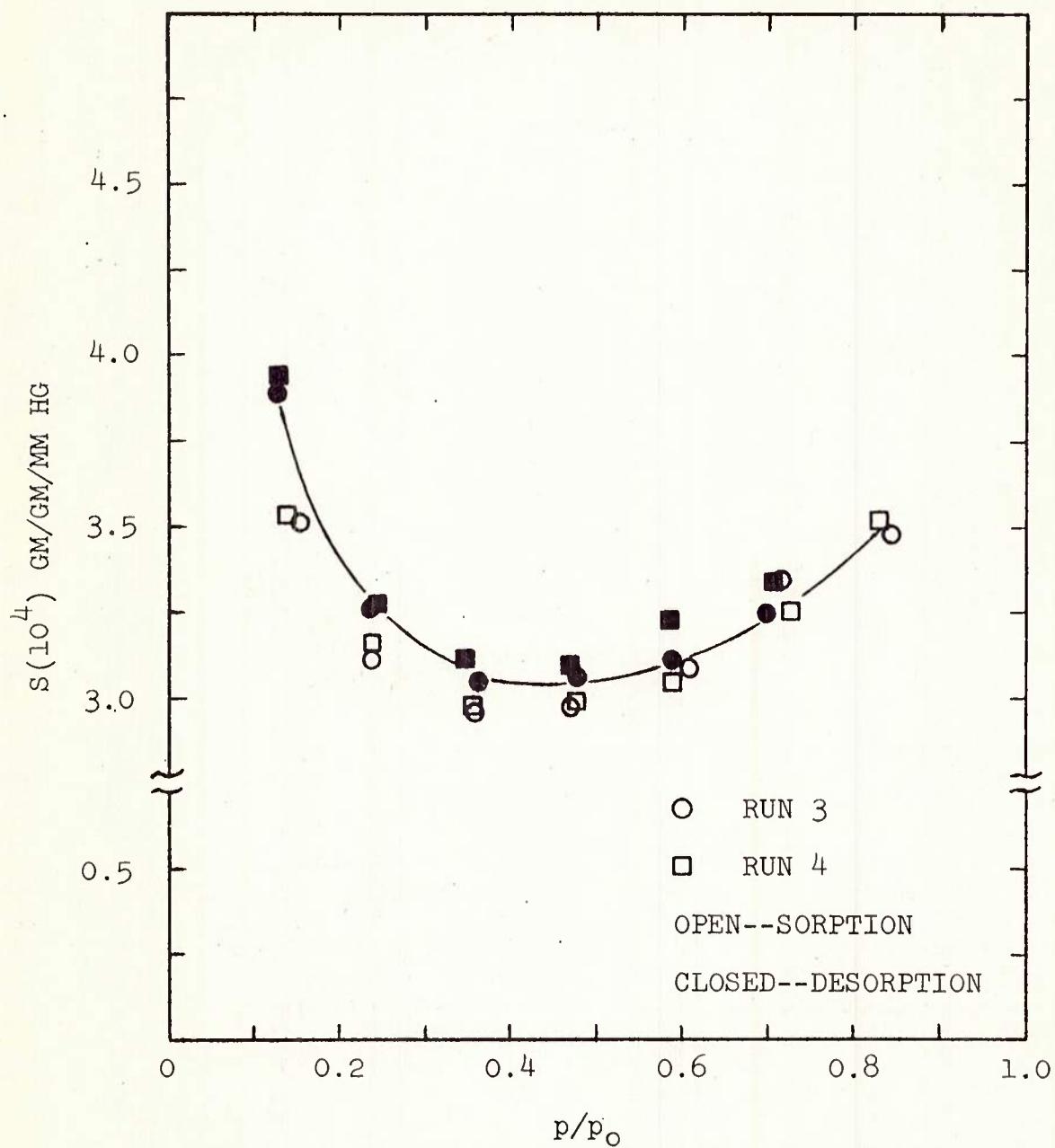


FIGURE D-24 VARIATION OF THE SOLUBILITY COEFFICIENT
WITH ACTIVITY AT 35°C

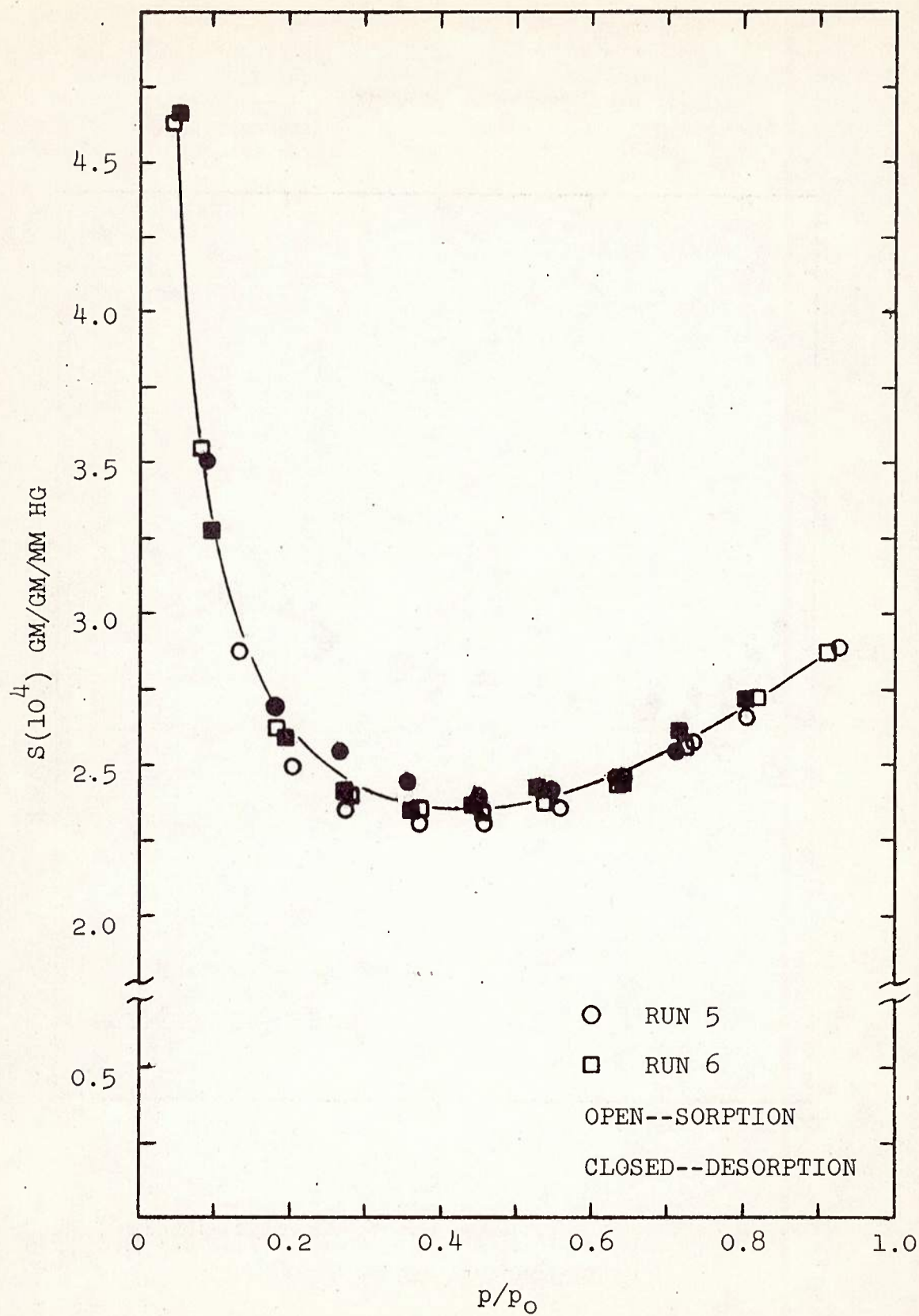


FIGURE D-25 VARIATION OF THE SOLUBILITY COEFFICIENT WITH ACTIVITY AT 40°C

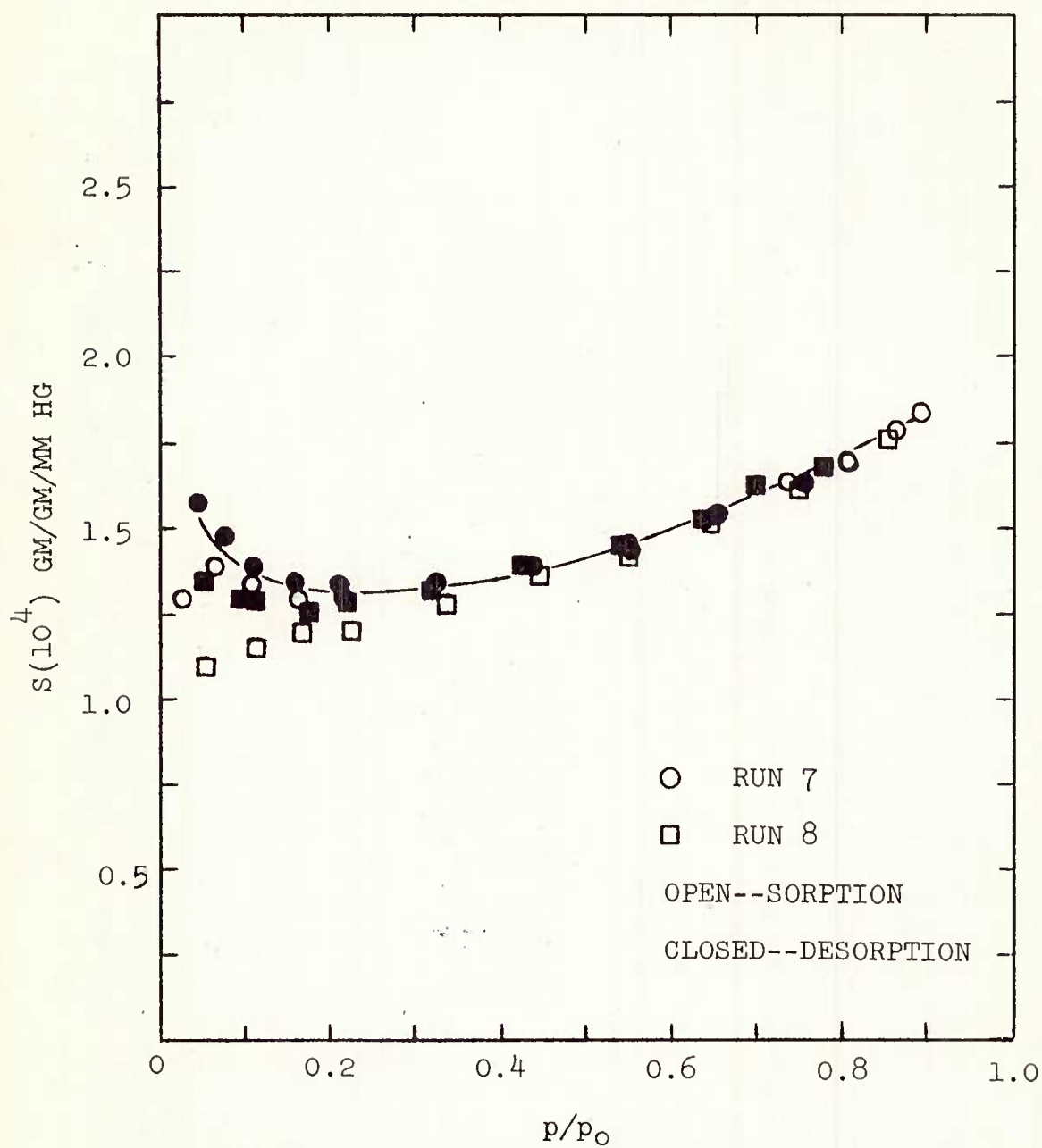


FIGURE D-26 VARIATION OF THE SOLUBILITY COEFFICIENT
WITH ACTIVITY AT 50°C

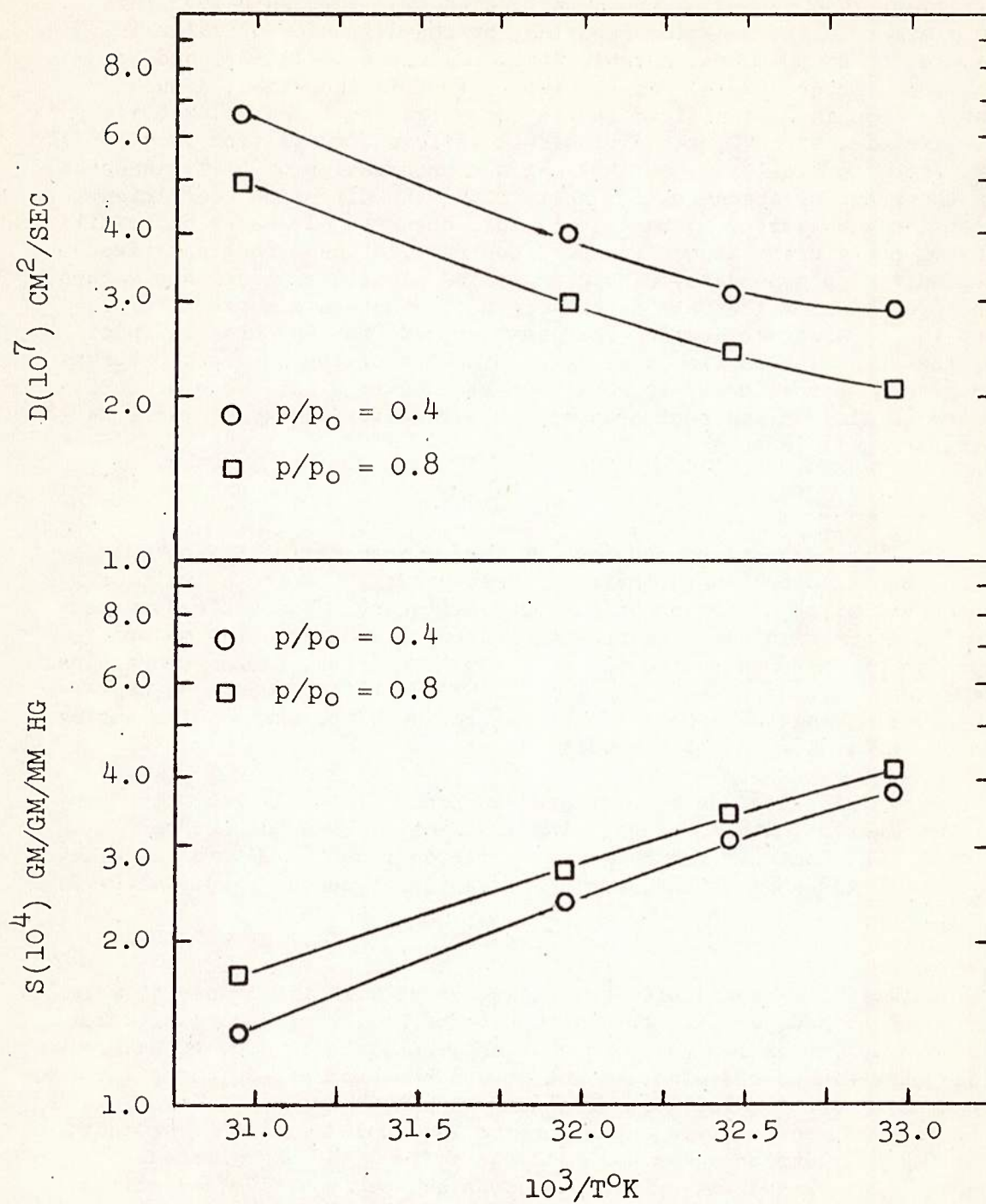


FIGURE D-27 EFFECT OF TEMPERATURE ON THE DIFFUSIVITY AND THE SOLUBILITY COEFFICIENT

A marked inverse concentration dependency of the diffusion coefficient is observed as shown in Figures D-19 through D-22. This is similar to the behavior reported for the diffusion of water in several other polymers, notably ethyl cellulose (D-11,-59) and silicone rubber. (D-14) As the temperature is increased, a much larger drop in \bar{D} is noticed in the concentration range below 0.1%. For example, at 50°C, the diffusion coefficient drops from $11.4(10^{-7})$ cm.²/sec. to $7.5(10^{-7})$ cm.²/sec. at a concentration of 0.1%. Whereas, in the range of concentration up to 1.5%, the diffusion coefficient drops only to $4.5(10^{-7})$ cm.²/sec. This observed decrease in the diffusion coefficient stands in sharp contrast to the strong positive concentration dependency displayed by the plasticizing organic vapors. The precision of the data did not permit an accurate curve fitting, but the apparent activation energies derived from an Arrhenius plot of the data removed from a straight-line fit of the \bar{D} versus C curves drop from approximately 10 kcal/mole at 50°C to 4 kcal/mole at 30°C. There is also an apparent drop of the activation energy as the concentration is increased.

B. Analysis

As has been stated previously, the interpretation given to an experimental sorption isotherm can help greatly in the analysis of a concentration dependent diffusion coefficient. The decreasing diffusion coefficient with increasing concentration, with the major portion of the drop taking place at low activities, could be explained as a large amount of specific site sorption at the lower concentrations, limiting the amount of free water, combined with an increasing amount of clustering of the water molecules.

This behavior has been treated in terms of the Langmuir isotherm in combination with the clustering function of Zimm and Lundberg. (D-63) The Langmuir isotherm was extracted from the data of this study by use of the form of the Langmuir equation presented by Dole. (D-25)

$$a/N = 1/c_1 N_s + a/N_s \quad \text{D-16}$$

The activity is represented by the letter a , N is the number of moles of vapor sorbed per unit of adsorbent, and N_s is the number of moles of sorption sites per unit of adsorbent. A plot was made to determine the constants of the equation and it was then replotted in the familiar form of a sorption isotherm of concentration versus activity. In Figure D-28, the resultant plot of the 40°C data has been reproduced. The Langmuir isotherm has been subtracted from the experimental curve. This resultant curve shows much sharper positive deviations from Henry's Law and has been ascribed to the polymerization of water

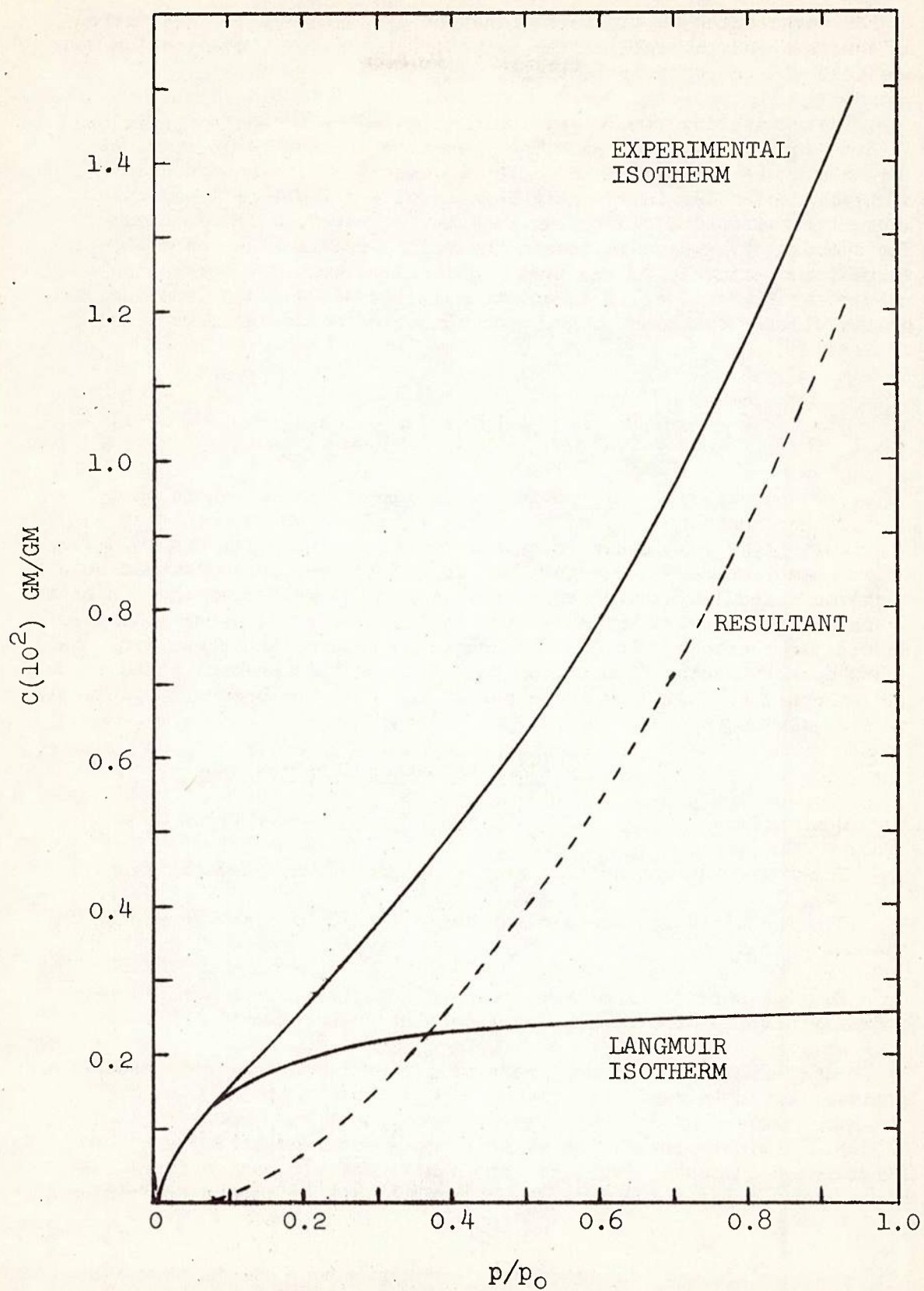


FIGURE D-28 | LANGMUIR ANALYSIS OF 40°C ISOTHERM

to form aggregates or clusters. The one disadvantage to this method of analysis was that all of the sorption at the low concentration was assigned to the Langmuir isotherm.

The clustering theory was further tested by the method developed by Zimm and Lundberg. (D-63) They identify a quantity $\Phi_1 G_{11}/v_1$ as the mean number of type 1 molecules in excess of the mean concentration of type 1 molecules in the neighborhood of a given type 1 molecule. Thus it measures the clustering tendency of the type 1 molecules. The symbols Φ_1 and v_1 represent the volume fraction and partial-molar volume, respectively, of the type 1 molecule. By using a relation developed by Zimm (D-62), a direct translation can be made from the value of the cluster function to the mean number of molecules clustering together.

$$G_{11}/v_1 = -\Phi_2 [\partial(a_1/\Phi_1)/\partial a_1] - 1 \quad D-17$$

If G_{11}/v_1 equals -1, as it would for an ideal solution whose activity coefficient does not vary with concentration, it would mean that a particular type 1 molecule in such a system excludes its own volume to other molecules. A cluster function of greater than -1 would mean that the molecules cluster together. As can be seen from the composite graph of Figure D-29, which is from the data of 50°C, water molecules do cluster together. Only a few questions remain, and these would be - how does the water cluster together and can this be controlled to give the higher diffusion rates needed for the development of a passive cooling system in space suits?

CONCLUSIONS AND RECOMMENDATIONS

A. Conclusions

The following conclusions were drawn from this investigation:

1. The diffusion coefficient has a marked inverse dependence on the concentration.
2. The sorption isotherms deviate positively from Henry's Law, possibly because of strong sorbent-sorbent interactions.
3. Very little, if any, heat of mixing is indicated by the superposition of the sorption isotherms.
4. A clustering of the water is apparent from a Zimm and Lundberg (D-63) analysis. This in combination with a specific site model could explain the inverse behavior of the diffusion coefficient.

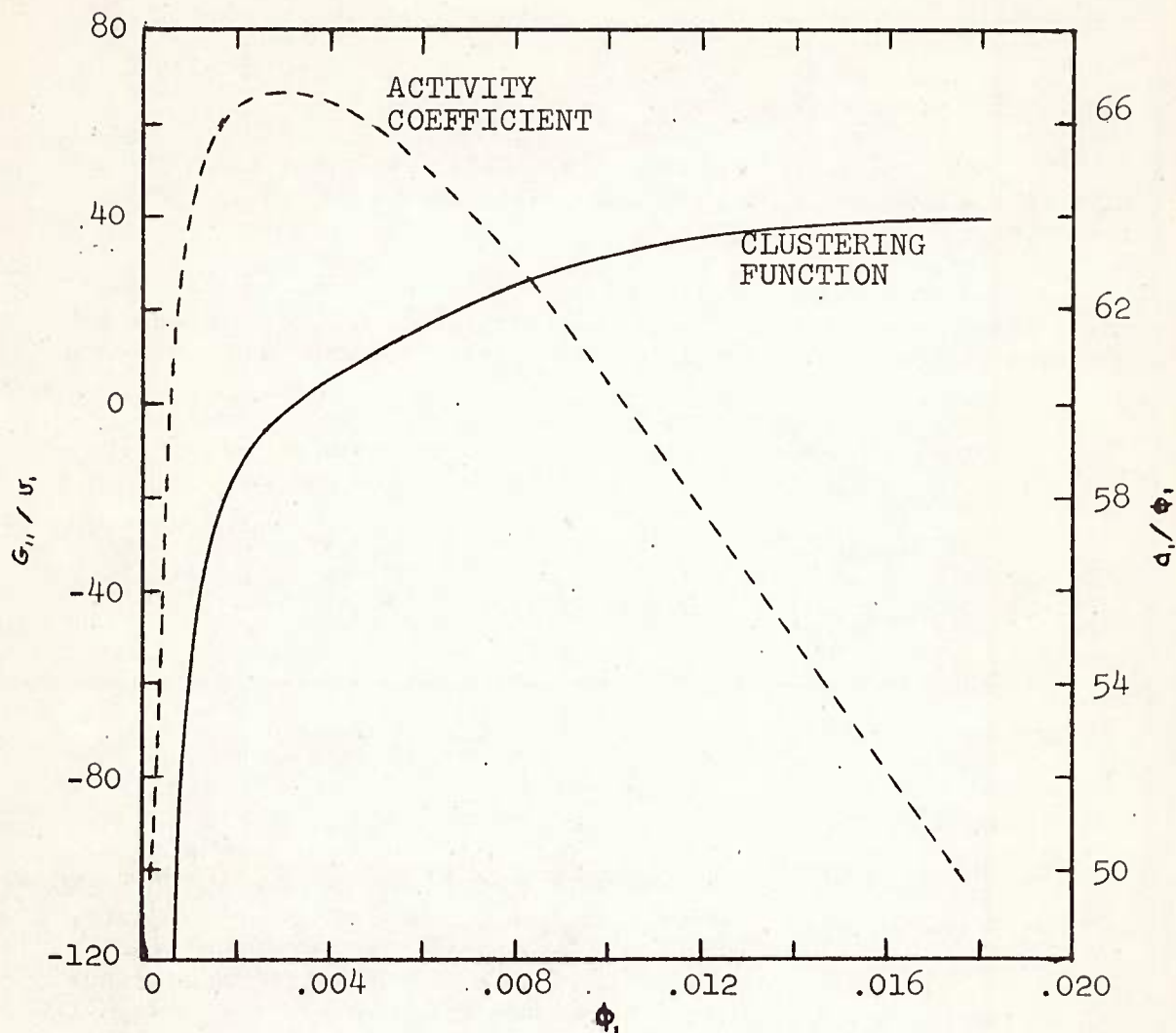


FIGURE [p-29] VOLUME FRACTION ACTIVITY COEFFICIENT AND CLUSTERING FUNCTION VERSUS VOLUME FRACTION

5. An Arrhenius plot of \bar{D} and S versus $1/T$ is not linear, i.e., varying activation energies of diffusion and solubility.

B. Recommendations

From the results of the experiment, the following recommendations are made:

1. A redesign of the sorption system is indicated to eliminate the initial draft against the balance beam.

2. The addition of extension arms to the valves through the outside of the oven would avoid thermal disturbances caused by opening the doors.

3. In order to study more closely the sharp drop in D at the lower concentrations displayed at 40°C and 50°C , more data should be gathered at these concentrations with greater accuracy and precision.

4. A more thorough investigation of other models presented in the literature is needed to find one that best explains the behavior, e.g., Barrie and Platt's (D-14) or Vieth, Michaels and Barrie. (D-47)

5. The need to conduct more studies on other well-characterized samples has been shown in order to find a structural parameter that might be the controlling factor in diffusion.

PART IV

SORPTION AND DIFFUSION OF ETHANOL

IN A POLYURETHANE

I. INTRODUCTION

In previous work, undertaken at the University of Rhode Island, (D-27,-54) the permeability of a polyester type polyurethane to a series of liquid alcohols was studied to obtain a better understanding of the aspects of penetrant structure which govern the permeability of polymers to small organic molecules. The family of alcohols lends itself especially well to this purpose since the normal alcohols provide a selection of penetrants of increasing chain length while the different side chain alcohols of the same molecular weight allow a study of the effects of branching on the permeability behavior.

The work at the University of Rhode Island was limited to the measurement of the steady-state permeation rate of different liquid

alcohols using conventional cup cells. The upstream (inside) surface of the polymer film is in contact with saturated vapor, or more commonly in contact with the liquid, while the downstream surface is exposed to air in which the alcohol concentration is negligibly small. This method is limited to steady-state measurements. Moreover, since the penetrant is always at unit activity, it is not possible to vary its concentration in the polymer independently of temperature as needed to determine the concentration or temperature dependence of the component sorption and diffusion processes.

In the present study, detailed measurements were made on the unsteady-state sorption of ethanol vapor into the polyurethane over a range of partial pressures using a quartz spring balance. As in the previous work on different alcohols and on water vapor (D-53), the polyurethane was composed of MDI, butanediol and polybutyleneadipate (molecular weight 2,000) in the molar ratios of 3.2:2:1.

II. EXPERIMENTAL PROCEDURE

The high vacuum system used for the collection of sorption data is shown in Figure D-30. The quartz spring (sensitivity = 1 mm/ng.) from which the polymer sample is suspended is inclosed by a water jacketed cell to thermostat the sample. The change in weight of the sample during the sorption process is determined by measuring the extension of the calibrated spring using a cathetometer that reads to 0.01 mm. Readings are reproducible to ± 0.02 mm.

A step-wise procedure was used for the sorption measurements with the result that the final uniform concentration of vapor in the polymer established at the previous pressure becomes the initial concentration when the film is exposed to the next pressure increment. Measurements were made only on the sorption cycle. The sample was first evacuated to less than five microns pressure for a period of 24 hours to determine the initial sample dry weight. At the start of the run the vapor is introduced to a predetermined pressure in the manifold and three liter flask. When the balance chamber is opened, the vapor pressure falls to a precalculated value that is constant for the run.

In taking measurements of the weight change due to vapor sorption, it was found convenient to space the readings at equal square root of time intervals starting at one minute. As discussed in the following section, the weight gain is generally a linear function of the square root of time over at least one half the sorption process. Therefore, spacing the readings in this way not only facilitates the data plotting but also provides a direct check on the value and constancy of the slope of the sorption-time curve, which is a measure of the diffusion constant.

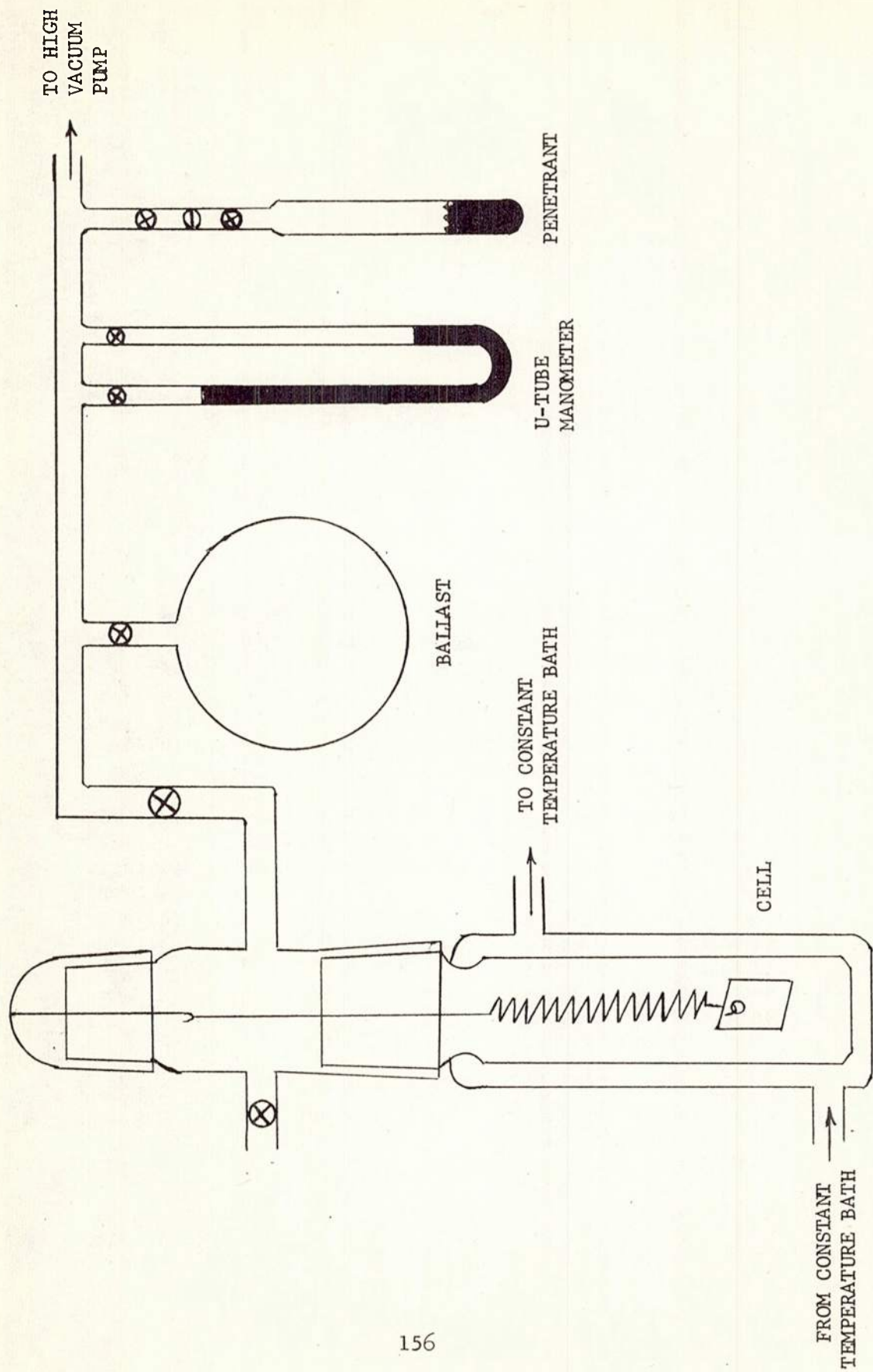


FIGURE D-30. DIAGRAM OF SORPTION SYSTEM

After the sample has reached equilibrium it is exposed to a new step increase in pressure and the same procedure is repeated until the maximum vapor pressure is reached. If the balance chamber is below room temperature, readings can be taken up to and, sometimes, including the saturation pressure. But if the balance chamber is above room temperature, the highest vapor pressure will be determined by the pressure at which vapor condenses in the portions of the manifold which are at ambient temperature.

III. TREATMENT OF THE DATA

The equilibrium data provide values of the amount of vapor sorbed as a function of the vapor pressure. When plotted as concentration (g/cc) against the partial pressure p/p_0 (where p_0 is the saturation vapor pressure), the curve is known as the sorption isotherm.

From the transient phase of the sorption measurement, the amount of penetrant adsorbed in the film as a function of time was obtained. This is usually expressed as weight of penetrant per unit weight of polymer M_t . When the film is exposed to a constant concentration of vapor, and when diffusion is Frickian and is not concentration dependent, then the fractional sorption $F = (M_t - M_0)/(M_\infty - M_0)$ plotted against the square root of time $t^{1/2}$ is a straight line through the origin over the first 60% of the sorption process. In the above expression for F , M_0 is the concentration of penetrant in the film at $t = 0$, and M_∞ is the concentration of penetrant when equilibrium is attained. The diffusion constant D can be calculated either from the half time $t_{1/2}$, the time required to reach one half the saturation concentration, (D-4,-22)

$$D = 0.494 L^2/t_{1/2} \quad D-18$$

or from the initial slope K

$$D = (\pi L^2/16)K^2 \quad D-19$$

where $K = dF/d(t^{1/2})$ and L is the sample thickness.

In many of the systems of interest the requirements set forth for the applicability of the above equations are not strictly obeyed. When the penetrant concentration is not restricted to very small values, ca. 1%, the swelling and plasticization of the polymer result in a diffusion constant which increases with the concentration. In general, the fractional sorption F versus $t^{1/2}$ remains linear over the first half or more of the sorption process. However, the value of D calculated from the proceeding equations then represents an average over the concentration interval of the sorption step.

$$\bar{D}(C_f) = \frac{1}{C_f - C_o} \int_{C_o}^{C_f} D(C)dc \quad D-20$$

where C_o and C_f are the initial and final concentration of penetrant in the film. This equation for the integral diffusion constant D is only approximate. (D-22,-30)

Other effects that might be important in the present study are the reduction in the concentration of mobile penetrant species in the polymer, either by reaction with polymer functional groups or by self-association of the penetrant molecules. If the reaction is irreversible or very much faster than the rate of diffusion, then F versus $t^{1/2}$ is still linear over the initial phase of sorption. (D-22,-58) However, the apparent diffusion constant calculated from the previous equations is less than the true diffusion constant due to the fraction of penetrant which is immobilized, and in such cases the apparent diffusion constant can decrease with increasing penetrant concentration. When the immobilization reaction is reversible and the rate constant for the back reaction which regenerates the original species is less than about one-thousandfold greater than the diffusion constant, then the sorption curve may become "S"-shaped or show other abnormalities. (D-22) Complex effects also occur due to structure changes in glassy or crystalline polymers (D-30) but this will not be important in the present studies of diffusion into a rubbery polymer.

IV RESULTS AND DISCUSSION

1. Equilibrium Results

The solubility of ethanol in polyurethane samples immersed in the liquid was determined at several temperatures overlapping the range of Foster's measurements, (D-27) with good agreement, as well as at 31.1°C. and 19.5°C. which are the temperatures at which the current unsteady-state sorption studies were made. The combined values from Foster's data (filled circles) and the current work (open circles) are presented in Figure D-31. Although the data fall on a curve of increasing concentration with increasing temperature, the slope at 50°C. is only one third the value at 20°C., indicating that the solubility is approaching a limiting value short of dissolution of the polymer.

The sorption isotherms, which represent the concentration as a function of vapor activity (p/p_o), are shown in Figure D-32. The concentration obtained at saturation at 19.5°C. was within 1% of the value obtained from samples immersed in liquid ethanol, indicating that no leaching of the polymer has occurred in the liquid and that non-equilibrium effects are probably absent. The curves at the two temperatures are strongly concave upward. This behavior differs

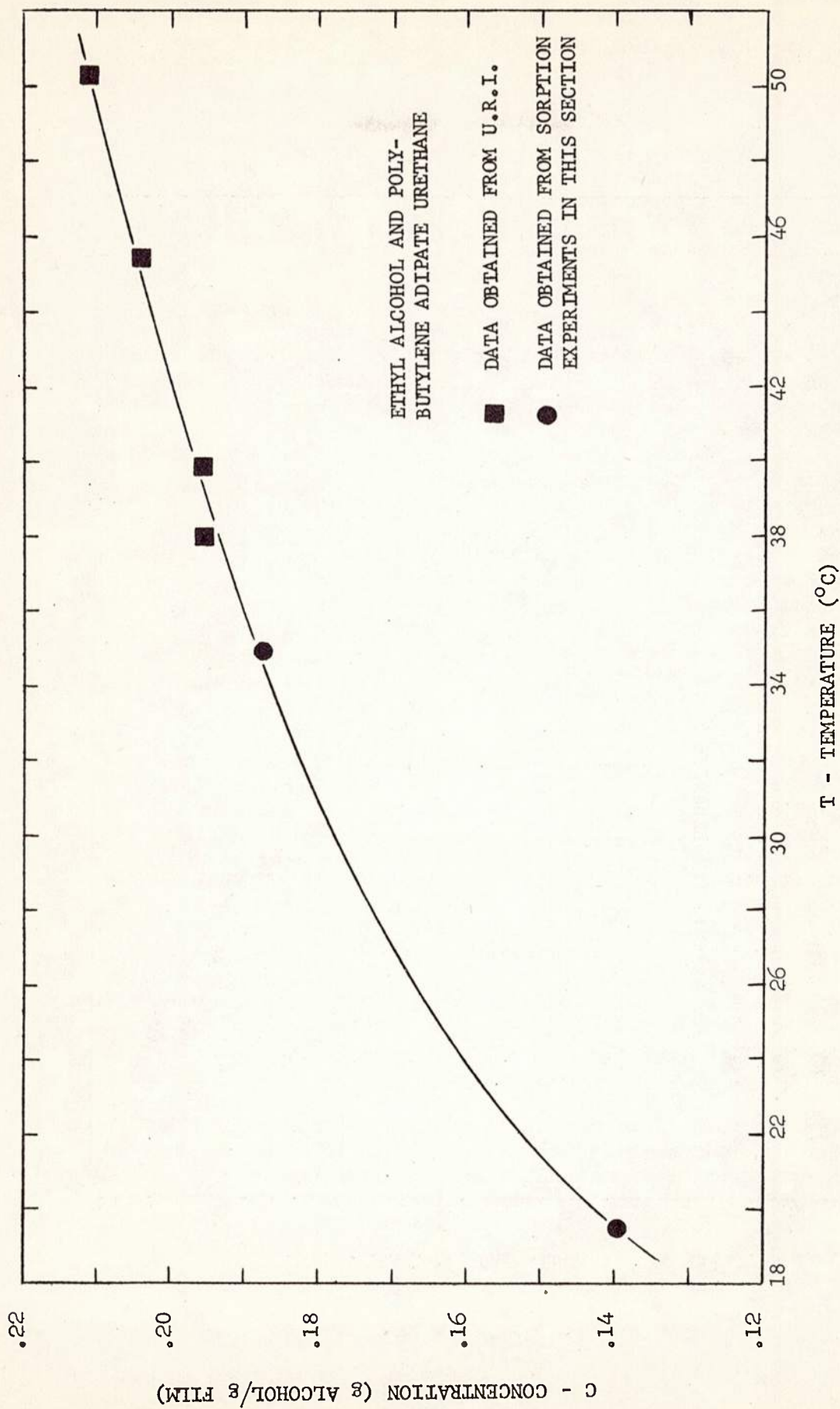


FIGURE D-31. TEMPERATURE DEPENDENCE OF ETHANOL SOLUBILITY IN THE POLYESTER POLYURETHANE; SAMPLES IMMersed IN THE LIQUID.

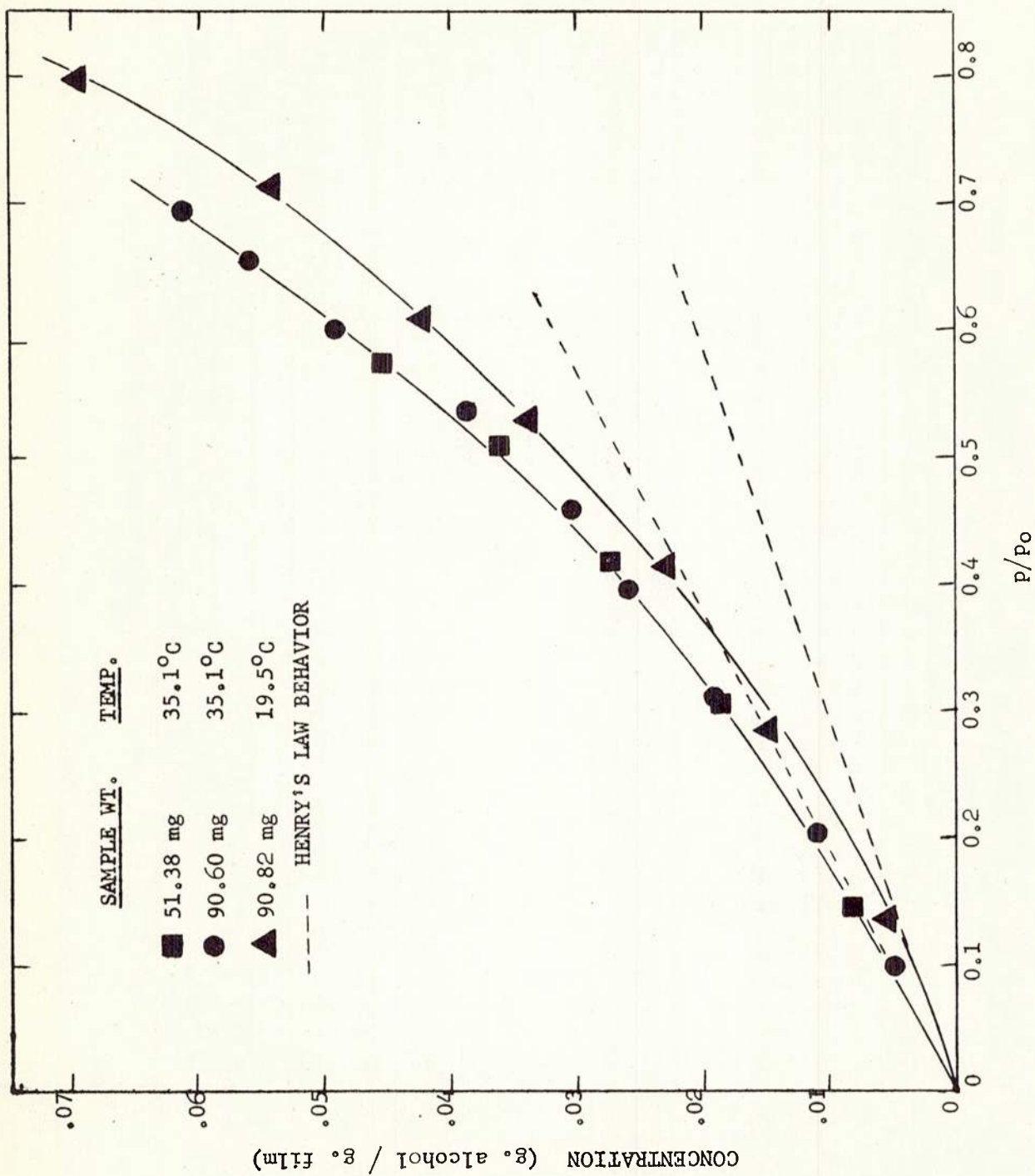


FIGURE D-32. SORPTION ISOTHERMS REPRESENTING CONCENTRATION OF ETHANOL (g/cc) AS A FUNCTION OF PARTIAL PRESSURE (p/p_0)

from the simple Henry's law behavior observed in the solution of most gases in polymers

$$C = k p$$

D-21

where the concentration is linearly dependent on the pressure. However, the isotherms are similar to the behavior obtained with polar penetrants in many polymers. (D-53) In Figure D-32, straight lines have been drawn through the origin to coincide with as much of the initial portion of the isotherm as possible. It is apparent that departures from Henry's Law behavior start at very low activities, of the order of 0.15.

Despite the marked deviations from Henry's law behavior, the isotherm at 35.1°C. falls only slightly above the curve for 19.5°C. This indicates that the heat of mixing is endothermic but very small. The value calculated from the equation

$$\Delta H = R[d(\ln a_1)/d(1/T)]_c$$

D-22

where a_1 is the solvent activity (p/p_0), C_1 is the solvent concentration and R is the gas constant, is only 1,060 calories. This suggests that the environment of ethanol molecules in the polyurethane is not very different energetically from the environment in liquid ethanol and, in particular, that many of the H - bonds present in the pure solvent are reformed in the polyurethane matrix.

The general behavior of the sorption isotherm is similar to that previously reported with water where, however, the saturation concentration is about 1.5%, a factor of 10 lower than ethanol. In both cases the sorption isotherms are strongly concave upward, and the heats of mixing very small, in fact, essentially zero for water. (D-53) Both the shape of the isotherm and the zero heat of mixing for water have been attributed to the aggregation of water molecules to form clusters. In view of the possibility of similar intermolecular H-bonding of ethanol molecules, this process is probably also important in determining the solubility behavior of ethanol.

2. Transient Results

A certain number of the sorption time curves were anomalous since F versus $t^{1/2}$ was not strictly linear over the first 60% of the sorption process. In the runs at the higher temperature, except for the first sorption step, there was an initial lag in the sorption process with the result that the curves were somewhat S-shaped and the linear portion of the curve extrapolated back to a positive intercept on the $t^{1/2}$ axis. For the first pressure step, both at the low and high temperature, there was a distinct break in the curve as illustrated by

the data plotted in Figure D-33. In the other sorption time curves at the lower temperature, the break in the curve was less marked and was shifted to higher ordinate values.

Figure D-34 presents the diffusion constants calculated from Equations D-18 and D-19 as a function of concentration. For the low temperature data there is good agreement between the half-time values (open circles) and slope values (filled circles) of D . It appears that D first decreases somewhat with increasing C and then increases for concentrations greater than 2.5%. However, the overall increase in D with C is very modest, especially compared to the order of magnitude changes frequently observed with swelling penetrants. (D-30)

At the higher temperature the half-time- and slope- calculated values of D are in poor agreement for at least half the data. In each of these cases, by correcting for the positive time intercept of the $F - t^{1/2}$ curve, the half-time values of D are brought into agreement with the slope value. An approximate curve of D versus C has been drawn through the slope values (filled points). It will be observed that there is a resemblance to the behavior at the lower temperature.

The appearance of the sorption-time curves is similar to the curves generated from Cranks analysis of diffusion with concurrent first order reaction, (D-22) when the ratio

$$b = \mu L^2 / D < 1 \quad \text{D-23}$$

Here μ is the rate constant for the back reaction which regenerates the free penetrant molecules. Under these circumstances the form of the curve and, therefore, the slope and half-time will be functions of the rate constant μ , an equilibrium association constant R , as well as L^2 and D separately. The presence of a break in the curve for the first sorption step at 19.5°C. facilitates an approximate analysis of this curve by comparison with the results which Crank has calculated. In Figure D-35, the experimental data are compared with the theoretical curve plotted from Crank's Table 8.2 for $R = 1$ (equal concentration of reacted and free species) and $b = 0.1$. The theoretical curve for $R = 1$ (equal concentration of reacted and free species) and $b = 0.1$. The theoretical curve for $R = 10$, $b = 0.01$ has also been included, in this case with the ordinate values multiplied by a factor of three, to illustrate the fact that the height of the break in the curve is a sensitive function of R . It is apparent that the shape of the experimental curve is in good agreement with the theoretical curve for $R = 1$, $b = 0.1$ up to $F = 0.5$ where the experimental curve begins to rise more steeply. Approximate values of the parameters have been calculated by identifying the experimental results with the theoretical curve. The

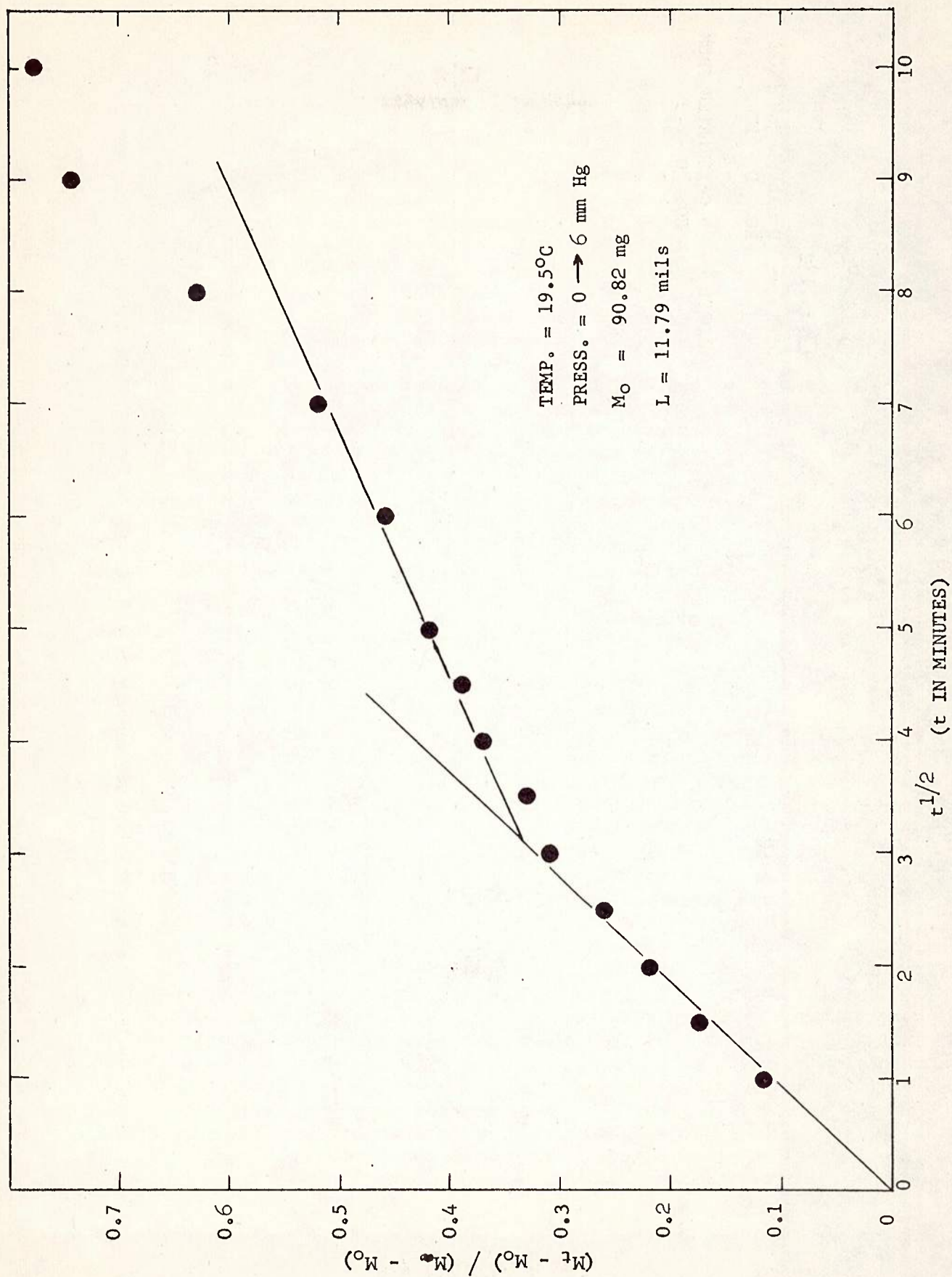


FIGURE D-33. SORPTION-TIME CURVE FOR ETHANOL

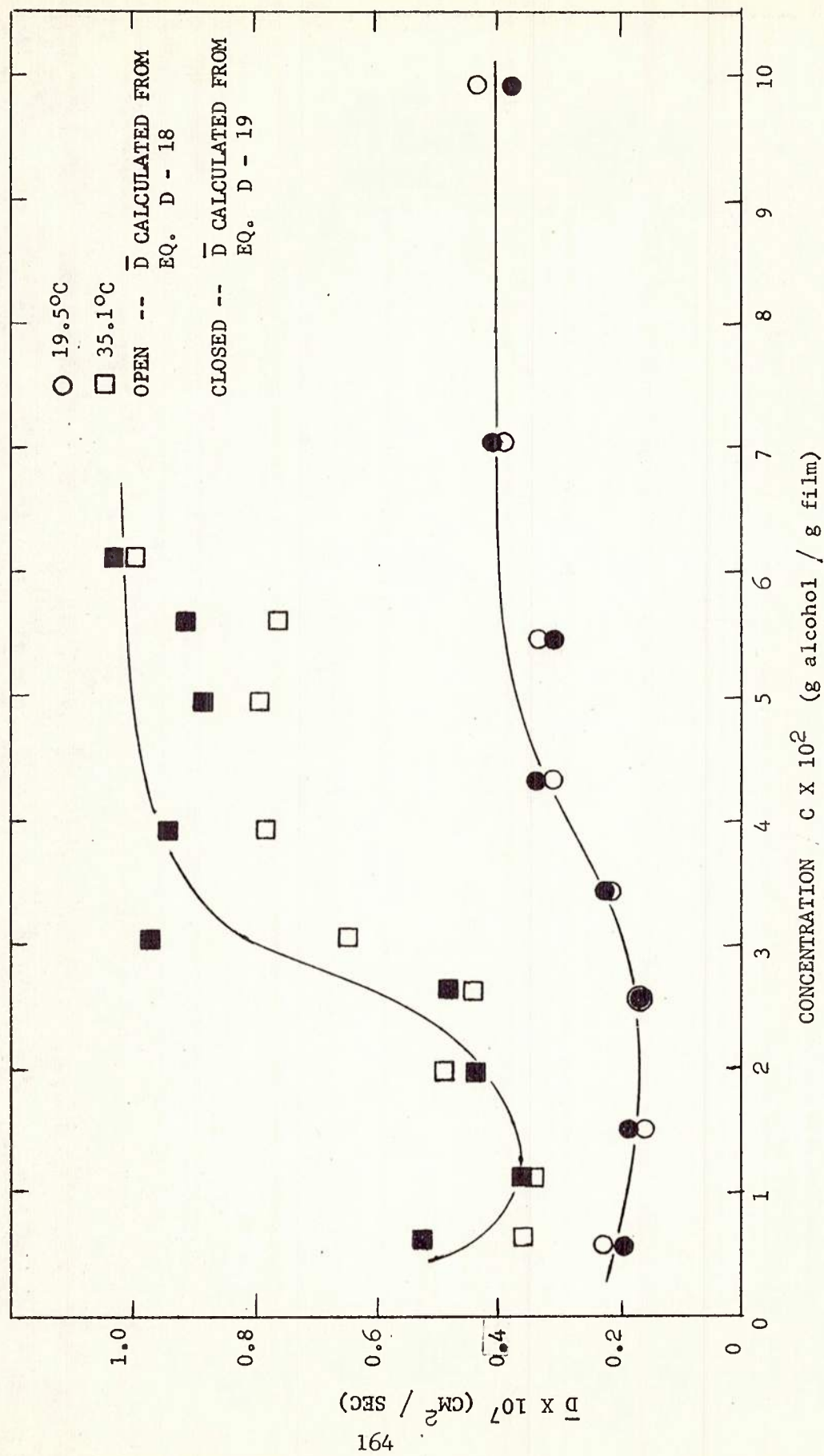


FIGURE D-34. CONCENTRATION DEPENDENCE OF THE DIFFUSION CONSTANT OF ETHANOL

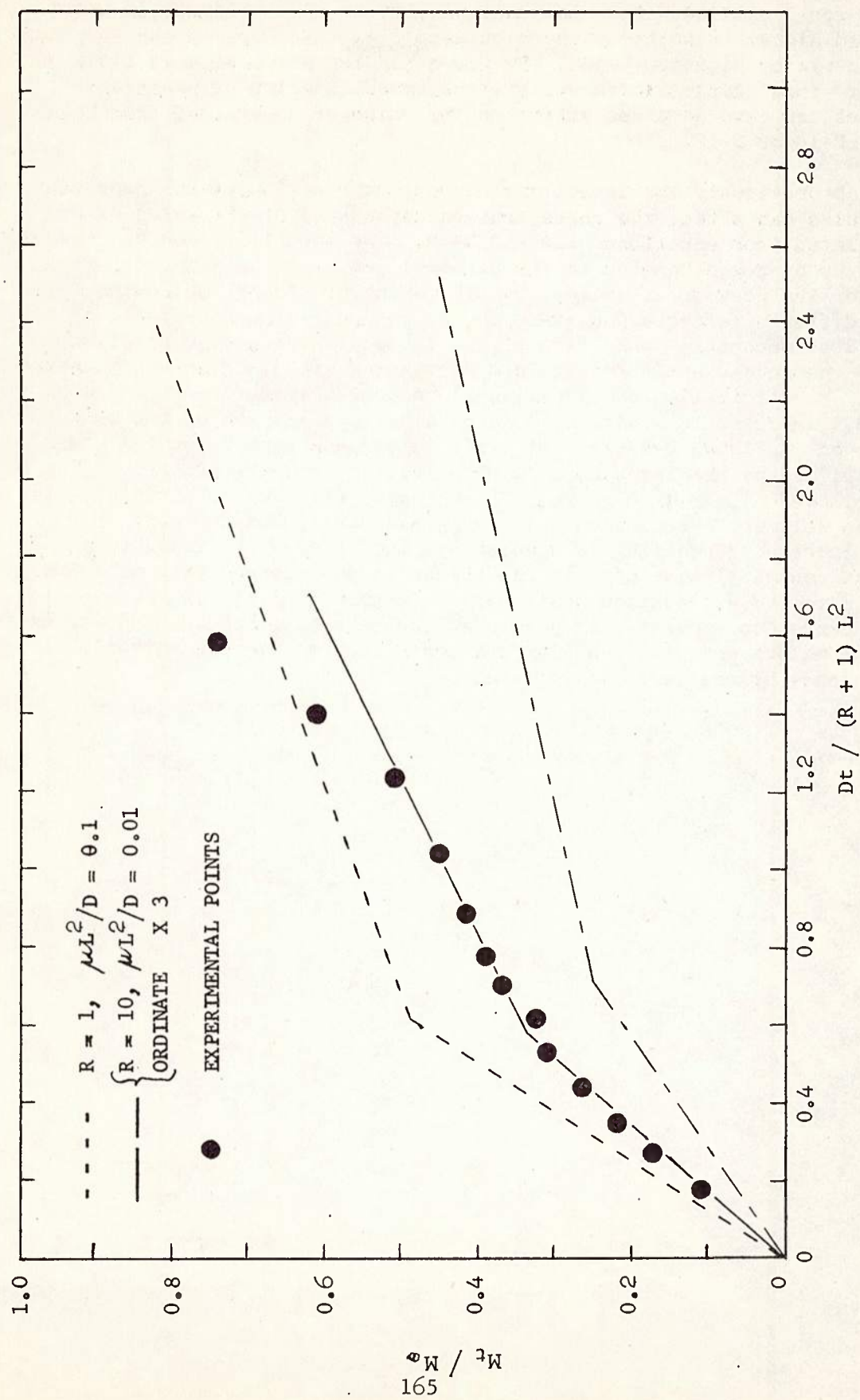


FIGURE D-35. COMPARISON OF SORPTION-TIME CURVE FOR ETHANOL AT 19.5°C, 0 → 6 MM Hg WITH THEORETICAL CURVES CALCULATED FOR DIFFUSION WITH CONCURRENT REACTION.

value for D obtained from this analysis, $2.3 \times 10^{-7} \text{ cm}^2/\text{sec}$, is about tenfold higher than the value calculated from the slope of the sorption-time curve by Equation D-19. The corresponding value of μ is $1.0 \times 10^{-4} \text{ sec}^{-1}$. This comparison shows that the immobilization of penetrant species can have a marked effect on the value of D obtained from Equations D-18 or D-19.

As previously mentioned, any concurrent reaction of the penetrant molecules can affect the concentration dependence of the value of D calculated from equations D-18 and D-19. The immobilization of ethanol can occur by hydrogen bonding to the carboxyl group of the polyester segment of the polymer as well as by clustering of ethanol molecules, with differing effects, however, on the concentration dependence of D. The first mechanism would result in D increasing with concentration while the second would result in D decreasing with increasing concentration. Plasticization and swelling alone should lead to a strong continuous increase in D with C. One possible explanation of the behavior observed in Figure D-34 is that, initially, penetrant molecules are immobilized by the interaction with polyester carboxyl groups. This is followed by a region in which D begins to rise due to plasticization of the polymer. But the normally expected continuous increase in D with increasing swelling is opposed by clustering which leads to an almost constant value of D at the higher ethanol concentrations. Any more detailed explanation must await a further analysis of the sorption-time curves to separate, if possible, the several factors which influence the anomalous sorption behavior and contribute to the concentration dependence of the diffusion constant.

REFERENCES

- D-1 Adamson, Arthur W. Physical Chemistry of Surfaces. New York: Interscience Publishers, 1960, 597 pp.
- D-2 Aithen, A., and R.M. Barrer. Trans. Faraday Soc., 51, 116 (1955).
- D-3 Amerongen, G.J. van. J. Polymer Sci., 5, 307 (1950).
- D-4 Amerongen, G.J. van. Rubber Chem. Technol., 37, 1065 (1964).
- D-5 Arkin, Herbert, and Colton, Statistical Methods, New York: Barnes and Noble, 1955.
- D-6 Auerbach, I., et al. J. Polymer Sci., 28, 129 (1958).
- D-7 Bagley, E., and F.A. Long. J. Am. Chem. Soc., 77, 2172 (1955).
- D-8 Barrer, R.M. Trans. Faraday Soc., 39, 237 (1943).
- D-9 Barrer, R.M. Diffusion In and Through Solids. London: Cambridge University Press, 1941, 464 pp.
- D-10 Barrer, R.M., J.A. Barrie, and J. Slater. J. Polymer Sci., 27, 177 (1958).
- D-11 Barrer, R.M., and J.A. Barrie. J. Polymer Sci., 28, 377 (1958).
- D-12 Barrer, R.M., and G. Skirrow. J. Polymer Sci., 3, 549 (1948).
- D-13 Barrer, R.M., and G. Skirrow. J. Polymer Sci., 3, 564 (1948).
- D-14 Barrier, J.A., and B. Platt. Polymer, 403, 303 (1963).
- D-15 Berliner, S.M. and D.L. Fiske. Advanced Space Suits for Extra-Vehicular and Lunar Exploration : Quarterly Progress Report No. 3. United States Army Natick Laboratories, Advanced Projects Branch, Natick, Massachusetts, 1965, 40 pp.
- D-16 B.F. Goodrich Data Sheet on Estane Polyurethanes.
- D-17 Brunauer, S., P.H. Emmett, and E. Teller. J. Am. Chem. Soc., 60, 309 (1938).
- D-18 Buckley, D.J., and M. Berger. Proc. Am. Chem. Soc., International Rubber Conference, 340, (Nov. 1959).

- D-19 Cesari, M., G. Perego, and A. Mazzei. Markomol. Chem., 83, 196 (1965).
- D-20 Cooper, S.L. and A.V. Tobolsky, Textile Res. J., 36, 800 (1966).
- D-21 Crank, J. Trans. Faraday Soc., 21, 1632 (1955).
- D-22 Crank, J. The Mathematics of Diffusion. London : Oxford University Press, 1956, 339 pp.
- D-23 Crank, J., and M.E. Henry. Trans. Faraday Soc., 45, 636 (1949).
- D-24 Crank, J., and G.S. Park. Trans. Faraday Soc., 45, 240 (1949).
- D-25 Dickenson, L.A. Rubber Age, 82, 96 (1957).
- D-26 Dole, M. Ann. N. Y. Acad. Sci., 51, 705 (1949).
- D-27 Foster, S. Honors Thesis, Dept. Chem. Eng., Univ. of Rhode Island, Kingston, Rhode Island, 1967.
- D-28 Freundlich, H. Colloid and Capillary Chemistry. London : Methuen and Co., Ltd., 1926.
- D-29 Frisch, H.L., and V. Stannett. J. Polymer Sci., 13, 131 (1954).
- D-30 Fujita, H. Fortschr. Hochpolym-Forsch., Bd. 3, S. 1-47 (1961).
- D-31 Fujita, H., A. Kishimoto, and K. Matsumoto, Trans. Faraday Soc., 56, 424 (1960).
- D-32 Garrett, R.R. Rubber and Plastics Age, 46, 915 (1965).
- D-33 Gordon, M., et al. Proc. Roy. Soc., 258A, 215 (1960).
- D-34 Hartley, G.S., and J. Crank. Trans. Faraday Soc., 52, 801 (1949).
- D-35 Hayes, M.J., and G.S. Park. Trans. Faraday Soc., 51, 1134 (1955).
- D-36 Hicks, E.M., Jr., A. J. Ultee, and J. Drougas. Science, 147, 373 (1965).
- D-37 Hill, T.L., and J.W. Rowen. J. Polymer Sci., 9, 93
- D-38 Hopfenberg, H.B., Water Transport In and Across Polyurethane Films : Quarterly Progress Report No. 5. United States Army Natick Laboratories, Advanced Projects Branch, Natick, Mass. 1965, 18 pp.
- D-39 Kokes, R.J., F.A. Long, and J.L. Hoard. J. Phys. Chem., 20, 1711 (1952).

- D-40 Langmuir, I. J. Am. Chem. Soc., 40, 1361 (1918).
- D-41 McBain, J.W. Phil. Mag., 18, 916 (1909).
- D-42 McBain, J.W., and A.M. Bakr. J. Am. Chem. Soc., 690 (1926).
- D-43 McClaren, A.D., and J.W. Rowen. J. Polymer Sci., 7, 289 (1951).
- D-44 Meares, P. J. App. Pol. Sci., 9, 917 (1965).
- D-45 Meares, P. Polymers -- Structure and Bulk Properties. London : D. Van Nostrand Company, Ltd., 1965, 366 pp.
- D-46 Michaels, A.S., and H.J. Bixler. J. Polymer Sci., 50, 413 (1961).
- D-47 Michaels, A.S., W.R. Vieth, and J.A. Barrie. Solution of Gases in Polyethylene Terephthalate. Paper read at the Annual Meeting of the American Physical Society, Division of High Polymer Physics, Baltimore, Maryland, 27-30 March, 1962.
- D-48 Prager, S., and F.A. Long. J. Am. Chem. Soc., 73, 4072 (1951).
- D-49 Rogers, C.E. Engineering Design for Plastics. Chap. 9, New York : Reinhold Publishing Corp., 1964.
- D-50 Rogers, C.E., V. Stanne H, and M. Szwerc. J. Polymer Sci., 45, 61 (1960).
- D-51 Saunders, J.H. Rubber Chem. and Technol., 33, 1259 (1960).
- D-52 Saunders, J.H., and H.K. Frisch, Polyurethanes, Chemistry and Technology, Pt. 1, New York : Interscience Publishers, 1962.
- D-53 Schneider, N.S., L.V. Dusablon, L.A. Spano, H. B. Hopfenberg, and F. Votta. J. Appl. Polymer Sci., in press.
- D-54 Sherman, D.P. Masters Thesis, Dept. Chem. Eng., Univ. of Rhode Island, Kingston, Rhode Island, 1966.
- D-55 Singh, A., and L. Weisshein, J. Polymer Sci., A-1 4, 2551 (1966).
- D-56 Votta, F. Analysis of Permeation Data. Memo for Record, United States Army Natick Laboratory, Advanced Projects Branch, Natick, Mass. 1966.
- D-57 Weisfeld, L.B., J.R. Little, and W.E. Wolstenholme. J. Polymer Sci., 56, 455 (1962).

- D-58 Weisz, P.B. Trans. Faraday Soc., 63, 1801 (1967).
- D-59 Wellons, J.D., and V. Stannett. J. Polymer Sci., A-1, 4, 593 (1966).
- D-60 Wetton, R.E. and G.A. Allen, Polymer, 7, 331 (1966).
- D-61 Yasuda, H., and V. Stannett. J. Polymer Sci., 57, 907 (1962).
- D-62 Zimm, B. H. J. Chem. Phys., 21, 934 (1953).
- D-63 Zimm, B.H., and J.L. Lundberg, J. Phys. Chem., 60, 425 (1956).

DOCUMENT CONTROL DATA - R & D

(Security classification of title, body of abstract and indexing annotation must be entered when the overall report is classified)

1. ORIGINATING ACTIVITY (Corporate author) U. S. Army Natick Laboratories Natick, Massachusetts 01760		2a. REPORT SECURITY CLASSIFICATION Unclassified	
		2b. GROUP	
3. REPORT TITLE Passive Thermal Control Systems for Advanced Space Suit Concepts			
4. DESCRIPTIVE NOTES (Type of report and inclusive dates) Final Report July 1964 - January 1968			
5. AUTHOR(S) (First name, middle initial, last name) Louise V. Dusablon, Ferdinand Votta, Jr., Nathaniel S. Schneider, Leo A. Spano			
6. REPORT DATE November 1968		7a. TOTAL NO. OF PAGES 170	7b. NO. OF REFS 84
8a. CONTRACT OR GRANT NO.		9a. ORIGINATOR'S REPORT NUMBER(S) 69-25-CE	
b. PROJECT NO.		9b. OTHER REPORT NO(S) (Any other numbers that may be assigned this report)	
c.		CEOM-54	
d.			
10. DISTRIBUTION STATEMENT This document has been approved for public release and sale; its distribution is unlimited.			
11. SUPPLEMENTARY NOTES		12. SPONSORING MILITARY ACTIVITY U. S. Army Natick Laboratories Natick, Mass. 01760	
13. ABSTRACT Pervaporation of water from a space suit has been proposed as a method of cooling an astronaut. The purpose of this program was to investigate the various principles, techniques and material designs applicable to the engineering of a system capable of transferring up to 3000 Btu/hr. Four different approaches were investigated with an eventual prototype kept in view. Simple diffusion of water through a membrane requires the development of a polymer with strong physical properties and chemical characteristics necessary to its application to a space suit. Presently no polymer has both required properties. Research was begun to design an appropriate polymer. A composite membrane was tested where the matrix had the required physical characteristics and a "filler" polymer enhanced the existing permeation qualities of the matrix. This system came within a factor of two of the required permeation rate of 1100 gms/24 hrs/100 in ² . A matrix with higher permeation rates and a more uniform method of mixing is needed before this method is capable of being incorporated in a prototype design. The principle of electroendosmosis was examined as a means of electrically controlling water transport through a membrane. It was shown to be theoretically capable of removing a sufficient quantity of moisture at no great cost of power. However, much developmental research is needed to bring the system to the prototype stage. A semipassive system ready for prototype development was also tested. With this method, the temperature of the man would be controlled by a valve which allows regulated amounts of water to evaporate and thus remove heat.			

14. KEY WORDS	LINK A		LINK B		LINK C	
	ROLE	WT	ROLE	WT	ROLE	WT
Protection	8				4	
Cooling	8				4	
Astronauts	9				4	
Pressure suits	9				4	
Diffusion	10		4		8	
Vapors	10		4		9	
Perspiration	10		4		9	
Development			8			
Polymers			9		10	
Membranes			9		10	
Composite materials			9		10	
Permeability			8			
Electrosomosis					10	
Control			4		4	
Temperature			4		4	